

000 001 002 003 004 005 006 007 008 009 010 011 012 013 014 015 016 017 018 019 020 021 022 023 024 025 026 027 028 029 030 031 032 033 034 035 036 037 038 039 040 041 042 043 044 045 046 047 048 049 050 051 052 053 IMPLICIT MODELS: EXPRESSIVE POWER SCALES WITH TEST-TIME COMPUTE

Anonymous authors

Paper under double-blind review

ABSTRACT

Implicit models, an emerging model class, compute outputs by iterating a single parameter block to a fixed point. This architecture realizes an infinite-depth, weight-tied network that trains with constant memory, significantly reducing memory needs for the same level of performance compared to explicit models. While it is empirically known that these compact models can often match or even exceed the accuracy of larger explicit networks by allocating more test-time compute, the underlying reasons are not yet well understood.

We study this gap through a non-parametric analysis of expressive power. We provide a strict mathematical characterization, showing that a simple and regular implicit operator can, through iteration, progressively express more complex mappings. We prove that for a broad class of implicit models, this process allows the model’s expressive power to grow with test-time compute, ultimately matching a much richer function class. The theory is validated across four domains: imaging, scientific computing, operations research, and LLM reasoning, demonstrating that as test-time iterations increase, the complexity of the learned mapping rises, while the solution quality simultaneously improves and stabilizes.

1 INTRODUCTION

Many machine-learning tasks can be cast as learning a mapping \mathcal{F} from input \mathbf{x} to the desired output \mathbf{y}_* , i.e., $\mathbf{y}_* = \mathcal{F}(\mathbf{x})$. An emerging alternative is the *implicit models*: train an operator \mathcal{G} whose fixed point matches the target, i.e., $\mathbf{y}_* = \mathcal{G}(\mathbf{y}_*, \mathbf{x})$ (Bai et al., 2019; El Ghaoui et al., 2021). At inference time, the fixed point is obtained via a root-finding solver. While advanced algorithms (e.g., Anderson acceleration or Broyden’s method) exist, the canonical approach is the Picard iteration:

$$y_1 = \mathcal{G}(y_0, \mathbf{x}), \quad y_2 = \mathcal{G}(y_1, \mathbf{x}), \quad y_3 = \mathcal{G}(y_2, \mathbf{x}), \quad \dots, \quad (1)$$

and expect $\mathbf{y}_t(\mathbf{x}) \rightarrow \mathbf{y}_*(\mathbf{x}) = \mathcal{F}(\mathbf{x})$ for all \mathbf{x} . Rather than producing \mathbf{y}_* in a single feed-forward pass, implicit models reach the target through gradual equilibrium-seeking updates. Here, “*test-time compute*” refers to the computational budget spent at inference—primarily the number of iterations. By tailoring the structure of \mathcal{G} , implicit models have shown strong results across many domains (e.g., imaging (Gilton et al., 2021), scientific computing (Marwah et al., 2023), generative modeling (Pokle et al., 2022; Geng et al., 2023), LLM reasoning (Geiping et al., 2025), etc.).

Behind these successes, the advantages of implicit models include: (i) they realize an infinite-depth, weight-tied network trainable with constant memory, which yields efficient training (Fung et al., 2022; Geng et al., 2021); (ii) they allow us to “implicitly bake in” domain constraints and structure (e.g., physics, geometry, safety), see Xie et al. (2022); Güngör et al. (2023); Oshin et al. (2024); and, most surprisingly, (iii) they can often match or even exceed the accuracy of larger explicit networks by allocating more iterations (Marwah et al., 2023; Wang et al., 2024; Geiping et al., 2025). Point (i) stems from the weight-tied architecture and avoiding full back-propagation. Point (ii) arises from the inherently implicit nature of many real-world, equation-based constraints. In contrast, the mechanism underlying the surprising effectiveness of (iii) remains less well understood.

We study this through the lens of expressive power—the set of input–output maps a model family can represent. We ask two questions. First, as a baseline: **(Q1)** Do implicit models (at least) match the expressive power of explicit ones? Concretely, for a target map $\mathcal{F} : \mathbf{x} \mapsto \mathbf{y}_*$, does there always exist an implicit operator \mathcal{G} such that the iterates of (1) satisfy $\mathbf{y}_t(\mathbf{x}) \rightarrow \mathcal{F}(\mathbf{x})$ for all \mathbf{x} ? If yes, a more insightful question follows: **(Q2)** Do implicit models offer an expressive advantage? In particular, can a relatively simple implicit operator \mathcal{G} , through iteration, represent a complex explicit map \mathcal{F} ? A positive answer to (Q2) would directly explain phenomenon (iii).

To our knowledge, these questions remain largely open. While universality has been touched upon in specific settings (Bai et al., 2019; Marwah et al., 2023) and separation results have demonstrated advantages over explicit models (Wu et al., 2024), a complete characterization of the representable function class of implicit models (and hence a direct answer to questions (Q1) and (Q2)) is still missing. Unlike studies focusing on infinite-width limits and kernel connections (Gao et al., 2022; Feng & Kolter, 2023; Ling et al., 2024), our work fills this gap from a *nonparametric, function-space perspective*, establishing that an implicit model’s expressive power scales with test-time compute. (See Appendix J for broader contextual discussions.) Specifically:

- **Expressive boundary.** We identify locally Lipschitz mappings as a natural target class and prove: every such map \mathcal{F} can be expressed as the fixed point of a “regular” (simple and well-behaved) \mathcal{G} , and conversely, every such fixed-point map is locally Lipschitz.
- **Emergent expressive power.** Our theory, combined with iterative solvers’ dynamics, yields a new viewpoint on implicit models: the expressive power is progressively unlocked by iterations.
- **Validation across domains.** We validate our theory with case studies in a wide range of applications (e.g., image reconstruction, scientific computing, operations research, and LLM reasoning).

Note that, while explicit networks are capable of expressing locally Lipschitz target maps (Beneventano et al., 2021) by scaling up the model size, implicit models are able to scale expressivity with test-time iterations and represent increasingly complex functions without adding parameters.

2 MAIN RESULTS

We now return to (Q1): given a target map \mathcal{F} , does there exist an implicit operator \mathcal{G} whose fixed-point iteration yields $\mathbf{y}_t(\mathbf{x}) \rightarrow \mathcal{F}(\mathbf{x})$? A naive construction answers “yes”: define, for $0 < \eta < 1$,

$$\mathcal{G}(\mathbf{y}, \mathbf{x}) := (1 - \eta)\mathbf{y} + \eta\mathcal{F}(\mathbf{x}). \quad (2)$$

Then the fixed-point iteration reduces to $\mathbf{y}_t = (1 - \eta)\mathbf{y}_{t-1} + \eta\mathcal{F}(\mathbf{x})$, hence $\mathbf{y}_t - \mathcal{F}(\mathbf{x}) = (1 - \eta)(\mathbf{y}_{t-1} - \mathcal{F}(\mathbf{x}))$. As $0 < \eta < 1$, it holds that, for all \mathbf{x} , $\mathbf{y}_t(\mathbf{x}) - \mathcal{F}(\mathbf{x}) \rightarrow \mathbf{0}$ as $t \rightarrow \infty$.

However, (2) is merely a trivial averaging of \mathbf{y} and $\mathcal{F}(\mathbf{x})$; learning such an implicit model is no different from learning \mathcal{F} directly. This prompts the natural follow-up: is there any *nontrivial* implicit representation that is able to indicate the expressive benefits of implicit models?

An illustrative example. Let $\mathcal{F}(x) = 1/x$ on $[-1, 1] \setminus \{0\}$. This function is smooth (differentiable to any order) almost everywhere, but blows up near the singular point $x = 0$:

$$|\mathcal{F}(x)| = \left| \frac{1}{x} \right| \rightarrow \infty, \quad \left| \frac{d\mathcal{F}}{dx} \right| = \left| -\frac{1}{x^2} \right| \rightarrow \infty, \quad \text{as } x \rightarrow 0.$$

Neural networks approximating $1/x$ on $[-1, -\delta] \cup (\delta, 1]$ typically demands higher network complexity—i.e., increasing depth/width as $\delta \rightarrow 0$ to capture the growing steepness near the singularity (Telgarsky, 2017). If we adopt the naive implicit form (2), $\mathcal{G}(y, x) = (1 - \eta)y + \eta/x$, nothing is gained: the model still inherits the singular behavior $|\partial\mathcal{G}/\partial x| = \eta/x^2 \rightarrow \infty$.

What would be a nontrivial implicit representation in this setting? Instead of writing $(1/x)$ explicitly, we can regard it as the solution of the equation $xy - 1 = 0$ (**implicit representation**). Inspired by this, we apply a fixed-point iteration to $xy - 1 = 0$: $\mathcal{G}(y, x) = y - \eta(xy - 1)$. Using the general scheme in (1), we have $y_t = y_{t-1} - \eta(xy_{t-1} - 1)$. Subtracting the true solution gives

$$y_t - \frac{1}{x} = y_{t-1} - \frac{1}{x} - \eta x \left(y_{t-1} - \frac{1}{x} \right) = (1 - \eta x) \left(y_{t-1} - \frac{1}{x} \right)$$

For any $0 < \eta < 1$ and any $x \in (0, 1]$, we have $0 < (1 - \eta x) < 1$ which implies $y_t \rightarrow 1/x$. (For $x < 0$, simply flip the stepsize sign, η to $-\eta$.) This implicit formulation is much simpler and more elegant: the operator $\mathcal{G}(y, x) = y - \eta(xy - 1)$ has *no singularity* and *no blow-up*.

The example indicates: intuitively, an implicit representation can realize a complicated map with singularities via a much simpler, smoother update operator \mathcal{G} . Next, we make it precise: we formally define what we mean by “simple” versus “complex,” and characterize—beyond the $1/x$ example—the class of target functions for which an implicit representation admits such a simple form.

Definition 2.1 (Lipschitz continuity). Let $(\mathbb{X}, \|\cdot\|)$ and $(\mathbb{Y}, \|\cdot\|)$ be normed spaces, and let $\mathcal{Q} : \mathbb{X} \rightarrow \mathbb{Y}$. We say \mathcal{Q} is *L-Lipschitz* (globally Lipschitz) on \mathbb{X} if there exists $L > 0$ such that

$$\|\mathcal{Q}(\mathbf{x}_1) - \mathcal{Q}(\mathbf{x}_2)\| \leq L \|\mathbf{x}_1 - \mathbf{x}_2\| \quad \text{for all } \mathbf{x}_1, \mathbf{x}_2 \in \mathbb{X},$$

and the smallest such L is the *Lipschitz constant* (or *Lipschitz modulus*), denoted as $\text{Lip}(\mathcal{Q})$. If the Lipschitz constant $L < 1$, we say \mathcal{Q} is *L-contractive* on \mathbb{X} . Given $\mathbf{x} \in \mathbb{X}$, we say \mathcal{Q} is *locally Lipschitz* at \mathbf{x} if there exists a neighborhood \mathbb{U} of \mathbf{x} on which \mathcal{Q} is $L_{\mathbb{U}}$ -Lipschitz continuous for some $L_{\mathbb{U}} > 0$. If \mathcal{Q} is locally Lipschitz at every $\mathbf{x} \in \mathbb{X}$, we say \mathcal{Q} is *locally Lipschitz* on \mathbb{X} .

108 Intuitively, Lipschitz continuity limits how quickly a function’s value can change. When a function
 109 is differentiable, its Lipschitz modulus can be characterized by the norm of its first derivative via
 110 the mean-value theorem. For example, $\mathcal{F}(x) = 1/x$ is locally Lipschitz on $[-1, 1] \setminus \{0\}$ but not
 111 globally Lipschitz there, since $|\mathrm{d}\mathcal{F}/\mathrm{d}x| = 1/x^2$ is unbounded as $x \rightarrow 0$, causing local Lipschitz
 112 constants to blow up near the singularity. In contrast, the implicit update $\mathcal{G}(y, x) = y - \eta(xy - 1)$
 113 has simple partial derivatives $|\partial\mathcal{G}/\partial x| = |\eta y|$ and $|\partial\mathcal{G}/\partial y| = |1 - \eta x|$ without singularity.

114 Locally Lipschitz mappings form a much richer class than globally Lipschitz ones. Typical examples
 115 (locally Lipschitz everywhere in their domains but not globally Lipschitz on the whole set) include:
 116 $\log x$ in $(0, 1]$, $\tan x$ in $(-\frac{\pi}{2}, \frac{\pi}{2})$, \sqrt{x} in $(0, 1]$, $\Gamma(x)$ in $\mathbb{R} \setminus \{0, -1, -2, \dots\}$, etc.

117 For this reason, we refer to globally Lipschitz maps as “simple” operators and locally Lipschitz maps
 118 (which may exhibit large local slopes near certain inputs) as “complex.” Next, we formally state our
 119 main result: identifying a broad family of target functions for which implicit representations provide
 120 such simple update operators while expressing complex fixed-point mappings.

121 **Assumption 2.2.** Let $\mathbb{X} \subset \mathbb{R}^d$ and $\mathcal{F} : \mathbb{X} \rightarrow \mathbb{R}^n$ be locally Lipschitz on \mathbb{X} .

122 We do NOT assume the domain \mathbb{X} to be bounded, compact, closed, or connected. For instance,
 123 $\mathbb{X} = \mathbb{R} \setminus \{0\}$ excludes the singular point and permits $\mathcal{F}(x) = 1/x$ to blow up at the interior gap $x = 0$
 124 while remaining locally Lipschitz on \mathbb{X} . Another example is $\mathbb{X} = \bigcup_{k \in \mathbb{Z}} (k\pi - \frac{\pi}{2}, k\pi + \frac{\pi}{2})$, where
 125 $\mathcal{F}(x) = \tan x$ remains locally Lipschitz despite blowing up at the singularity points $\{k\pi + \frac{\pi}{2}\}_{k \in \mathbb{Z}}$.

126 We now formalize what we mean by “simple” update rules—namely, *regular implicit operators*.

127 **Definition 2.3** (Regular implicit operator). Let $\mathbb{X} \subset \mathbb{R}^d$ be bounded. An operator $\mathcal{G} : \mathbb{R}^n \times \mathbb{X} \rightarrow \mathbb{R}^n$
 128 is *regular* if: (i) For any $\mathbf{y} \in \mathbb{R}^n$, the map $\mathbf{x} \mapsto \mathcal{G}(\mathbf{y}, \mathbf{x})$ is globally Lipschitz (w.r.t. \mathbf{x}) on \mathbb{X} , and
 129 the Lipschitz constant grows linearly w.r.t. $\|\mathbf{y}\|$, and (ii) For each $\mathbf{x} \in \mathbb{X}$, there exists $\mu(\mathbf{x}) \in (0, 1)$,
 130 the map $\mathbf{y} \mapsto \mathcal{G}(\mathbf{y}, \mathbf{x})$ is $\mu(\mathbf{x})$ -contractive on \mathbb{R}^n , and $\mu(\mathbf{x})$ is continuous w.r.t. \mathbf{x} .

131 A regular \mathcal{G} satisfies: (i) Fixing \mathbf{y} , $\mathcal{G}(\mathbf{y}, \cdot)$ is *globally Lipschitz in \mathbf{x}* , this makes it a “simple” operator,
 132 and (ii) Fixing \mathbf{x} , $\mathcal{G}(\cdot, \mathbf{x})$ is *contractive in \mathbf{y}* ; by Banach’s theorem, this yields a unique fixed point
 133 $\mathbf{y}_*(\mathbf{x})$ and guarantees that iterates of (1) converge to it: $\mathbf{y}_t(\mathbf{x}) \rightarrow \mathbf{y}_*(\mathbf{x})$. An example of regular \mathcal{G}
 134 is the aforementioned $\mathcal{G}(y, x) = y - \eta(xy - 1)$ on $x \in (0, 1]$ with $0 < \eta < 1$. **Moreover, regularity**
 135 **does not require joint Lipschitz properties.** With this definition, we present our main results.

136 **Theorem 2.4** (Sufficiency). *Under Assumption 2.2, for any \mathcal{F} there exists a regular implicit operator*
 137 $\mathcal{G} : \mathbb{R}^n \times \mathbb{X} \rightarrow \mathbb{R}^n$ *whose fixed-point map reproduces \mathcal{F} : $\mathrm{Fix}(\mathcal{G}(\cdot, \mathbf{x})) = \mathcal{F}(\mathbf{x})$ for all $\mathbf{x} \in \mathbb{X}$.*

138 **Theorem 2.5** (Necessity). *Let $\mathbb{X} \subset \mathbb{R}^d$ and let $\mathcal{G} : \mathbb{R}^n \times \mathbb{X} \rightarrow \mathbb{R}^n$ be regular. For every $\mathbf{x} \in \mathbb{X}$,*
 139 *$\mathcal{G}(\cdot, \mathbf{x})$ has a unique fixed point \mathbf{y}_* , and the fixed-point map $\mathbf{x} \mapsto \mathbf{y}_*(\mathbf{x})$ is locally Lipschitz on \mathbb{X} .*

140 Proofs are deferred to Appendix A. Theorem 2.4 provides an affirmative answer to (Q1) and (Q2)
 141 posed in the introduction. It proves that for any locally Lipschitz target \mathcal{F} on a bounded domain,
 142 there exists a *regular* implicit operator \mathcal{G} , whose iterations converge to the target $\mathbf{y}_t(\mathbf{x}) \rightarrow \mathcal{F}(\mathbf{x})$
 143 for all \mathbf{x} . This demonstrates that the expressive power of implicit models **not only matches** that
 144 of explicit models **but also provides a distinct expressive benefit**: *a relatively simple (regular)*
 145 *implicit representation can yield a complex fixed-point mapping.* Complementarily, Theorem 2.5
 146 shows the boundary is tight: fixed points induced by any regular \mathcal{G} are *necessarily* locally Lipschitz.
 147 Together, the two results give an exact expressivity characterization for regular implicit models.

148 **What does our theory imply?** Take a locally Lipschitz target \mathcal{F} (e.g., the curve in Fig. 1). Our re-
 149 sults guarantee the existence of a *regular* implicit operator \mathcal{G} such that the iteration $\mathbf{y}_t = \mathcal{G}(\mathbf{y}_{t-1}, \mathbf{x})$
 150 with $\mathbf{y}_0 = \mathbf{0}$ converges: $\mathbf{y}_t(\mathbf{x}) \rightarrow \mathcal{F}(\mathbf{x})$. Consider the first iterate **and its Lipschitz property**:

$$151 \quad \mathbf{y}_1(\mathbf{x}) = \mathcal{G}(\mathbf{0}, \mathbf{x}) \quad \Rightarrow \quad \mathrm{Lip}(\mathbf{y}_1) = \sup_{\mathbf{x}, \mathbf{x}'} \frac{\|\mathcal{G}(\mathbf{0}, \mathbf{x}) - \mathcal{G}(\mathbf{0}, \mathbf{x}')\|}{\|\mathbf{x} - \mathbf{x}'\|} = \mathrm{Lip}(\mathcal{G}(\mathbf{0}, \cdot)).$$

153 Because a regular operator \mathcal{G} is *globally Lipschitz* by definition, $\mathbf{y}_1(\cdot)$ is restricted to representing
 154 “simple,” globally smooth mappings. However, as iterations progress, \mathbf{y}_t converges toward \mathcal{F} . If the
 155 target \mathcal{F} features singularities (regions where local slopes become large or unbounded), the effective
 156 Lipschitz constant of the iterate $\mathbf{y}_t(\cdot)$ naturally grows with t to match that complexity:

$$157 \quad \lim_{t \rightarrow \infty} \frac{\|\mathbf{y}_t(\mathbf{x}) - \mathbf{y}_t(\mathbf{x}')\|}{\|\mathbf{x} - \mathbf{x}'\|} = \frac{\|\mathcal{F}(\mathbf{x}) - \mathcal{F}(\mathbf{x}')\|}{\|\mathbf{x} - \mathbf{x}'\|}.$$

159 This dynamic highlights a fundamental distinction: While explicit networks scale their *model size* to
 160 approximate locally Lipschitz targets (Beneventano et al., 2021), implicit models can scale expres-
 161 sivity with *test-time compute*. Since our theory guarantees a regular operator can define a complex
 equilibrium, iterating this single operator realizes this complexity *without adding parameters*.

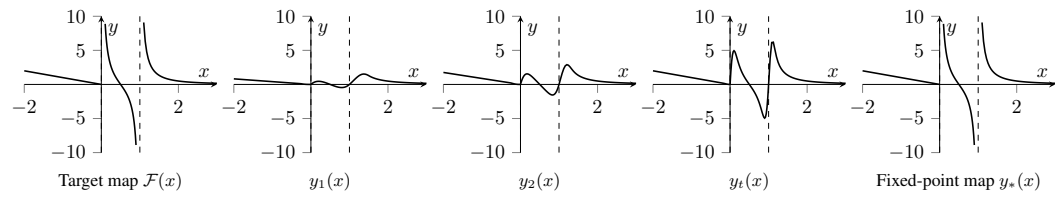


Figure 1: (Conceptual diagram) A simple implicit update expresses a complex map via iteration.

Generalization. Someone may ask: does a large Lipschitz constant of the fixed-point map $y_*(x)$ imply sensitivity or poor generalization (cf. Pabaraju et al. (2021))? Our view is that this sensitivity is *inherent to the target \mathcal{F}* , not to the implicit representation—any faithful model, explicit or implicit, must track \mathcal{F} ’s sharp variations. Our case studies in Section 3 confirm this: the target \mathcal{F} in many tasks is indeed steep somewhere and the effective Lipschitz *grows* as accuracy improves. Crucially, the implicit formulation can realize such targets with a *simple* operator \mathcal{G} , which regularizes training and supports good generalization in practice.

Insights for practitioners. A substantial line of work (e.g., El Ghaoui et al. (2021); Winston & Kolter (2020); Jafarpour et al. (2021); Revay et al. (2020); Havens et al. (2023)) enforces a global Lipschitz bound on the fixed-point map $y_*(x)$. Typically, the model is parameterized as $\mathcal{G}(y, x) = \sigma(\mathbf{A}y + \mathbf{B}x + b)$, and by imposing specific algebraic structure on \mathbf{A} and \mathbf{B} , one ensures that $y_*(x)$ is globally Lipschitz in x . While this indeed improves robustness, our theory shows it **constrains expressivity and undercuts the unique advantage of implicit models**. Our recommendation is different: rather than imposing uniform Lipschitz constraints, incorporate case-by-case *domain-specific knowledge, priors, or constraints* (as illustrated in our case studies Sec. 3). This method provides effective regularization, leading to robustness and strong test performance while unlocking the full power of implicit models—representing complex maps with relatively simple operators.

3 CASE STUDIES

In this section, we present four case studies. For the first three tasks, we (i) verify that the target satisfies Assumption 2.2; (ii) specify a domain-informed architecture for \mathcal{G} ; (iii) confirm empirically that, under standard training without explicitly enforcing \mathcal{G} to be regular, *the learned operators \mathcal{G} exhibit these properties*—i.e., \mathcal{G} is Lipschitz in x and iterates y_t converge (see Appendix F for training strategies and discussions regarding regularity guarantees); and (iv) demonstrate that expressive power scales with test-time iterations. Finally, we extend this analysis to LLM reasoning to validate our predictions in a domain where strict mathematical definitions are less applicable.

3.1 CASE STUDY 1: IMAGE RECONSTRUCTION (INVERSE PROBLEMS)

Inverse problems in imaging seek to recover an image $y_* \in \mathbb{R}^n$ from partial, noisy measurements $x = \mathbf{A}y_* + \mathbf{n} \in \mathbb{R}^d$ ($d < n$), where \mathbf{A} is a known linear operator and \mathbf{n} is noise. A common prior is that y_* lies near a smooth data manifold $\mathbb{M} \subset \mathbb{R}^n$. To recover y_* , a standard estimator solves

$$\min_{y \in \mathbb{R}^n} \frac{1}{2} \|x - \mathbf{A}y\|^2 + \frac{\alpha}{2} \text{dist}^2(y, \mathbb{M}), \quad (3)$$

or, equivalently, a variable-splitting surrogate

$$\min_{y, z \in \mathbb{R}^n} \frac{1}{2} \|x - \mathbf{A}y\|^2 + \frac{\alpha}{2} \text{dist}^2(z, \mathbb{M}) + \frac{\beta}{2} \|y - z\|^2. \quad (4)$$

Next we will show that, under mild assumptions, both (3) and (4) admit a unique minimizer for each x in a bounded set, and the solution map $x \mapsto \hat{y}(x)$ is *locally Lipschitz*. Hence the reconstruction target falls within Assumption 2.2 and is covered by our expressivity results in Section 2.

Assumption 3.1. Let $\mathbb{M} \subset \mathbb{R}^n$ be a compact, \mathcal{C}^2 , embedded (possibly nonconvex) submanifold with positive reach $\tau > 0$. Assume the forward operator $\mathbf{A} : \mathbb{R}^n \rightarrow \mathbb{R}^d$ is (μ, L) -bi-Lipschitz when restricted to \mathbb{M} and let σ_{\max} denote the maximal singular value of \mathbf{A} .

These assumptions are modest: they are standard in prior work and supported by existing theory. Formal definitions (reach and bi-Lipschitz continuity) and relevant literature appear in Appendix C.

Definition 3.2. Define the admissible set of observations x for (3) and (4):

$$\mathbb{X} := \left\{ x : x = \mathbf{A}y_* + \mathbf{n}, \quad \text{for some } y_* \in \mathbb{M}, \quad \|\mathbf{n}\| < \frac{1}{80} \frac{\mu^5}{\sigma_{\max}^2 L^2} \tau. \right\}$$

Theorem 3.3. Under Assumption 3.1, there exists $\alpha > 0$ for all $x \in \mathbb{X}$ such that the minimization problem (3) yields a unique minimizer \hat{y} . Let $\mathcal{F}_{1a} : x \mapsto \hat{y}$ denote the associated solution map from input x to the recovery \hat{y} . Then \mathcal{F}_{1a} is locally Lipschitz continuous on \mathbb{X} .

Theorem 3.4. Under Assumption 3.1, there exist $\alpha, \beta > 0$ for all $\mathbf{x} \in \mathbb{X}$ such that the minimization problem (4) yields a unique minimizer $(\hat{\mathbf{y}}, \hat{\mathbf{z}})$. Let $\mathcal{F}_{1b}: \mathbf{x} \mapsto \hat{\mathbf{y}}$ denote the associated solution map from input \mathbf{x} to the recovery $\hat{\mathbf{y}}$. Then \mathcal{F}_{1b} is locally Lipschitz continuous on \mathbb{X} .

Corollary 3.5. There must be a regular implicit operator $\mathcal{G}(\mathbf{y}, \mathbf{x})$ such that $\text{Fix}(\mathcal{G}(\cdot, \mathbf{x})) = \mathcal{F}_{1a}(\mathbf{x})$ for all $\mathbf{x} \in \mathbb{X}$. The same conclusion holds for $\mathcal{F}_{1b}(\mathbf{x})$.

Proofs of the theorems are deferred to Appendix C, and Corollary 3.5 follows immediately from Theorems 2.4, 3.3, and 3.4. This corollary guarantees the existence of regular implicit models \mathcal{G} for image reconstruction. Next, we present how to implement \mathcal{G} in this context.

Problem-specific \mathcal{G} . We adopt *algorithm-inspired* designs that mirror classical solvers for (3) and (4). Parameterizing these iterative solvers gives problem-tailored implicit models. In particular,

- Option I (PGD-style). To solve (3), if \mathbb{M} were known, one would use proximal gradient descent (PGD): $\mathbf{y}_{t+1} = \text{prox}_\sigma(\mathbf{y}_t - \gamma \mathbf{A}^\top(\mathbf{A}\mathbf{y}_t - \mathbf{x}))$, with parameters $\sigma, \gamma > 0$, where prox_σ is the proximal map of $(\sigma/2)\text{dist}^2(\mathbf{y}, \mathbb{M})$ (see Appendix C.1). In practice, we replace prox_σ by a learnable neural network denoiser $\mathcal{H}_{\theta, \sigma}$ (parameters θ and noise level input σ) and obtain

$$\mathcal{G}_\Theta(\mathbf{y}, \mathbf{x}) = \mathcal{H}_{\theta, \sigma}(\mathbf{y} - \gamma \mathbf{A}^\top(\mathbf{A}\mathbf{y} - \mathbf{x})), \quad \Theta = \{\theta, \sigma, \gamma\}. \quad (5)$$

- Option II (HQS-style). For (4), a standard solver is half-quadratic splitting (HQS, see Appendix C.2). Similar to Option I, we replace the proximal map by a learned module and obtain

$$\mathcal{G}_\Theta(\mathbf{y}, \mathbf{x}) = \mathcal{H}_{\theta, \sigma}((\mathbf{A}^\top \mathbf{A} + \beta \mathbf{I})^{-1}(\mathbf{A}^\top \mathbf{x} + \beta \mathbf{y})), \quad \Theta = \{\theta, \sigma, \beta\}. \quad (6)$$

Here we follow the long-standing “plug-in denoiser” idea from Plug-and-Play (PnP) methods (Venkatakrishnan et al., 2013), which replaces a proximal operator with an off-the-shelf denoiser inside an iterative solver (see brief bibliography in Appendix C.2). Unlike PnP, one can also train the *entire* \mathcal{G}_Θ as an implicit model, in both PGD-style (Gilton et al., 2021; Winston & Kolter, 2020; Zou et al., 2023; Yu & Dansereau, 2024; Daniele et al., 2025; Shenoy et al., 2025) and HQS-style (Gkillas et al., 2023) formulations. We adopt the latter.

Questions. Given the parameterizations in (5) and (6), we examine: (i) are these \mathcal{G}_Θ operators Lipschitz with respect to \mathbf{x} ; and (ii) do they, as our theory predicts, realize progressively more complex input–output mappings over iterations despite having simple per-iteration operators?

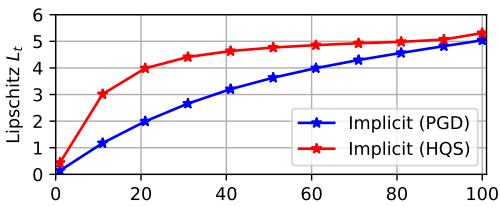
Experiment settings. We study image deblurring, $\mathbf{x} = \mathbf{A}(\mathbf{y}_*) + \mathbf{n}$, where \mathbf{A} is a motion-blur operator and \mathbf{n} is additive Gaussian noise. Using BSDS500 (Martin et al., 2001), we construct 200 training, 100 validation, and 200 test pairs $(\mathbf{x}, \mathbf{y}_*)$, yielding datasets $\mathbb{D}_{\text{inv,train}}$, $\mathbb{D}_{\text{inv,valid}}$, and $\mathbb{D}_{\text{inv,test}}$. Implementation details (data preprocessing, model choices, and training) are in Appendix G.

For evaluation, we analyze 100 iterations of the learned dynamics, $\mathbf{y}_{t+1}(\mathbf{x}) = \mathcal{G}_\Theta(\mathbf{y}_t(\mathbf{x}), \mathbf{x})$, $0 \leq t \leq 99$ and $\mathbf{y}_0 = \mathbf{0}$, on the test set $\mathbb{D}_{\text{inv,test}} = \{(\mathbf{x}_i, \mathbf{y}_i^*)\}_{i=1}^{200}$. For each i , we create 5 perturbed ground truths $\mathbf{y}_{i,j}^*$, $1 \leq j \leq 5$, and for each $\mathbf{y}_{i,j}^*$, we apply \mathbf{A} , add noise, and then obtain $\mathbf{x}_{i,j}$. The perturbed pairs $\{(\mathbf{x}_{i,j}, \mathbf{y}_{i,j}^*)\}_{i,j}$ form the perturbed dataset $\mathbb{D}'_{\text{inv,test}}$. Details appear in Appendix G. We track two metrics, including an empirical Lipschitz estimate and reconstruction quality in PSNR (i.e., Peak Signal-to-Noise Ratio, higher PSNR means more accurate reconstruction, see appendix):

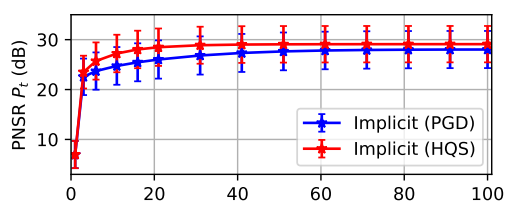
$$L_t := \max_{1 \leq i \leq 200} \max_{1 \leq j \leq 5} \frac{\|\mathbf{y}_t(\mathbf{x}_i) - \mathbf{y}_t(\mathbf{x}_{i,j})\|}{\|\mathbf{x}_i - \mathbf{x}_{i,j}\|}, \quad \text{and} \quad P_t(i, j) := \text{PSNR}(\mathbf{y}_t(\mathbf{x}_{i,j}), \mathbf{y}_{i,j}^*),$$

for $1 \leq i \leq 200$, $0 \leq j \leq 5$, where $j = 0$ means the original (unperturbed) sample, $\mathbf{x}_{i,0} := \mathbf{x}_i$, $\mathbf{y}_{i,0}^* := \mathbf{y}_i^*$. Here, L_t estimates how complex the t -th iterate map $\mathbf{y}_t(\cdot)$ is, while P_t measures the reconstruction quality on *both* the original dataset $\mathbb{D}_{\text{inv,test}}$ and the perturbed set $\mathbb{D}'_{\text{inv,test}}$.

Experiment results. (i) Results in Figure 2 support our theory. Figure 2a plots L_t versus t , while Figure 2b reports the mean \pm std of $\{P_t(i, j)\}_{i,j}$ versus t . At $t = 1$, the mapping $\mathbf{y}_1(\mathbf{x}) = \mathcal{G}_\Theta(\mathbf{0}, \mathbf{x})$ reflects a *single application* of \mathcal{G}_Θ and exhibits low Lipschitz constant: $L_1 = 0.140$ for PGD and $L_1 = 0.436$ for HQS. As t increases, \mathbf{y}_t approaches the fixed point and L_t grows substantially, saturating around ≈ 5.0 for both models (Figure 2a). Meanwhile, the PSNR rises and stabilizes, indicating that $\mathbf{y}_t(\mathbf{x})$ converges toward the ground truth (Figure 2b). Thus, the increase in L_t does not reflect divergence or instability; rather, it captures the greater complexity of the underlying target mapping $\mathbf{x} \mapsto \mathbf{y}_*$, which is progressively expressed through iteration. (ii) We also provide a comparison (both visually and quantitatively) to an explicit model in Figure 3. This baseline uses the identical DRUNet and is trained on the deblurring dataset with an end-to-end MSE loss. A visual inspection reveals that implicit models, particularly implicit HQS (6), produce sharper images with



(a) Empirical Lipschitz L_t of $\mathbf{y}_t(\cdot)$ vs. iteration. L_t starts small at $t=1$ and grows to a plateau (~ 5), indicating increasing expressivity of $\mathbf{y}_t(\cdot)$.



(b) Reconstruction quality P_t (mean \pm std over the original and perturbed test samples) increases and stabilizes: $\mathbf{y}_t(\mathbf{x})$ converges toward the truth.

Figure 2: Validation on image deblurring. Iterating a simple operator \mathcal{G}_Θ produces a complex fixed-point mapping: Lipschitz (a) grows, while accuracy (b) improves and stabilizes.



Figure 3: Visual results for deblurring. The top PSNR values (28.49, 30.03, or 31.53 dB) correspond to the single visualized image; the second line shows the average (\pm std) over all test samples.

better-recovered textures and fewer artifacts than the explicit baseline. This perceptual advantage is corroborated by the quantitative metrics, where the DEQ-HQS model achieves a significant PSNR gain of over 2dB on average across the entire test set. *(iii)* Additional experiments showing a small implicit model outperforming larger explicit ones appear in Appendix G.

3.2 CASE STUDY 2: SCIENTIFIC COMPUTING

The Navier-Stokes (NS) equations are foundational to computational fluid dynamics. We focus on the 2D steady-state incompressible case on a periodic domain $\Omega := [0, 2\pi]^2$:

$$(u \cdot \nabla)u + \nabla p = \nu \Delta u + f, \quad \nabla \cdot u = 0 \quad \text{on } \Omega \quad (7)$$

where $u : \Omega \rightarrow \mathbb{R}^2$ is the velocity field, $p : \Omega \rightarrow \mathbb{R}$ is the pressure, $\nu > 0$ is the viscosity, $f : \Omega \rightarrow \mathbb{R}^2$ is the external force. Solving NS equations refers to determining u given f . Although global existence/smoothness of the solution given general forcings is famously open, classical results guarantee well-posedness under suitable conditions on f .

Theorem 3.6 (Temam (1995)). *There exists a constant $c > 0$ depending only on Ω such that, if $\|f\|_{L^2(\Omega)} \leq c\nu^2$, then (7) admits a unique solution $u_*(f)$. Let \mathbb{H} denote the space of admissible forcings¹, and set $\mathbb{B}_\nu := \{f \in \mathbb{H} : \|f\|_{L^2(\Omega)} \leq c\nu^2\}$. Then there exists a subset $\mathbb{H}_\nu \subset \mathbb{B}_\nu$ that is dense in \mathbb{B}_ν , on which the solution map $f \mapsto u_*(f)$ is locally Lipschitz.*

Vorticity form. Let $\omega := \nabla \times u$ (and hence $\omega_* := \nabla \times u_*$). Under periodic boundary and zero-mean conditions, one can recover the velocity u from vorticity ω by solving a Poisson equation (Majda et al., 2002). We hence focus on the solution map in vorticity: $f \mapsto \omega_*$.

While Theorem 3.6 gives a local Lipschitz result in function spaces, our expressivity results (Section 2) are stated for finite-dimensional spaces. To bridge this gap, we discretize the NS equations.

Discretization. Partition Ω into N_h cells $\Omega_h := \{C_i\}_{i=1}^{N_h}$ and define the cell-average restriction $\mathcal{R}_h(f)|_C := \frac{1}{|C|} \int_C f(\xi) d\xi$ (similarly for ω). We work with the discrete forcings and vorticities:

$$\mathbf{x} := \mathcal{R}_h(f) \in \mathbb{R}^{N_h \times 2}, \quad \mathbf{y} := \mathcal{R}_h(\omega) \in \mathbb{R}^{N_h}$$

and aim to learn $\mathbf{x} \mapsto \mathbf{y}_*$ where $\mathbf{y}_* := \mathcal{R}_h(\omega_*)$ is the discrete solution in vorticity form. Back to the continuum setting, let the lifting operator \mathcal{E}_h be the piecewise-constant reconstruction $\mathcal{E}_h(\mathbf{x}) := \sum_{C \in \Omega_h} x_C \mathbf{1}_C$, and let \mathcal{P} be the orthogonal projection onto divergence-free, zero-mean fields.

¹Details regarding the function spaces are provided in Appendix D.

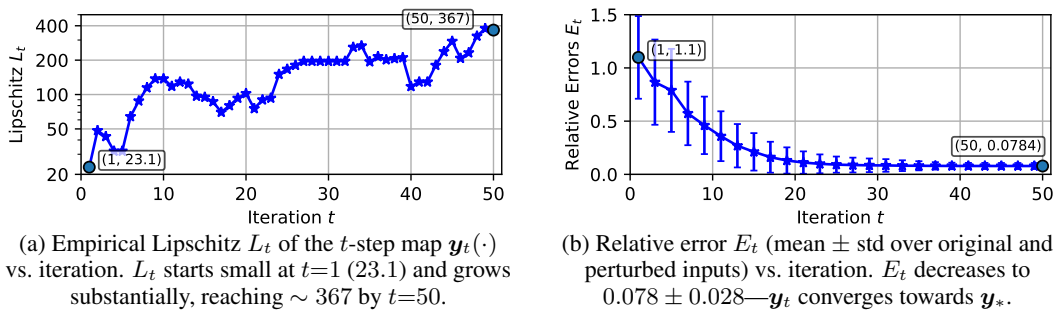


Figure 4: Validation on the steady Navier–Stokes task. Iterating a simple operator \mathcal{G}_Θ yields a complex fixed-point mapping: Lipschitz constant (a) increases, while error (b) decreases.

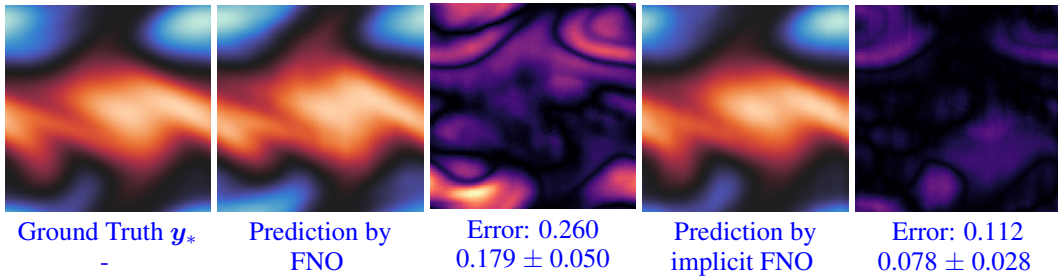


Figure 5: Visual results for NS equations. The top value (0.260 and 0.112) means the relative error (between the prediction and the ground truth) on the single visualized sample; the second line shows the average relative error (\pm std) over all test samples. Both models have 2.376 M parameters.

Corollary 3.7. $\mathcal{F}_2 : \mathbf{x} \mapsto \mathbf{y}_*$ is locally Lipschitz on $\mathbb{X}_{\nu,h} := \{\mathbf{x} \in \mathbb{R}^{N_h \times 2} : \mathcal{P}(\mathcal{E}_h(\mathbf{x})) \in \mathbb{H}_\nu\}$ and there exists a regular implicit operator $\mathcal{G}(\mathbf{y}, \mathbf{x})$ satisfying $\text{Fix}(\mathcal{G}(\cdot, \mathbf{x})) = \mathcal{F}_2(\mathbf{x})$ on $\mathbb{X}_{\nu,h}$.

The corollary instantiates our expressivity theory for steady-state NS, guaranteeing the existence of a *regular* implicit model \mathcal{G} . As in the image–reconstruction case, we now (i) choose a problem-specific parameterization of \mathcal{G} and (ii) verify our theory numerically on this architecture.

Problem-tailored parameterization. We use Marwah et al. (2023) as our code base. In particular,

$$\mathbf{z}_* = \mathcal{G}_\Theta(\mathbf{z}_*, \mathcal{Q}_\Phi(\mathbf{x})), \quad \mathbf{y}_* = \mathcal{Q}_\Psi(\mathbf{z}_*).$$

The core \mathcal{G}_Θ is implemented as a Fourier Neural Operator (FNO) (Li et al., 2021), and both the encoder \mathcal{Q}_Φ and decoder \mathcal{Q}_Ψ use pointwise MLPs². Details appear in Appendix H.

Experiments. We use the dataset of Marwah et al. (2023) with viscosity $\nu = 0.01$, which provides 4500 training pairs and 500 test pairs $(\mathbf{x}, \mathbf{y}^*)$, where \mathbf{x} is the discretized force and \mathbf{y}^* is the corresponding vorticity; we denote these sets by $\mathbb{D}_{\text{pde,train}}$ and $\mathbb{D}_{\text{pde,test}}$. Details are given in Appendix H.

We test iteration-wise behavior for 50 steps starting from $\mathbf{z}_0 = \mathbf{0}$: $\mathbf{z}_{t+1} = \mathcal{G}_\Theta(\mathbf{z}_t, \mathcal{Q}_\Phi(\mathbf{x}))$ for $0 \leq t \leq 49$, and $\mathbf{y}_t(\mathbf{x}) = \mathcal{Q}_\Psi(\mathbf{z}_t)$. Analogous to the inverse-problem study, we augment the test set with perturbations. For each $(\mathbf{x}_i, \mathbf{y}_i^*) \in \mathbb{D}_{\text{pde,test}}$, we construct 15 perturbed vorticities $\{\mathbf{y}_{i,j}^*\}_{j=1}^{15}$; we then compute compatible forces $\{\mathbf{x}_{i,j}\}_{j=1}^{15}$ by evaluating the NS operator (see Appendix H for details). The perturbed test set is $\mathbb{D}'_{\text{pde,test}} = \{(\mathbf{x}_{i,j}, \mathbf{y}_{i,j}^*) : 1 \leq i \leq 500, 1 \leq j \leq 15\}$. Across iterations we report an empirical Lipschitz estimate L_t and relative reconstruction error E_t :

$$L_t := \max_{1 \leq i \leq 500} \max_{1 \leq j \leq 15} \frac{\|\mathbf{y}_t(\mathbf{x}_i) - \mathbf{y}_t(\mathbf{x}_{i,j})\|}{\|\mathbf{x}_i - \mathbf{x}_{i,j}\|}, \quad \text{and} \quad E_t(i, j) := \frac{\|\mathbf{y}_t(\mathbf{x}_{i,j}) - \mathbf{y}_{i,j}^*\|}{\|\mathbf{y}_{i,j}^*\| + \epsilon},$$

for $1 \leq i \leq 500, 0 \leq j \leq 15$, where $j = 0$ means the original (unperturbed) sample, $\mathbf{x}_{i,0} := \mathbf{x}_i, \mathbf{y}_{i,0}^* := \mathbf{y}_i^*$. Therefore, E_t evaluates accuracy on both $\mathbb{D}_{\text{pde,test}}$ and $\mathbb{D}'_{\text{pde,test}}$.

The results in Figure 4 align with our theory. At $t = 1$, the mapping $\mathbf{y}_1(\mathbf{x})$ reflects a single application of \mathcal{G}_Θ and exhibits low Lipschitz constant: $L_1 = 23.1$. As iterations proceed toward the fixed point, the complexity grows markedly: L_t increases to ≈ 367 by $t = 50$ (Figure 4a). Meanwhile,

²Introducing additional encoder and decoder is common in practice. Compared to the vanilla formulation $\mathbf{y}_* = \mathcal{G}(\mathbf{y}_*, \mathbf{x})$, it does not change our expressivity results in Section 2. Details appear in Appendix B.

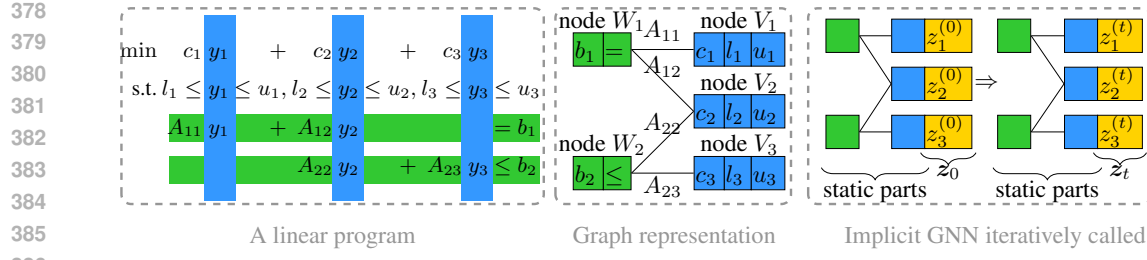


Figure 6: The graph representation of LP and implicit GNN applied on this graph

the relative error E_t decreases monotonically and stabilizes at 0.078 ± 0.028 (Figure 4b), indicating convergence to a good approximation of \mathbf{y}_* . Thus, *the learned operator \mathcal{G}_Θ is simple (Lipschitz in \mathbf{x}), while additional test-time iterations let \mathbf{y}_t realize progressively more complex mappings*. In addition, a comparison with an explicit baseline (vanilla FNO) in Figure 5 shows the implicit model produces more accurate solutions, both visually and quantitatively. Additional experiments showing a small implicit model outperforming larger explicit ones appear in Appendix H.

3.3 CASE STUDY 3: OPERATIONS RESEARCH

Linear program (LP) is fundamental to operations research, of which a general form is given by

$$\min_{\mathbf{y} \in \mathbb{R}^n} \mathbf{c}^\top \mathbf{y}, \quad \text{s.t. } \mathbf{A}\mathbf{y} \circ \mathbf{b}, \quad \mathbf{l} \leq \mathbf{y} \leq \mathbf{u}. \quad (8)$$

Here, $\mathbf{A} \in \mathbb{R}^{m \times n}$, $\mathbf{b} \in \mathbb{R}^m$, $\mathbf{c} \in \mathbb{R}^n$, $\mathbf{l} \in \mathbb{R}^n$, $\mathbf{u} \in \mathbb{R}^n$, and $\circ \in \{=, \leq\}^m$ denotes componentwise relations, i.e., each $\circ_i \in \{=, \leq\}$ specifies whether $(\mathbf{A}\mathbf{y})_i$ equals or is bounded above by b_i . Let $\mathbf{x} := (\mathbf{A}, \mathbf{b}, \mathbf{c}, \circ, \mathbf{l}, \mathbf{u})$ as the input that describes the LP in (8). To define the solution mapping \mathcal{F}_3 that maps \mathbf{x} to the solution of LP, we require feasibility and boundedness (which ensure an optimal solution (Bertsimas & Tsitsiklis, 1997)). Accordingly, let

$$\mathbb{X} := \{(\mathbf{A}, \mathbf{b}, \mathbf{c}, \circ, \mathbf{l}, \mathbf{u}) : \text{The resulting LP is feasible and bounded}\}$$

Within \mathbb{X} , there are some LPs where the solution mapping is not single-valued or not continuous. By excluding these LPs, it forms a subset $\mathbb{X}_{\text{sub}} \subset \mathbb{X}$ on which \mathcal{F}_3 is single-valued and locally Lipschitz. The strict definition of \mathbb{X}_{sub} and the proof of Theorem 3.8 are provided in Appendix E.

Theorem 3.8. *There is a subset $\mathbb{X}_{\text{sub}} \subset \mathbb{X}$ that is dense in \mathbb{X} , on which each LP admits a unique solution \mathbf{y}_* , and the solution map $\mathcal{F}_3 : \mathbf{x} \mapsto \mathbf{y}_*$ is locally Lipschitz continuous on \mathbb{X}_{sub} .*

Corollary 3.9. *There exists a regular implicit model $\mathcal{G}(\mathbf{y}, \mathbf{x})$ with $\text{Fix}(\mathcal{G}(\cdot, \mathbf{x})) = \mathcal{F}_3(\mathbf{x})$ on \mathbb{X}_{sub} .*

Corollary 3.9 follows immediately from Theorems 2.4 and 3.8. It indicates the existence of implicit models with desired properties that solves LP. As in the previous case studies, we now (i) choose a problem-specific parameterization of \mathcal{G} and (ii) verify the theory numerically on this architecture.

Implicit GNN parameterization. We model the implicit operator \mathcal{G} for LP with a *graph neural network (GNN)*. First, express an LP instance $\mathbf{x} = (\mathbf{A}, \mathbf{b}, \mathbf{c}, \circ, \mathbf{l}, \mathbf{u})$ as a bipartite graph (Figure 6). We create n variable nodes $\{V_j\}_{j=1}^n$ and m constraint nodes $\{W_i\}_{i=1}^m$. Node features collect the data of the LP: each V_j stores (c_j, l_j, u_j) ; each W_i stores (b_i, \circ_i) . We connect W_i to V_j if $A_{ij} \neq 0$, and place A_{ij} on that edge as its feature. Given this representation, an (explicit) GNN can map the LP to a solution, i.e., $\mathbf{y}_* = \text{GNN}(\mathbf{x})$ where \mathbf{x} denotes the graph-encoded LP. This approach was proposed in Gasse et al. (2019), and Chen et al. (2023) subsequently showed that (explicit) GNNs offer a universal framework for representing LPs. Built on this, we propose an *implicit GNN*:

$$\mathbf{z}_* = \mathcal{G}_\Theta(\mathbf{z}_*, \mathcal{Q}_\Phi(\mathbf{x})), \quad \mathbf{y}_* = \mathcal{Q}_\Psi(\mathbf{z}_*) \quad (9)$$

where \mathcal{G}_Θ is the core GNN, \mathcal{Q}_Φ encodes instance-specific (static) features from \mathbf{x} , and \mathcal{Q}_Ψ decodes per-variable states to the solution. Both \mathcal{Q}_Φ and \mathcal{Q}_Ψ are small MLPs shared across all nodes. At inference, we repeatedly call \mathcal{G}_Θ with initialization $\mathbf{z}_0 = \mathbf{0}$: $\mathbf{z}_t = \mathcal{G}_\Theta(\mathbf{z}_{t-1}, \mathcal{Q}_\Phi(\mathbf{x}))$ for $t = 1, 2, \dots, T$, and finally output $\mathbf{y}_t = \mathcal{Q}_\Psi(\mathbf{z}_t)$. Relative to prior work, our only modification is to attach to each variable node an additional *dynamic* state $z_j^{(t)} \in \mathbb{R}$. Details appear in Appendix I.

There is a rapidly growing literature on implicit GNNs with diverse applications and theories (Gu et al., 2020; Park et al., 2022; Chen et al., 2022a;b; Baker et al., 2023; Lin et al., 2024; Nastorg et al., 2024; Zhong et al., 2024; Yang et al., 2025). Our LP case study is complementary to this line of work: rather than adopting a particular implicit-GNN architecture, we start from a standard explicit GNN for LP and convert it into a fixed-point formulation tailored to linear programs.

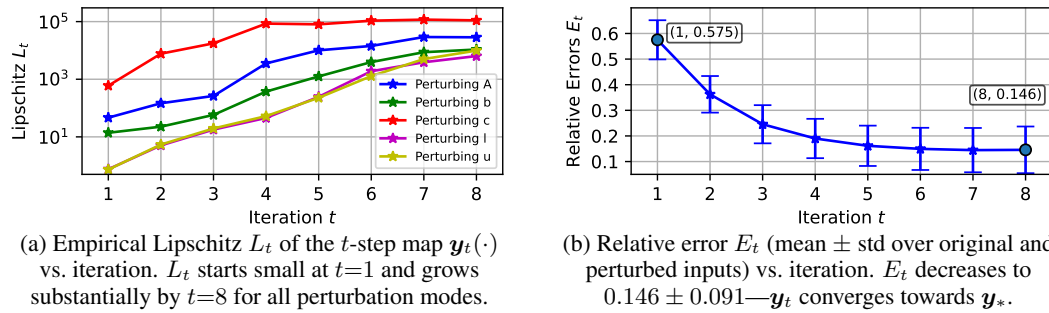


Figure 7: Numerical validation on the linear-program task.

Table 1: Comparison between explicit GNNs and implicit GNNs on the LP task.

	Emb. size	4	8	16	32
Exp-GNNs	# Params.	580	2,088	7,888	30,624
	Err (Train)	0.387 ± 0.103	0.233 ± 0.084	0.183 ± 0.070	0.112 ± 0.049
	Err (Test)	0.397 ± 0.107	0.273 ± 0.104	0.283 ± 0.111	0.318 ± 0.122
	Emb. size	4	8	16	32
Imp-GNNs	# Params.	722	2,350	8,390	31,606
	Err (Train)	0.203 ± 0.107	0.162 ± 0.094	0.131 ± 0.080	0.118 ± 0.073
	Err (Test)	0.218 ± 0.117	0.177 ± 0.105	0.152 ± 0.098	0.156 ± 0.109

Experiments. We sample LP instances $\mathbf{x} = (\mathbf{A}, \mathbf{b}, \mathbf{c}, \circ, \mathbf{l}, \mathbf{u})$, solve it to obtain an optimal solution \mathbf{y}_* , and form 2,500 training pairs and 1,000 test pairs like $(\mathbf{x}, \mathbf{y}_*)$, denoted $\mathbb{D}_{\text{LP,train}}$ and $\mathbb{D}_{\text{LP,test}}$. We also create five perturbed test sets $\{\mathbb{D}_{\text{LP,test}}^{(j)}\}_{j=1}^5$ by altering exactly one block among $(\mathbf{A}, \mathbf{b}, \mathbf{c}, \mathbf{l}$, or $\mathbf{u})$. For each $(\mathbf{x}_i, \mathbf{y}_i^*) \in \mathbb{D}_{\text{LP,test}}$ and each perturbation type j , we form a perturbed instance $\mathbf{x}_{i,j}$, solve it to obtain $\mathbf{y}_{i,j}^*$, and collect $\mathbb{D}_{\text{LP,test}}^{(j)} = \{(\mathbf{x}_{i,j}, \mathbf{y}_{i,j}^*)\}_{i=1}^{1000}$. Details in Appendix I. We report:

$$L_t(j) := \max_{1 \leq i \leq 1000} \frac{\|\mathbf{y}_t(\mathbf{x}_i) - \mathbf{y}_t(\mathbf{x}_{i,j})\|}{\|\mathbf{x}_i - \mathbf{x}_{i,j}\|}, \quad \text{and} \quad E_t(i, j) := \frac{\|\mathbf{y}_t(\mathbf{x}_{i,j}) - \mathbf{y}_{i,j}^*\|}{\|\mathbf{y}_{i,j}^*\| + \epsilon},$$

for $1 \leq i \leq 1000, 0 \leq j \leq 5$, where $j = 0$ denotes the unperturbed pair $(\mathbf{x}_{i,0}, \mathbf{y}_{i,0}^*) := (\mathbf{x}_i, \mathbf{y}_i^*)$.

Results support our theory. (i) Figure 7a plots the five curves $L_t(j)$ (one for each perturbation type). At $t = 1$, a single application of (9) yields relatively small empirical Lipschitz constants for *all* perturbation modes. As iterations proceed toward the fixed point, Lipschitz constants grow markedly. (ii) Figure 7b reports the mean \pm std of $E_t(i, j)$: E_t decreases and stabilizes at 0.146, indicating that the growth of L_t reflects the higher intrinsic complexity of the solution mapping $\mathbf{y}_*(\mathbf{x})$ rather than divergence or instability. (iii) Table 1 contrasts implicit and explicit GNNs. At matched embedding sizes, implicit GNNs match or beat explicit ones—most clearly at small/mid sizes (4/8/16). In addition, a smaller implicit model can outperform a larger explicit model on training error. For example, implicit-4 vs. explicit-8 (0.203 vs. 0.233) and implicit-8 vs. explicit-16 (0.162 vs. 0.183). This supports our theory that iterating a simple implicit operator can yield strong expressivity.

Discussion on generalization. While generalization is not our main focus, a trend in Table 1 is informative: explicit GNNs improve as width increases from 4 to 8 but then *overfit* (test error significantly rises at 16/32), whereas implicit GNNs improve from 4 to 8 to 16 and only tick up slightly at 32. We attribute this to: (i) LP constraints $\mathbf{A}\mathbf{y} \circ \mathbf{b}$ in (8) are specified implicitly rather than as an explicit set; implicit models align naturally with such a structure, and (ii) while fixed-point maps $\mathbf{y}_*(\mathbf{x})$ can be sensitive to inputs \mathbf{x} , the implicit formulation allows us realize them via a simpler, smaller operator \mathcal{G} , which “implicitly” regularizes training and support good generalization in practice.

3.4 CASE STUDY 4: LLM REASONING

While previous case studies focused on domains with strict mathematical definitions (inverse problems, PDEs, LPs), we now investigate if our theory extends to broader applications where metrics like “smoothness” and “Lipschitz continuity” are less formally defined. We examine the looped transformer for LLM reasoning, utilizing the pre-trained model from Geiping et al. (2025). Unlike standard feed-forward transformers, this architecture recycles a shared block \mathcal{G}_Θ to iteratively update a latent “thought” vector \mathbf{z} : $\mathbf{z}_t = \mathcal{G}_\Theta(\mathbf{z}_{t-1}, \mathcal{Q}_\Phi(\mathbf{x}))$, $\mathbf{y}_t = \mathcal{Q}_\Psi(\mathbf{z}_t)$ where \mathcal{Q}_Φ encodes the input \mathbf{x} , and \mathcal{Q}_Ψ decodes the latent state into the output sequence \mathbf{y}_t obtained after t recurrent blocks.

486
487
488
489
490
491
492
493
494
495
496
497
498
499
500
501
502
503
504
505
506
507
508
509
510
511
512
513
514
515
516
517
518
519
520
521
522
523
524
525
526
527
528
529
530
531
532
533
534
535
536
537
538
539

Table 2: Evolution of model outputs for the inputs “charge and voltage” vs. “charge and pay”, showing how the semantic difference emerges over iterations.

Input/Output 1	Input/Output 2	Comments
x : explain the difference between charge and voltage.	x' : explain the difference between charge and pay.	Prompts differ in a <i>single word</i> , but the context shifts from Physics to Finance.
$y_2(x)$: explain the difference between charge and voltage.	$y_2(x')$: explain the difference between charge and pay.	Both outputs merely echo inputs.
$y_4(x)$: explain the difference between charge and voltage. explain the difference between current and voltage.	$y_4(x')$: explain the difference between charge and pay. explain the difference between the two.	Outputs repeat the inputs with slight variations; contexts are not yet separated.
$y_6(x)$: The difference between voltage and charge is that voltage is the difference between the potential difference between two points, while charge is the difference between the electric field between two points.	$y_6(x')$: explain the difference between charge and pay. Explain the difference between charge and pay.	Separation begins: Output 1 moves into a Physics explanation (potential difference), while Output 2 still stays near the prompt.
$y_8(x)$: The difference between charge and voltage is that voltage is the difference in electric potential between two points in an electric field, while charge is the amount of electric charge in a system.	$y_8(x')$: Charge is the amount of money that a person owes to a company or organization. Pay is the amount of money that a person receives from a company or organization.	Full separation: Output 1 gives a Physics definition; Output 2 correctly adopts the Financial interpretation (money owed vs. received).
$y_{32}(x)$: Charge is the amount of electric charge present in a body. Voltage is the difference in electric potential between two points.	$y_{32}(x')$: Charge is the amount of money that a person or company owes to a credit card company. Pay is the amount of money that a person or company has paid to the credit card company.	Refinement: both domains have stable, concise, and accurate definitions specialized to Physics versus Finance.

Strictly extending our Lipschitz theory to the discrete space of language tokens is challenging, as standard norms do not apply. However, we can empirically test the core prediction of our theory: can the model express increasingly complex mappings as iterations increase? In this context, complexity implies: *subtle differences in the input correspond to substantial shifts in context*. A capable model must effectively distinguish these semantic nuances and produce vastly different responses.

Qualitative Results. Table 2 visualizes the evolution of reasoning on a typical example. At early iterations ($t = 2, 4$), the model fails to differentiate context (Physics vs. Finance), producing repetitions or shallow associations. Conversely, with more iterations ($t = 6, 8$ or more), the model utilizes increased test-time compute to resolve this ambiguity, correctly defining “charge” as electric potential versus financial debt. This confirms the implicit operator’s ability to progressively realize complex, context-sensitive mappings.

Quantitative Results. To quantitatively measure this, we define an “Empirical Lipschitz” constant L_t using Levenshtein distance $d(\cdot, \cdot)$:

$$L_t(i) := \frac{d(y_t(x_i), y_t(x'_i))}{d(x_i, x'_i)}$$

We construct $\{(x_i, x'_i)\}_{i=1}^{200}$, a dataset of 200 pairs where inputs differ by only 1–2 words but require vastly different semantic contexts³. Figure 8 plots the geometric mean of L_t , which rises from ≈ 29.2 at $t = 2$ (indicating relative insensitivity) to saturate at ≈ 52.5 by $t = 16$. The model’s emergent capacity to map proximal inputs to semantically distinct outputs. Even in the discrete domain of language reasoning, iterating a fixed operator allows the model to scale its expressive power, evolving from simple surface-level processing to complex, context-aware reasoning.

4 CONCLUSIONS AND FUTURE DIRECTIONS

We have provided a strict characterization of the representational capacity of regular implicit models. Our analysis reveals that iterating a simple operator allows the model to progressively realize increasingly complex mappings, ultimately covering the entire class of locally Lipschitz functions. This theory is validated through four diverse case studies, showing that the empirical Lipschitz constant rises alongside solution quality. A key direction for future work is to quantify the precise rate of this Lipschitz growth to inform optimal test-time iteration heuristics.

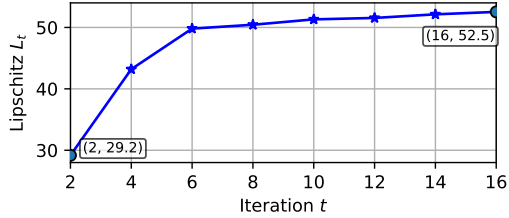


Figure 8: Empirical Lipschitz of the output sequence $y_t(\cdot)$ generated by Geiping et al. (2025) using t recurrent blocks. L_t grows as t increases.

Consistent with our theory, this growth reflects the model’s emergent capacity to map proximal inputs to semantically distinct outputs. Even in the discrete domain of language reasoning, iterating a fixed operator allows the model to scale its expressive power, evolving from simple surface-level processing to complex, context-aware reasoning.

³ Available at: https://anonymous.4open.science/r/semantic_contrast_pairs-4F4F/semantic_contrast_pairs_200.csv

540 REFERENCES
541

542 Eddie Aamari, Jisu Kim, Frédéric Chazal, Bertrand Michel, Alessandro Rinaldo, and Larry Wasser-
543 man. Estimating the reach of a manifold. *Electronic Journal of Statistics*, 13(1):1359–1399,
544 2019.

545 Iskander Azangulov, George Deligiannidis, and Judith Rousseau. Convergence of diffusion models
546 under the manifold hypothesis in high-dimensions. *arXiv preprint arXiv:2409.18804*, 2024.

547 Shaojie Bai, J Zico Kolter, and Vladlen Koltun. Deep equilibrium models. *Advances in Neural
548 Information Processing Systems*, 32, 2019.

549 550 Justin Baker, Qingsong Wang, Cory D Hauck, and Bao Wang. Implicit graph neural networks: A
551 monotone operator viewpoint. In *International Conference on Machine Learning*, pp. 1521–1548.
552 PMLR, 2023.

553 Richard G Baraniuk and Michael B Wakin. Random projections of smooth manifolds. *Foundations
554 of computational mathematics*, 9(1):51–77, 2009.

555 556 Pierfrancesco Beneventano, Patrick Cheridito, Robin Graeber, Arnulf Jentzen, and Benno Kuck-
557 uck. Deep neural network approximation theory for high-dimensional functions. *arXiv preprint
558 arXiv:2112.14523*, 2021.

559 Dimitris Bertsimas and John N Tsitsiklis. *Introduction to linear optimization*, volume 6. Athena
560 scientific Belmont, MA, 1997.

561 562 Stephen P Boyd and Lieven Vandenberghe. *Convex optimization*. Cambridge university press, 2004.

563 Gregery T Buzzard, Stanley H Chan, Suhas Sreehari, and Charles A Bouman. Plug-and-play un-
564 plugged: Optimization-free reconstruction using consensus equilibrium. *SIAM Journal on Imag-
565 ing Sciences*, 11(3):2001–2020, 2018.

566 567 Emmanuel J Candes and Terence Tao. Near-optimal signal recovery from random projections: Uni-
568 versal encoding strategies? *IEEE Transactions on Information Theory*, 52(12):5406–5425, 2006.

569 Stanley H Chan, Xiran Wang, and Omar A Elgendy. Plug-and-play ADMM for image restoration:
570 Fixed-point convergence and applications. *IEEE Transactions on Computational Imaging*, 3(1):
571 84–98, 2016.

572 573 Qi Chen, Yifei Wang, Yisen Wang, Jianlong Chang, Qi Tian, Jiansheng Yang, and Zhouchen Lin.
574 Efficient and scalable implicit graph neural networks with virtual equilibrium. In *IEEE Interna-
575 tional Conference on Big Data (Big Data)*, pp. 864–873. IEEE, 2022a.

576 577 Qi Chen, Yifei Wang, Yisen Wang, Jiansheng Yang, and Zhouchen Lin. Optimization-induced graph
578 implicit nonlinear diffusion. In *International Conference on Machine Learning*, pp. 3648–3661.
PMLR, 2022b.

579 Tianlong Chen, Weiyi Zhang, Zhou Jingyang, Shiyu Chang, Sijia Liu, Lisa Amini, and Zhangyang
580 Wang. Training stronger baselines for learning to optimize. *Advances in Neural Information
581 Processing Systems*, 33:7332–7343, 2020.

582 583 Tianlong Chen, Xiaohan Chen, Wuyang Chen, Howard Heaton, Jialin Liu, Zhangyang Wang, and
584 Wotao Yin. Learning to optimize: A primer and a benchmark. *Journal of Machine Learning
585 Research*, 23(189):1–59, 2022c.

586 587 Xiaohan Chen, Jialin Liu, Zhangyang Wang, and Wotao Yin. Theoretical linear convergence of un-
588 folded ISTA and its practical weights and thresholds. *Advances in Neural Information Processing
589 Systems*, 31, 2018.

590 591 Ziang Chen, Jialin Liu, Xinshang Wang, and Wotao Yin. On representing Linear Programs by
592 Graph Neural Networks. In *International Conference on Learning Representations*, 2023. URL
<https://openreview.net/forum?id=cP2QVK-uygd>.

593 Kenneth L Clarkson. Tighter bounds for random projections of manifolds. In *Proceedings of the
Twenty-Fourth Annual Symposium on Computational Geometry*, pp. 39–48, 2008.

594 Christian Daniele, Silvia Villa, Samuel Vaiter, and Luca Calatroni. Deep equilibrium models for
 595 Poisson imaging inverse problems via Mirror Descent. *arXiv preprint arXiv:2507.11461*, 2025.
 596

597 Manfredo P Do Carmo. *Differential geometry of curves and surfaces: revised and updated second*
 598 *edition*. Courier Dover Publications, 2016.

599 David L Donoho and Carrie Grimes. Image manifolds which are isometric to Euclidean space.
 600 *Journal of Mathematical Imaging and Vision*, 23(1):5–24, 2005.
 601

602 Asen L Dontchev and R Tyrrell Rockafellar. Characterizations of strong regularity for variational
 603 inequalities over polyhedral convex sets. *SIAM Journal on Optimization*, 6(4):1087–1105, 1996.

604 Asen L Dontchev and R Tyrrell Rockafellar. *Implicit functions and solution mappings*, volume 543.
 605 Springer, 2009.

606 Laurent El Ghaoui, Fangda Gu, Bertrand Travacca, Armin Askari, and Alicia Tsai. Implicit deep
 607 learning. *SIAM Journal on Mathematics of Data Science*, 3(3):930–958, 2021.

608 Herbert Federer. Curvature measures. *Transactions of the American Mathematical Society*, 93(3):
 609 418–491, 1959.

610 Zhili Feng and J Zico Kolter. On the Neural Tangent Kernel of equilibrium models. *arXiv preprint*
 611 *arXiv:2310.14062*, 2023.

612 Gerald B. Folland. *Advanced Calculus*. University of Washington, Seattle, WA, 2nd edition, 2023.
 613 Freely available at <https://sites.math.washington.edu/~folland/AdvCalc/>.

614 Samy Wu Fung and Benjamin Berkels. A generalization bound for a family of implicit networks.
 615 *arXiv preprint arXiv:2410.07427*, 2024.

616 Samy Wu Fung, Howard Heaton, Qiuwei Li, Daniel McKenzie, Stanley Osher, and Wotao Yin. JFB:
 617 Jacobian-free backpropagation for implicit networks. In *Proceedings of the AAAI Conference on*
 618 *Artificial Intelligence*, 2022.

619 Tianxiang Gao, Hailiang Liu, Jia Liu, Hridesh Rajan, and Hongyang Gao. A global convergence
 620 theory for deep ReLU implicit networks via over-parameterization. In *International Conference on*
 621 *Learning Representations*, 2022. URL <https://openreview.net/forum?id=R332S76Rjxs>.

622 Maxime Gasse, Didier Chételat, Nicola Ferroni, Laurent Charlin, and Andrea Lodi. Exact combi-
 623 natorial optimization with graph convolutional neural networks. *Advances in Neural Information*
 624 *Processing Systems*, 32, 2019.

625 Ruraj Gavaskar and Kunal N Chaudhury. Plug-and-play ISTA converges with kernel denoisers.
 626 *IEEE Signal Processing Letters*, 27:610–614, 2020.

627 Jonas Geiping, Sean McLeish, Neel Jain, John Kirchenbauer, Siddharth Singh, Brian R Bartoldson,
 628 Bhavya Kailkhura, Abhinav Bhatele, and Tom Goldstein. Scaling up test-time compute with
 629 latent reasoning: A recurrent depth approach. *arXiv preprint arXiv:2502.05171*, 2025.

630 Zhengyang Geng, Xin-Yu Zhang, Shaojie Bai, Yisen Wang, and Zhouchen Lin. On training implicit
 631 models. *Advances in Neural Information Processing Systems*, 34:24247–24260, 2021.

632 Zhengyang Geng, Ashwini Pokle, and J Zico Kolter. One-step diffusion distillation via deep equi-
 633 librium models. *Advances in Neural Information Processing Systems*, 36:41914–41931, 2023.

634 Davis Gilton, Gregory Ongie, and Rebecca Willett. Deep equilibrium architectures for inverse
 635 problems in imaging. *IEEE Transactions on Computational Imaging*, 7:1123–1133, 2021.

636 Alexandros Gkillas, Dimitris Ampeliotis, and Kostas Berberidis. An optimization-based Deep
 637 Equilibrium Model for hyperspectral image deconvolution with convergence guarantees. *arXiv*
 638 *preprint arXiv:2306.06378*, 2023.

639 Fangda Gu, Heng Chang, Wenwu Zhu, Somayeh Sojoudi, and Laurent El Ghaoui. Implicit graph
 640 neural networks. *Advances in Neural Information Processing Systems*, 33:11984–11995, 2020.

648 Alper Güngör, Baris Askin, Damla Alptekin Soydan, Can Barış Top, Emine Ulku Saritas, and Tolga
 649 Cukur. DEQ-MPI: A deep equilibrium reconstruction with learned consistency for magnetic
 650 particle imaging. *IEEE Transactions on Medical Imaging*, 43(1):321–334, 2023.

651

652 Aaron Havens, Alexandre Araujo, Siddharth Garg, Farshad Khorrami, and Bin Hu. Exploiting
 653 connections between Lipschitz structures for certifiably robust deep equilibrium models. *Advances
 654 in Neural Information Processing Systems*, 36:21658–21674, 2023.

655

656 Chinmay Hegde and Richard G Baraniuk. Signal recovery on incoherent manifolds. *IEEE Transac-
 657 tions on Information Theory*, 58(12):7204–7214, 2012.

658

659 Samuel Hurault, Arthur Leclaire, and Nicolas Papadakis. Gradient step denoiser for convergent
 660 Plug-and-Play. In *International Conference on Learning Representations*, 2022a. URL <https://openreview.net/forum?id=fPhKeld3Okz>.

661

662 Samuel Hurault, Arthur Leclaire, and Nicolas Papadakis. Proximal denoiser for convergent plug-
 663 and-play optimization with nonconvex regularization. In *International Conference on Machine
 664 Learning*, pp. 9483–9505. PMLR, 2022b.

665

666 Mark A Iwen and Mauro Maggioni. Approximation of points on low-dimensional manifolds via
 667 random linear projections. *Information and Inference: A Journal of the IMA*, 2(1):1–31, 2013.

668

669 Saber Jafarpour, Alexander Davydov, Anton Proskurnikov, and Francesco Bullo. Robust implicit
 670 networks via non-Euclidean contractions. *Advances in Neural Information Processing Systems*,
 34:9857–9868, 2021.

671

672 Ulugbek S Kamilov, Hassan Mansour, and Brendt Wohlberg. A plug-and-play priors approach for
 673 solving nonlinear imaging inverse problems. *IEEE Signal Processing Letters*, 24(12):1872–1876,
 2017.

674

675 Ulugbek S Kamilov, Charles A Bouman, Gregery T Buzzard, and Brendt Wohlberg. Plug-and-
 676 play methods for integrating physical and learned models in computational imaging: Theory,
 677 algorithms, and applications. *IEEE Signal Processing Magazine*, 40(1):85–97, 2023.

678

679 Gunther Leobacher and Alexander Steinicke. Existence, uniqueness and regularity of the projection
 680 onto differentiable manifolds. *Annals of global analysis and geometry*, 60(3):559–587, 2021.

681

682 Anat Levin, Yair Weiss, Frédo Durand, and William T. Freeman. Understanding and evaluating
 683 Blind Deconvolution algorithms. In *IEEE Conference on Computer Vision and Pattern Recog-
 684 nition (CVPR)*, pp. 1964–1971, 2009. doi: 10.1109/CVPR.2009.5206815.

685

686 Zongyi Li, Nikola Borislavov Kovachki, Kamyar Azizzadenesheli, Burigede liu, Kaushik Bhat-
 687 tacharya, Andrew Stuart, and Anima Anandkumar. Fourier Neural Operator for parametric par-
 688 tial differential equations. In *International Conference on Learning Representations*, 2021. URL
 689 <https://openreview.net/forum?id=c8P9NQVtmnO>.

690

691 Junchao Lin, Zenan Ling, Zhanbo Feng, Jingwen Xu, Minxuan Liao, Feng Zhou, Tianqi Hou,
 692 Zhenyu Liao, and Robert C Qiu. IGNN-Solver: A graph neural solver for Implicit Graph Neural
 693 Networks. *arXiv preprint arXiv:2410.08524*, 2024.

694

695 Zenan Ling, Xingyu Xie, Qiuhan Wang, Zongpeng Zhang, and Zhouchen Lin. Global convergence
 696 of over-parameterized deep equilibrium models. In *International Conference on Artificial Intelli-
 697 gence and Statistics*, pp. 767–787. PMLR, 2023.

698

699 Zenan Ling, Longbo Li, Zhanbo Feng, Yixuan Zhang, Feng Zhou, Robert C Qiu, and Zhenyu
 700 Liao. Deep Equilibrium Models are almost equivalent to not-so-deep explicit models for high-
 701 dimensional Gaussian mixtures. In *International Conference on Machine Learning*, pp. 30585–
 30609. PMLR, 2024.

702

703 Jialin Liu, Xiaohan Chen, Zhangyang Wang, and Wotao Yin. ALISTA: Analytic weights are as good
 704 as learned weights in LISTA. In *International Conference on Learning Representations*, 2019.

702 Jiaming Liu, Salman Asif, Brendt Wohlberg, and Ulugbek Kamilov. Recovery analysis for plug-and-
 703 play priors using the restricted eigenvalue condition. *Advances in Neural Information Processing*
 704 *Systems*, 34:5921–5933, 2021.

705 Andrew J Majda, Andrea L Bertozzi, and A Ogawa. Vorticity and incompressible flow. cambridge
 706 texts in applied mathematics. *Appl. Mech. Rev.*, 55(4):B77–B78, 2002.

708 Olvi L Mangasarian and T-H Shiau. Lipschitz continuity of solutions of linear inequalities, programs
 709 and complementarity problems. *SIAM Journal on Control and Optimization*, 25(3):583–595,
 710 1987.

711 D. Martin, C. Fowlkes, D. Tal, and J. Malik. A database of human segmented natural images and its
 712 application to evaluating segmentation algorithms and measuring ecological statistics. In *IEEE*
 713 *International Conference on Computer Vision (ICCV)*, volume 2, pp. 416–423, July 2001.

714 Tanya Marwah, Ashwini Pokle, J Zico Kolter, Zachary Lipton, Jianfeng Lu, and Andrej Risteski.
 715 Deep equilibrium based neural operators for steady-state PDEs. *Advances in Neural Information*
 716 *Processing Systems*, 36:15716–15737, 2023.

718 Takeru Miyato, Toshiki Kataoka, Masanori Koyama, and Yuichi Yoshida. Spectral normalization
 719 for Generative Adversarial Networks. In *International Conference on Learning Representations*,
 720 2018. URL <https://openreview.net/forum?id=B1QRgziT->.

721 Davide Murari, Takashi Furuya, and Carola-Bibiane Schönlieb. Approximation theory for 1-
 722 lipschitz resnets. *arXiv preprint arXiv:2505.12003*, 2025.

724 Florent Nacry and Lionel Thibault. Distance function associated to a prox-regular set. *Set-Valued*
 725 *and Variational Analysis*, pp. 1–20, 2022.

726 Matthieu Nastorg, Michele-Alessandro Bucci, Thibault Faney, Jean-Marc Gratien, Guillaume
 727 Charpiat, and Marc Schoenauer. An implicit GNN solver for Poisson-like problems. *Computers*
 728 *& Mathematics with Applications*, 176:270–288, 2024.

730 Alex Oshin, Hassan Almubarak, and Evangelos A. Theodorou. Differentiable Robust Model
 731 Predictive Control. In *Robotics: Science and Systems (RSS)*, 2024. URL <https://roboticsconference.org/2024/program/papers/3/>.

733 Chirag Pabbaraju, Ezra Winston, and J Zico Kolter. Estimating Lipschitz constants of monotone
 734 deep equilibrium models. In *International Conference on Learning Representations*, 2021.

736 Junyoung Park, Jinyun Choo, and Jinkyoo Park. Convergent graph solvers. In *International Conference on Learning Representations*, 2022. URL <https://openreview.net/forum?id=ItkxLQU011D>.

739 Ashwini Pokle, Zhengyang Geng, and J Zico Kolter. Deep equilibrium approaches to diffusion
 740 models. *Advances in Neural Information Processing Systems*, 35:37975–37990, 2022.

741 René Poliquin, R Rockafellar, and Lionel Thibault. Local differentiability of distance functions.
 742 *Transactions of the American mathematical Society*, 352(11):5231–5249, 2000.

744 Peter Potaptchik, Iskander Azangulov, and George Deligiannidis. Linear convergence of diffusion
 745 models under the manifold hypothesis. *arXiv preprint arXiv:2410.09046*, 2024.

747 Arash Rasti-Meymandi, Aboozar Ghaffari, and Emad Fatemizadeh. Plug and play augmented HQS:
 748 Convergence analysis and its application in MRI reconstruction. *Neurocomputing*, 518:1–14,
 749 2023.

750 Max Revay, Ruigang Wang, and Ian R Manchester. Lipschitz bounded equilibrium networks. *arXiv*
 751 *preprint arXiv:2010.01732*, 2020.

752 Stephen M Robinson. Strongly regular generalized equations. *Mathematics of Operations Research*,
 753 5(1):43–62, 1980.

755 Sam T Roweis and Lawrence K Saul. Nonlinear dimensionality reduction by locally linear embed-
 756 ding. *Science*, 290(5500):2323–2326, 2000.

756 Ernest Ryu, Jialin Liu, Sicheng Wang, Xiaohan Chen, Zhangyang Wang, and Wotao Yin. Plug-and-
 757 play methods provably converge with properly trained denoisers. In *International Conference on*
 758 *Machine Learning*, pp. 5546–5557. PMLR, 2019.

759

760 Franco Scarselli, Marco Gori, Ah Chung Tsoi, Markus Hagenbuchner, and Gabriele Monfardini.
 761 The graph neural network model. *IEEE Transactions on Neural Networks*, 20(1):61–80, 2008.

762

763 Vineet R Shenoy, Suhas Lohit, Hassan Mansour, Rama Chellappa, and Tim K Marks. Recovering
 764 Pulse Waves from video using Deep Unrolling and Deep Equilibrium Models. *arXiv preprint*
 765 *arXiv:2503.17269*, 2025.

766

767 Yu Sun, Brendt Wohlberg, and Ulugbek S Kamilov. An online plug-and-play algorithm for regular-
 768 ized image reconstruction. *IEEE Transactions on Computational Imaging*, 5(3):395–408, 2019.

769

770 Julián Tachella, Matthieu Terris, Samuel Hurault, Andrew Wang, Dongdong Chen, Minh-Hai
 771 Nguyen, Maxime Song, Thomas Davies, Leo Davy, Jonathan Dong, Paul Escande, Johannes
 772 Hertrich, Zhiyuan Hu, Tobías I. Liaudat, Nils Laurent, Brett Levac, Mathurin Massias, Thomas
 773 Moreau, Thibaut Modrzyk, Brayan Monroy, Sebastian Neumayer, Jérémie Scanvic, Florian Sar-
 774 rron, Victor Sechaud, Georg Schramm, Romain Vo, and Pierre Weiss. DeepInverse: A Python
 775 package for solving imaging inverse problems with deep learning. Technical Report 2505.20160,
 776 arXiv, 2025. <https://arxiv.org/abs/2505.20160>.

777

778 Rong Tang and Yun Yang. Adaptivity of diffusion models to manifold structures. In *International*
 779 *Conference on Artificial Intelligence and Statistics*, pp. 1648–1656. PMLR, 2024.

780

781 Matus Telgarsky. Neural networks and rational functions. In *International Conference on Machine*
 782 *Learning*, pp. 3387–3393. PMLR, 2017.

783

784 Roger Temam. *Navier–Stokes equations and nonlinear functional analysis*. SIAM, 1995.

785

786 Lan V. Truong. Global convergence rate of deep equilibrium models with general activations.
 787 *Transactions on Machine Learning Research*, 2025. ISSN 2835-8856. URL <https://openreview.net/forum?id=XPReQ1AM0>.

788

789 Singanallur V Venkatakrishnan, Charles A Bouman, and Brendt Wohlberg. Plug-and-play priors for
 790 model based reconstruction. In *IEEE Global Conference on Signal and Information Processing*
 791 (*GlobalSIP*), pp. 945–948. IEEE, 2013.

792

793 Aladin Virmaux and Kevin Scaman. Lipschitz regularity of deep neural networks: analysis and
 794 efficient estimation. *Advances in Neural Information Processing Systems*, 31, 2018.

795

796 Michael B Wakin. Manifold-based signal recovery and parameter estimation from compressive
 797 measurements. *arXiv preprint arXiv:1002.1247*, 2010.

798

799 Haixin Wang, Jianlong Chang, Yihang Zhai, Xiao Luo, Jinan Sun, Zhouchen Lin, and Qi Tian. Lion:
 800 Implicit vision prompt tuning. In *Proceedings of the AAAI Conference on Artificial Intelligence*,
 801 2024.

802

803 Ezra Winston and J Zico Kolter. Monotone operator equilibrium networks. *Advances in Neural*
 804 *Information Processing Systems*, 33:10718–10728, 2020.

805

806 Zhoutong Wu, Yimu Zhang, Cong Fang, and Zhouchen Lin. Separation and bias of deep equilib-
 807 rium models on expressivity and learning dynamics. *Advances in Neural Information Processing*
 808 *Systems*, 37:32476–32511, 2024.

809

810 Xingyu Xie, Qiuhan Wang, Zenan Ling, Xia Li, Guangcan Liu, and Zhouchen Lin. Optimization in-
 811 duced equilibrium networks: An explicit optimization perspective for understanding equilibrium
 812 models. *IEEE Transactions on Pattern Analysis and Machine Intelligence*, 45(3):3604–3616,
 813 2022.

814

815 Keyulu Xu, Weihua Hu, Jure Leskovec, and Stefanie Jegelka. How powerful are Graph Neural
 816 Networks? In *International Conference on Learning Representations*, 2019. URL <https://openreview.net/forum?id=ryGs6iA5Km>.

810 Chengda Yang. Nonlinear image recovery with half-quadratic regularization. *IEEE Transactions on*
811 *Image Processing*, 4(7):932–946, 1995.

812

813 Yongyi Yang, Tang Liu, Yangkun Wang, Zengfeng Huang, and David Wipf. Implicit vs unfolded
814 Graph Neural Networks. *Journal of Machine Learning Research*, 26(82):1–46, 2025.

815 Youhao Yu and Richard M Dansereau. MsDC-DEQ-Net: Deep Equilibrium Model (DEQ) with
816 multiscale dilated convolution for image compressive sensing (CS). *IET Signal Processing*, 2024
817 (1):6666549, 2024.

818

819 Kai Zhang, Yawei Li, Wangmeng Zuo, Lei Zhang, Luc Van Gool, and Radu Timofte. Plug-and-play
820 image restoration with deep denoiser prior. *IEEE Transactions on Pattern Analysis and Machine*
821 *Intelligence*, 44(10):6360–6376, 2021.

822

823 Yongjian Zhong, Hieu Vu, Tianbao Yang, and Bijaya Adhikari. Efficient and effective implicit dy-
824 namic graph neural network. In *Proceedings of the 30th ACM SIGKDD Conference on Knowledge*
825 *Discovery and Data Mining*, pp. 4595–4606, 2024.

826

827 Zihao Zou, Jiaming Liu, Brendt Wohlberg, and Ulugbek S Kamilov. Deep equilibrium learning of
828 explicit regularization functionals for imaging inverse problems. *IEEE Open Journal of Signal*
829 *Processing*, 4:390–398, 2023.

830

831

832

833

834

835

836

837

838

839

840

841

842

843

844

845

846

847

848

849

850

851

852

853

854

855

856

857

858

859

860

861

862

863

864 A PROOFS OF MAIN RESULTS
865866 The core intuition behind our proofs is an extension of the $1/x$ example discussed in the introduction.
867868 For Theorem 2.4 (Sufficiency), we construct the implicit operator \mathcal{G} as a dynamic interpolation:
869 $\mathcal{G}(\mathbf{y}, \mathbf{x}) = (1 - \varepsilon(\mathbf{x}))\mathbf{y} + \varepsilon(\mathbf{x})\mathcal{F}(\mathbf{x})$, which iteratively pulls the state \mathbf{y} toward the target $\mathcal{F}(\mathbf{x})$ with
870 a step size $\varepsilon(\mathbf{x})$. The key theoretical innovation is making this step size adaptive: we construct $\varepsilon(\mathbf{x})$
871 to be inversely proportional to the local steepness (Lipschitz constant) of the target $\mathbf{y}_*(\mathbf{x})$. In regions
872 where the target function becomes extremely steep or singular (like $x \rightarrow 0$ for $1/x$), our constructed
873 $\varepsilon(\mathbf{x})$ naturally vanishes. This effectively “slows down” the dynamics, ensuring the operator \mathcal{G} itself
874 remains globally smooth and contractive.
875876 Theorem 2.5 (Necessity) establishes the converse: we show that for any regular operator, the local
877 steepness of the fixed point is mathematically bounded by the operator’s parameters (y -contraction
878 modulus $\mu(\mathbf{x})$); and the fixed point map $\mathbf{y}_*(\mathbf{x})$ can only become singular if the convergence rate
879 slows down (contraction modulus $\rightarrow 1$), perfectly matching the mechanism used in our sufficiency
880 construction.
881882 A.1 PROOF OF SUFFICIENCY
883884 *Proof of Theorem 2.4.* Given any \mathcal{F} satisfying Assumption 2.2, the existence of \mathcal{G} is proved by the
885 following construction:
886

887
$$\mathcal{G}(\mathbf{y}, \mathbf{x}) = \mathcal{F}(\mathbf{x}) + (1 - \varepsilon(\mathbf{x}))(\mathbf{y} - \mathcal{F}(\mathbf{x})). \quad (10)$$

888

889 The proof will be done by choosing a function $\varepsilon : \mathbb{X} \rightarrow \mathbb{R}$ such that
890891

- Functions $\varepsilon(\mathbf{x})$ and $\varepsilon(\mathbf{x})\mathcal{F}(\mathbf{x})$ are both globally Lipschitz continuous on \mathbb{X} .
- $0 < \varepsilon(\mathbf{x}) < 1$ for any $\mathbf{x} \in \mathbb{X}$.

892893 The existence of such a ε function is deferred to [Theorem A.4](#). Now let’s suppose such a $\varepsilon(\mathbf{x})$ is
894 given and finish the whole proof. First let’s check the contractivity of \mathcal{G} in (10) as \mathbf{x} fixed. For any
895 $\mathbf{y}, \hat{\mathbf{y}} \in \mathbb{R}^n$, it holds that
896

897
$$\mathcal{G}(\mathbf{y}, \mathbf{x}) - \mathcal{G}(\hat{\mathbf{y}}, \mathbf{x}) = (1 - \varepsilon(\mathbf{x}))(\mathbf{y} - \mathcal{F}(\mathbf{x})) - (1 - \varepsilon(\mathbf{x}))(\hat{\mathbf{y}} - \mathcal{F}(\mathbf{x})) = (1 - \varepsilon(\mathbf{x}))(\mathbf{y} - \hat{\mathbf{y}}).$$

898

899 Since $0 < \varepsilon(\mathbf{x}) < 1$ for $\mathbf{x} \in \mathbb{X}$, we conclude that $\mathcal{G}(\cdot, \mathbf{x})$ is a contractor for $\mathbf{x} \in \mathbb{X}$. In addition,
900 the continuity of the contractive factor $(1 - \varepsilon(\mathbf{x}))$ is directly resulted from the continuity of $\varepsilon(\mathbf{x})$.
901 Finally, we check the Lipschitz continuity as \mathbf{y} fixed. For any $\mathbf{x}, \hat{\mathbf{x}} \in \mathbb{X}$ and any $\mathbf{y} \in \mathbb{R}^n$, it holds
902 that

903
$$\begin{aligned} & \mathcal{G}(\mathbf{y}, \mathbf{x}) - \mathcal{G}(\mathbf{y}, \hat{\mathbf{x}}) \\ &= (\mathcal{G}(\mathbf{y}, \mathbf{x}) - \mathbf{y}) - (\mathcal{G}(\mathbf{y}, \hat{\mathbf{x}}) - \mathbf{y}) \\ &= (\mathcal{F}(\mathbf{x}) - \mathbf{y} + (1 - \varepsilon(\mathbf{x}))(\mathbf{y} - \mathcal{F}(\mathbf{x}))) - (\mathcal{F}(\hat{\mathbf{x}}) - \mathbf{y} + (1 - \varepsilon(\hat{\mathbf{x}}))(\mathbf{y} - \mathcal{F}(\hat{\mathbf{x}}))) \\ &= -\varepsilon(\mathbf{x})(\mathbf{y} - \mathcal{F}(\mathbf{x})) + \varepsilon(\hat{\mathbf{x}})(\mathbf{y} - \mathcal{F}(\hat{\mathbf{x}})) \\ &= (-\varepsilon(\mathbf{x}) + \varepsilon(\hat{\mathbf{x}}))\mathbf{y} + (\varepsilon(\mathbf{x})\mathcal{F}(\mathbf{x}) - \varepsilon(\hat{\mathbf{x}})\mathcal{F}(\hat{\mathbf{x}})) \end{aligned}$$

904

905 With a fixed $\mathbf{y} \in \mathbb{R}^n$, the Lipschitz continuity of $\mathcal{G}(\mathbf{y}, \cdot)$ follows from the Lipschitz continuity of
906 $\varepsilon(\mathbf{x})$ and $\varepsilon(\mathbf{x})\mathcal{F}(\mathbf{x})$. In particular, by denoting the Lipschitz constants of $\varepsilon(\mathbf{x})$ and $\varepsilon(\mathbf{x})\mathcal{F}(\mathbf{x})$ as L_ε
907 and $L_{\varepsilon\mathcal{F}}$ respectively, we have
908

909
$$\|\mathcal{G}(\mathbf{y}, \mathbf{x}) - \mathcal{G}(\mathbf{y}, \hat{\mathbf{x}})\| \leq L_\varepsilon \|\mathbf{x} - \hat{\mathbf{x}}\| \cdot \|\mathbf{y}\| + L_{\varepsilon\mathcal{F}} \|\mathbf{x} - \hat{\mathbf{x}}\| \leq (L_\varepsilon \|\mathbf{y}\| + L_{\varepsilon\mathcal{F}}) \|\mathbf{x} - \hat{\mathbf{x}}\|$$

910

911 where the Lipschitz constant of \mathcal{G} , $L := L_\varepsilon \|\mathbf{y}\| + L_{\varepsilon\mathcal{F}}$, grows linearly w.r.t. $\|\mathbf{y}\|$, which finishes the
912 whole proof. \square
913914 Below we provide the core theorems used in the proof of Theorem 2.4. We first consider \mathbb{X} to be
915 bounded ([Theorem A.1](#)) and then extend the results to the unbounded domain ([Theorem A.4](#)).
916

918 **Theorem A.1.** For any \mathcal{F} satisfying Assumption 2.2 *defined on a bounded domain $\mathbb{X} \subset \mathbb{R}^d$* , there
 919 exists a function $\varepsilon : \mathbb{X} \rightarrow \mathbb{R}$ such that $0 < \varepsilon(\mathbf{x}) < 1$ for $\mathbf{x} \in \mathbb{X}$, and $\varepsilon(\mathbf{x})$ and $\varepsilon(\mathbf{x})\mathcal{F}(\mathbf{x})$ are both
 920 globally Lipschitz continuous on \mathbb{X} .

922 *Proof.* Let $\bar{\mathbb{X}}$ be the closure of set \mathbb{X} . In this proof, we will first extend \mathcal{F} to $\bar{\mathbb{X}}$, construct the ε
 923 function on $\bar{\mathbb{X}}$, and finally prove the global Lipschitz continuity of $\varepsilon(\mathbf{x})$ and $\varepsilon(\mathbf{x})\mathcal{F}(\mathbf{x})$ on $\bar{\mathbb{X}}$.

924 **Step 1: Extension to $\bar{\mathbb{X}}$.** First we extend \mathcal{F} to $\bar{\mathbf{x}} \in \bar{\mathbb{X}} \setminus \mathbb{X}$ by the limit relative to \mathbb{X} :

$$\mathcal{F}(\bar{\mathbf{x}}) = \begin{cases} \lim_{\mathbb{X} \ni \mathbf{x} \rightarrow \bar{\mathbf{x}}} \mathcal{F}(\mathbf{x}), & \text{if } \lim_{\mathbb{X} \ni \mathbf{x} \rightarrow \bar{\mathbf{x}}} \mathcal{F}(\mathbf{x}) \text{ exists,} \\ 0, & \text{otherwise.} \end{cases}$$

929 Note that even if \mathcal{F} is continuously extendable to $\bar{\mathbf{x}}$, it is still possible that \mathcal{F} is not locally Lipschitz
 930 continuous at the point $\bar{\mathbf{x}}$. A simple example is the function \sqrt{x} , which is continuous as $x \geq 0$ and
 931 locally Lipschitz continuous for all points $x > 0$ but NOT locally Lipschitz at $x = 0$. We collect all
 932 these points (where \mathcal{F} is not locally Lipschitz) into the set $\mathbb{D}(\mathcal{F})$:

$$\mathbb{D}(\mathcal{F}) := \{\mathbf{x} \in \bar{\mathbb{X}} : \mathcal{F} \text{ is not locally Lipschitz continuous at } \mathbf{x}\}$$

934 For brevity, we will use \mathbb{D} to denote $\mathbb{D}(\mathcal{F})$. It holds that \mathbb{D} is a closed set (ref. to Lemma A.2) and
 935 $\mathbb{D} \subset \bar{\mathbb{X}} \setminus \mathbb{X}$.

937 **Step 2: Constructing a function $\varepsilon : \bar{\mathbb{X}} \rightarrow \mathbb{R}_{\geq 0}$.** Now let's define a set including all points that
 938 are very "safe", i.e., sufficiently far from the discontinuity set \mathbb{D} . In particular, given a positive real
 939 number $r > 0$, the set \mathbb{D}_r is define by

$$\mathbb{D}_r := \{\mathbf{x} \in \bar{\mathbb{X}} : d(\mathbf{x}, \mathbb{D}) \geq r\},$$

941 where $d(\mathbf{x}, \mathbb{D})$ means the distance of \mathbf{x} and \mathbb{D} , and the closedness of \mathbb{D}_r can be derived from the
 942 continuity of the distance function. Since $\mathbb{D}_r \subset \bar{\mathbb{X}}$ and $\bar{\mathbb{X}}$ is compact, \mathbb{D}_r must be compact. Note that
 943 \mathbb{D}_r and \mathbb{D} are disjoint, hence \mathcal{F} is locally Lipschitz continuous everywhere on \mathbb{D}_r . Thanks to the fact
 944 that local Lipschitz continuity on a compact set implies global Lipschitz continuity (ref to Lemma
 945 A.3), we can conclude that \mathcal{F} is bounded and globally Lipschitz continuous on \mathbb{D}_r for all $r > 0$.
 946 Therefore, the following two supremums exist, as long as the cardinality (number of elements) of
 947 \mathbb{D}_r is large enough:

$$h_1(r) = \begin{cases} \sup_{\mathbf{x}_1, \mathbf{x}_2 \in \mathbb{D}_r, \mathbf{x}_1 \neq \mathbf{x}_2} \frac{\|\mathcal{F}(\mathbf{x}_1) - \mathcal{F}(\mathbf{x}_2)\|}{\|\mathbf{x}_1 - \mathbf{x}_2\|}, & \text{card}(\mathbb{D}_r) \geq 2, \\ 0, & \text{otherwise.} \end{cases}$$

$$h_2(r) = \begin{cases} \sup_{\mathbf{x} \in \mathbb{D}_r} \|\mathcal{F}(\mathbf{x})\|, & \text{card}(\mathbb{D}_r) \geq 1, \\ 0, & \text{otherwise.} \end{cases}$$

955 Here, both h_1 and h_2 are non-negative and monotone non-increasing on $(0, +\infty)$. Then we define:

$$\hat{h}(r) = \frac{1}{h_1(r) + h_2(r) + 1}.$$

958 It has the following properties:

- 961 • Bounded: $0 < \hat{h}(r) \leq 1$ as $r > 0$.
- 962 • Monotone : $\hat{h}(r_1) \leq \hat{h}(r_2)$ as $0 < r_1 \leq r_2$. (Due to the monotonicity of h_1 and h_2)
- 963 • Naturally extended to $r = 0$: $\lim_{r \rightarrow 0^+} \hat{h}(r)$ exists. (Due to the monotonicity of \hat{h})
- 964 • $\hat{h}(r)h_i(r) < 1$ for $r \geq 0$ and $i = 1, 2$.

968 These properties implies that \hat{h} is Riemann integrable on $[0, +\infty)$. Then we can define the following
 969 function:

$$\hat{\varepsilon}(r) := \int_0^r \hat{h}(s) ds$$

970 with the following properties:

972 • $\hat{\varepsilon}(0) = 0$.
 973
 974 • Monotone increasing. This is a straightforward result of the fact that $\hat{h}(s) > 0$ for $s > 0$.
 975
 976 • Strictly positive as $r > 0$. This is also straightforward as $\hat{h}(s) > 0$ for $s > 0$.
 977 • 1-Lipschitz continuous on $[0, +\infty)$. For any r_1, r_2 with $0 \leq r_1 \leq r_2 < +\infty$, we have
 978
 979 $|\hat{\varepsilon}(r_1) - \hat{\varepsilon}(r_2)| = \hat{\varepsilon}(r_2) - \hat{\varepsilon}(r_1) = \int_{r_1}^{r_2} \hat{h}(s) ds \leq \left(\sup_{r \geq 0} \hat{h}(r) \right) |r_1 - r_2| = |r_1 - r_2|$.
 980
 981

982 With such a $\hat{\varepsilon}(r)$, we can define $\varepsilon(\mathbf{x})$ by

$$983 \quad 984 \quad 985 \quad 986 \quad \varepsilon(\mathbf{x}) = \frac{\hat{\varepsilon}(d(\mathbf{x}, \mathbb{D}))}{1 + \hat{\varepsilon}(d(\mathbf{x}, \mathbb{D}))}.$$

987 It holds that $\varepsilon(\mathbf{x}) = 0$ for $\mathbf{x} \in \mathbb{D}$ and $0 < \varepsilon(\mathbf{x}) < 1$ for $\mathbf{x} \in \overline{\mathbb{X}} \setminus \mathbb{D}$. As $\mathbb{D} \subset \overline{\mathbb{X}} \setminus \mathbb{X}$, we have
 988 $0 < \varepsilon(\mathbf{x}) < 1$ for $\mathbf{x} \in \mathbb{X}$.

989 **Step 3: Establishing the Lipschitz continuity.** Since the distance function $d(\mathbf{x}, \mathbb{D})$ is 1-Lipschitz
 990 continuous (Federer, 1959, Theorem 4.8 (1)), the Lipschitz continuity of $\hat{\varepsilon}$ implies the Lipschitz
 991 continuity of ε . In particular, for all $\mathbf{x}_1, \mathbf{x}_2 \in \overline{\mathbb{X}}$, it holds that

$$992 \quad 993 \quad \begin{aligned} & |\varepsilon(\mathbf{x}_1) - \varepsilon(\mathbf{x}_2)| \\ &= \left| \frac{\hat{\varepsilon}(d(\mathbf{x}_1, \mathbb{D}))}{1 + \hat{\varepsilon}(d(\mathbf{x}_1, \mathbb{D}))} - \frac{\hat{\varepsilon}(d(\mathbf{x}_2, \mathbb{D}))}{1 + \hat{\varepsilon}(d(\mathbf{x}_2, \mathbb{D}))} \right| \quad \left(\frac{x}{1+x} \text{ is 1-Lipschitz as } \left(\frac{x}{1+x} \right)' = \frac{1}{(1+x)^2} \right) \\ &\leq \left| \hat{\varepsilon}(d(\mathbf{x}_1, \mathbb{D})) - \hat{\varepsilon}(d(\mathbf{x}_2, \mathbb{D})) \right| \quad (\text{Lipschitz continuity of } \hat{\varepsilon}) \\ &\leq |d(\mathbf{x}_1, \mathbb{D}) - d(\mathbf{x}_2, \mathbb{D})| \leq \|\mathbf{x}_1 - \mathbf{x}_2\| \quad (\text{Lipschitz continuity of } d) \end{aligned}$$

1000 Therefore, to complete the whole proof, it's enough to show the global Lipschitz continuity of $\varepsilon \mathcal{F}$
 1001 on $\overline{\mathbb{X}}$. As $\overline{\mathbb{X}}$ is compact, and thanks to Lemma A.3, it's enough to show $\varepsilon \mathcal{F}$ is locally Lipschitz
 1002 everywhere on $\overline{\mathbb{X}}$.

1003 First, we consider the local Lipschitz continuity of $\varepsilon \mathcal{F}$ on $\overline{\mathbb{X}} \setminus \mathbb{D}$. Due to Lemma A.2, $\overline{\mathbb{X}} \setminus \mathbb{D}$ must
 1004 be open relative to $\overline{\mathbb{X}}$. For any $\mathbf{x} \in \overline{\mathbb{X}} \setminus \mathbb{D}$, there must be a small enough $r > 0$ such that $\mathbb{U} :=$
 1005 $\mathbb{B}(\mathbf{x}, r) \cap \overline{\mathbb{X}} \subset \overline{\mathbb{X}} \setminus \mathbb{D}$. Pick $\mathbf{x}_1, \mathbf{x}_2 \in \mathbb{U}$. For any $\mathbf{x}_1, \mathbf{x}_2$, it holds that

$$1006 \quad 1007 \quad \begin{aligned} & \|\varepsilon(\mathbf{x}_1) \mathcal{F}(\mathbf{x}_1) - \varepsilon(\mathbf{x}_2) \mathcal{F}(\mathbf{x}_2)\| \\ &= \|\varepsilon(\mathbf{x}_1) \mathcal{F}(\mathbf{x}_1) - \varepsilon(\mathbf{x}_1) \mathcal{F}(\mathbf{x}_2) + \varepsilon(\mathbf{x}_1) \mathcal{F}(\mathbf{x}_2) - \varepsilon(\mathbf{x}_2) \mathcal{F}(\mathbf{x}_2)\| \quad (11) \\ &\leq \varepsilon(\mathbf{x}_1) \|\mathcal{F}(\mathbf{x}_1) - \mathcal{F}(\mathbf{x}_2)\| + |\varepsilon(\mathbf{x}_1) - \varepsilon(\mathbf{x}_2)| \cdot \|\mathcal{F}(\mathbf{x}_2)\|. \end{aligned}$$

1008 Since both ε and \mathcal{F} are locally Lipschitz and locally bounded everywhere on $\overline{\mathbb{X}} \setminus \mathbb{D}$, they must be
 1009 Lipschitz and bounded within \mathbb{U} . Then the local Lipschitz continuity of $\varepsilon \mathcal{F}$ at \mathbf{x} immediately follows
 1010 from (11). Note that \mathbf{x} is arbitrarily picked from $\overline{\mathbb{X}} \setminus \mathbb{D}$, hence $\varepsilon \mathcal{F}$ is locally Lipschitz everywhere on
 1011 $\overline{\mathbb{X}} \setminus \mathbb{D}$.

1012 Next, we consider the local Lipschitz continuity of $\varepsilon \mathcal{F}$ on \mathbb{D} . For any $\mathbf{x} \in \mathbb{D}$, we consider its
 1013 neighborhood $\mathbb{U} := \mathbb{B}(\mathbf{x}, 1) \cap \overline{\mathbb{X}}$ and pick $\mathbf{x}_1, \mathbf{x}_2 \in \mathbb{U}$. Then we need to consider three cases. The
 1014 first case is both $\mathbf{x}_1, \mathbf{x}_2$ belong to the discontinuity set \mathbb{D} : $\mathbf{x}_1, \mathbf{x}_2 \in \mathbb{D}$. In this case, it holds that
 1015 $\varepsilon(\mathbf{x}_1) = \varepsilon(\mathbf{x}_2) = 0$ and hence

$$1016 \quad 1017 \quad \|\varepsilon(\mathbf{x}_1) \mathcal{F}(\mathbf{x}_1) - \varepsilon(\mathbf{x}_2) \mathcal{F}(\mathbf{x}_2)\| = 0 \leq \|\mathbf{x}_1 - \mathbf{x}_2\|.$$

1018 The second case is that one of the point is in \mathbb{D} while the other is not, we suppose $\mathbf{x}_1 \in \mathbb{D}, \mathbf{x}_2 \in \overline{\mathbb{X}} \setminus \mathbb{D}$,
 1019 then

$$1020 \quad 1021 \quad \|\varepsilon(\mathbf{x}_1) \mathcal{F}(\mathbf{x}_1) - \varepsilon(\mathbf{x}_2) \mathcal{F}(\mathbf{x}_2)\|$$

$$\begin{aligned}
&= \|\varepsilon(\mathbf{x}_2)\mathcal{F}(\mathbf{x}_2)\| \leq \hat{\varepsilon}(d(\mathbf{x}_2, \mathbb{D})) \|\mathcal{F}(\mathbf{x}_2)\| \\
&= \left(\int_0^{d(\mathbf{x}_2, \mathbb{D})} \hat{h}(s) ds \right) \|\mathcal{F}(\mathbf{x}_2)\| \\
&\leq \hat{h}(d(\mathbf{x}_2, \mathbb{D})) \cdot d(\mathbf{x}_2, \mathbb{D}) \cdot \|\mathcal{F}(\mathbf{x}_2)\| \quad (\text{Monontonicity of } \hat{h}) \\
&\leq \hat{h}(d(\mathbf{x}_2, \mathbb{D})) \cdot d(\mathbf{x}_2, \mathbb{D}) \cdot h_2(d(\mathbf{x}_2, \mathbb{D})) \quad (\text{Definition of } h_2) \\
&< d(\mathbf{x}_2, \mathbb{D}) \quad (\hat{h}(r) \cdot h_2(r) < 1 \text{ as } r \geq 0) \\
&= d(\mathbf{x}_2, \mathbb{D}) - d(\mathbf{x}_1, \mathbb{D}) \leq \|\mathbf{x}_1 - \mathbf{x}_2\|
\end{aligned}$$

Finally, we consider the last case where $\mathbf{x}_1, \mathbf{x}_2 \in \bar{\mathbb{X}} \setminus \mathbb{D}$. Without loss of generality, we assume

$$0 < d(\mathbf{x}_1, \mathbb{D}) \leq d(\mathbf{x}_2, \mathbb{D}).$$

Then the definition of h_1 and h_2 implies that

$$\begin{aligned}
&\|\mathcal{F}(\mathbf{x}_1) - \mathcal{F}(\mathbf{x}_2)\| \\
&\leq \max(h_1(d(\mathbf{x}_1, \mathbb{D})), h_1(d(\mathbf{x}_2, \mathbb{D}))) \cdot \|\mathbf{x}_1 - \mathbf{x}_2\| \\
&= h_1(d(\mathbf{x}_1, \mathbb{D})) \cdot \|\mathbf{x}_1 - \mathbf{x}_2\|,
\end{aligned}$$

and

$$\|\mathcal{F}(\mathbf{x}_2)\| \leq h_2(d(\mathbf{x}_2, \mathbb{D})).$$

Consequently, applying (11) and the above inequalities, we have

$$\begin{aligned}
&\|\varepsilon(\mathbf{x}_1)\mathcal{F}(\mathbf{x}_1) - \varepsilon(\mathbf{x}_2)\mathcal{F}(\mathbf{x}_2)\| \\
&\leq \varepsilon(\mathbf{x}_1) \|\mathcal{F}(\mathbf{x}_1) - \mathcal{F}(\mathbf{x}_2)\| + |\varepsilon(\mathbf{x}_1) - \varepsilon(\mathbf{x}_2)| \cdot \|\mathcal{F}(\mathbf{x}_2)\| \\
&\leq \varepsilon(\mathbf{x}_1) \cdot h_1(d(\mathbf{x}_1, \mathbb{D})) \cdot \|\mathbf{x}_1 - \mathbf{x}_2\| + |\varepsilon(\mathbf{x}_1) - \varepsilon(\mathbf{x}_2)| \cdot h_2(d(\mathbf{x}_2, \mathbb{D})) \\
&\leq \hat{\varepsilon}(d(\mathbf{x}_1, \mathbb{D})) \cdot h_1(d(\mathbf{x}_1, \mathbb{D})) \cdot \|\mathbf{x}_1 - \mathbf{x}_2\| + |\hat{\varepsilon}(d(\mathbf{x}_1, \mathbb{D})) - \hat{\varepsilon}(d(\mathbf{x}_2, \mathbb{D}))| \cdot h_2(d(\mathbf{x}_2, \mathbb{D})) \\
&= \left(\int_0^{d(\mathbf{x}_1, \mathbb{D})} \hat{h}(s) ds \right) \cdot h_1(d(\mathbf{x}_1, \mathbb{D})) \cdot \|\mathbf{x}_1 - \mathbf{x}_2\| + \left(\int_{d(\mathbf{x}_1, \mathbb{D})}^{d(\mathbf{x}_2, \mathbb{D})} \hat{h}(s) ds \right) \cdot h_2(d(\mathbf{x}_2, \mathbb{D})) \\
&\leq d(\mathbf{x}_1, \mathbb{D}) \cdot \hat{h}(d(\mathbf{x}_1, \mathbb{D})) \cdot h_1(d(\mathbf{x}_1, \mathbb{D})) \cdot \|\mathbf{x}_1 - \mathbf{x}_2\| \\
&\quad + |d(\mathbf{x}_1, \mathbb{D}) - d(\mathbf{x}_2, \mathbb{D})| \cdot \hat{h}(d(\mathbf{x}_2, \mathbb{D})) \cdot h_2(d(\mathbf{x}_2, \mathbb{D})) \\
&< d(\mathbf{x}_1, \mathbb{D}) \cdot \|\mathbf{x}_1 - \mathbf{x}_2\| + |d(\mathbf{x}_1, \mathbb{D}) - d(\mathbf{x}_2, \mathbb{D})| \\
&\leq d(\mathbf{x}_1, \mathbb{D}) \cdot \|\mathbf{x}_1 - \mathbf{x}_2\| + \|\mathbf{x}_1 - \mathbf{x}_2\|
\end{aligned}$$

The last inequality results from $\hat{h}(r) \cdot (h_1(r) + h_2(r)) < 1$ for all $r > 0$. And the above inequalities imply

$$\|\varepsilon(\mathbf{x}_1)\mathcal{F}(\mathbf{x}_1) - \varepsilon(\mathbf{x}_2)\mathcal{F}(\mathbf{x}_2)\| \leq (\text{diam}(\bar{\mathbb{X}}) + 1) \cdot \|\mathbf{x}_1 - \mathbf{x}_2\|.$$

Combining all the results together, we have $\varepsilon\mathcal{F}$ is locally $(\text{diam}(\bar{\mathbb{X}}) + 1)$ -Lipschitz at any $\mathbf{x} \in \bar{\mathbb{X}}$. Then the compactness of $\bar{\mathbb{X}}$ concludes the global Lipschitz continuous of $\varepsilon\mathcal{F}$, which finishes the whole proof. \square

Follows are some lemmas (as well as their proofs) that we used in the proof of Theorem A.1.

Lemma A.2. *Let $\mathbb{T} \subset \mathbb{R}^d$ be closed and let $\mathcal{F} : \mathbb{T} \rightarrow \mathbb{R}^n$. Denote by $\mathbb{D}(\mathcal{F}) \subset \mathbb{T}$ the set of points at which \mathcal{F} is not locally Lipschitz. Then $\mathbb{D}(\mathcal{F})$ is closed (in \mathbb{T} , hence in \mathbb{R}^d).*

Proof. Recall that \mathcal{F} is locally Lipschitz (relative to \mathbb{T}) at $\mathbf{x} \in \mathbb{T}$ if there exist $r > 0$ and $L > 0$ such that

$$\|\mathcal{F}(\mathbf{u}) - \mathcal{F}(\mathbf{v})\| \leq L \|\mathbf{u} - \mathbf{v}\| \quad \text{for all } \mathbf{u}, \mathbf{v} \in \mathbb{T} \cap \mathbb{B}(\mathbf{x}, r).$$

Let $\mathbb{G} := \mathbb{T} \setminus \mathbb{D}(\mathcal{F})$ be the set of points where \mathcal{F} is locally Lipschitz. We first show that \mathbb{G} is relatively open in \mathbb{T} . Fix $\mathbf{x} \in \mathbb{G}$ and choose r, L as above. If $\mathbf{x}' \in \mathbb{T} \cap \mathbb{B}(\mathbf{x}, r/2)$, then $\mathbb{B}(\mathbf{x}', r/2) \subset$

1080 $\mathbb{B}(\mathbf{x}, r)$; hence the same L works on $\mathbb{T} \cap \mathbb{B}(\mathbf{x}', r/2)$, so \mathcal{F} is locally Lipschitz at \mathbf{x}' . Therefore
 1081 $\mathbb{T} \cap \mathbb{B}(\mathbf{x}, r/2) \subset \mathbb{G}$, proving that \mathbb{G} is open in \mathbb{T} . Consequently, $\mathbb{D}(\mathcal{F}) = \mathbb{T} \setminus \mathbb{G}$ is closed in \mathbb{T} .
 1082 Since \mathbb{T} is closed in \mathbb{R}^d , every set closed in \mathbb{T} is also closed in \mathbb{R}^d . Hence $\mathbb{D}(\mathcal{F})$ is closed in \mathbb{R}^d as
 1083 well. \square

1084 **Lemma A.3.** *Let \mathbb{T} be a compact set. If \mathcal{F} is locally Lipschitz everywhere on \mathbb{T} , then it must be
 1085 globally Lipschitz on \mathbb{T} .*

1087 *Proof.* Assume, to the contrary, that \mathcal{F} is not globally Lipschitz on \mathbb{T} . Then we can choose se-
 1088 quences $\{\mathbf{x}_k\}_{k \geq 1}, \{\mathbf{y}_k\}_{k \geq 1} \subset \mathbb{T}$ such that
 1089

$$\frac{\|\mathcal{F}(\mathbf{x}_k) - \mathcal{F}(\mathbf{y}_k)\|}{\|\mathbf{x}_k - \mathbf{y}_k\|} \xrightarrow{k \rightarrow \infty} \infty. \quad (12)$$

1090 Local Lipschitzness implies continuity of \mathcal{F} on \mathbb{T} , so by compactness \mathcal{F} is bounded: there exists
 1091 $C < \infty$ with $\|\mathcal{F}(\mathbf{z})\| \leq C$ for all $\mathbf{z} \in \mathbb{T}$. Consequently,
 1092

$$\|\mathcal{F}(\mathbf{x}_k) - \mathcal{F}(\mathbf{y}_k)\| \leq 2C \quad \text{for all } k,$$

1093 and therefore (12) forces $\|\mathbf{x}_k - \mathbf{y}_k\| \rightarrow 0$.
 1094

1095 By sequential compactness of \mathbb{T} , passing to a subsequence (not relabeled) we may assume $\mathbf{x}_k \rightarrow \mathbf{x} \in \mathbb{T}$; since $\|\mathbf{x}_k - \mathbf{y}_k\| \rightarrow 0$, we also have $\mathbf{y}_k \rightarrow \mathbf{x}$. Since \mathcal{F} is locally Lipschitz at \mathbf{x} , for k large
 1096 enough we have
 1097

$$\frac{\|\mathcal{F}(\mathbf{x}_k) - \mathcal{F}(\mathbf{y}_k)\|}{\|\mathbf{x}_k - \mathbf{y}_k\|} \leq L,$$

1098 for some $L > 0$, which contradicts (12). Therefore \mathcal{F} must be globally Lipschitz on \mathbb{T} . \square
 1099

1100 Now we relax the condition in Theorem A.1 and extend it to unbounded domains.
 1101

1102 **Theorem A.4.** *For any $\mathbb{X} \subset \mathbb{R}^d$ (not necessarily bounded) and any locally Lipschitz function $\mathcal{F} : \mathbb{X} \rightarrow \mathbb{R}$, there exists a function $\varepsilon : \mathbb{X} \rightarrow \mathbb{R}$ such that $0 < \varepsilon(\mathbf{x}) < 1$ for $\mathbf{x} \in \mathbb{X}$, and $\varepsilon(\mathbf{x})\mathcal{F}(\mathbf{x})$ are both globally Lipschitz continuous on \mathbb{X} .*

1103 *Proof.* We consider the following grids in \mathbb{R}^d :

$$\mathbf{k} = (2k_1, 2k_2, \dots, 2k_d), \quad k_i \in \mathbb{Z}, i \in [d].$$

1104 We define the closed d -dimensional cubic centered at \mathbf{k} by
 1105

$$\mathcal{C}_{\mathbf{k}} = \left[2k_1 - \frac{3}{2}, 2k_1 + \frac{3}{2} \right] \times \left[2k_2 - \frac{3}{2}, 2k_2 + \frac{3}{2} \right] \times \cdots \times \left[2k_d - \frac{3}{2}, 2k_d + \frac{3}{2} \right].$$

1106 According to Theorem A.1, there exists a function $\varepsilon_{\mathbf{k}}$ defined on $\mathcal{C}_{\mathbf{k}} \cap \mathbb{X}$, so that
 1107

- 1108 • $0 < \varepsilon_{\mathbf{k}}(\mathbf{x}) < 1$ on $\mathcal{C}_{\mathbf{k}} \cap \mathbb{X}$.
- 1109 • $\varepsilon_{\mathbf{k}}(\mathbf{x})$ is 1-Lipschitz on $\mathcal{C}_{\mathbf{k}} \cap \mathbb{X}$.
- 1110 • $\varepsilon_{\mathbf{k}}(\mathbf{x})\mathcal{F}(\mathbf{x})$ is $(\text{diam}(\mathcal{C}_{\mathbf{k}}) + 1)$ -Lipschitz on $\mathcal{C}_{\mathbf{k}} \cap \mathbb{X}$.

1111 Next, we concatenate all these $\varepsilon_{\mathbf{k}}$ functions and get a global $\varepsilon : \mathbb{X} \rightarrow \mathbb{R}$. We define the following
 1112 concatenation function in 1-dimensional space:
 1113

$$\rho(x) = \begin{cases} x + \frac{3}{2}, & x \in \left[-\frac{3}{2}, -\frac{1}{2} \right], \\ 1, & x \in \left[-\frac{1}{2}, \frac{1}{2} \right], \\ -x + \frac{3}{2}, & x \in \left[\frac{1}{2}, \frac{3}{2} \right], \\ 0, & \text{otherwise.} \end{cases}$$

1134 Then we define the d-dimensional concatenation function. Let $\mathbf{x} = (x_1, x_2, \dots, x_d)$.
 1135

$$1136 \quad \rho^{(d)}(\mathbf{x}) = \prod_{i=1}^d \rho(x_i).$$

$$1137$$

$$1138$$

1139 We define the shifting function $\rho_{\mathbf{k}}^{(d)}(\mathbf{x}) = \rho^{(d)}(\mathbf{x} - \mathbf{k})$. On \mathbb{X} , we construct
 1140

$$1141 \quad \varepsilon(\mathbf{x}) = \sum_{\mathbf{k} \in \{\mathbf{k}: \mathbf{x} \in \mathcal{C}_{\mathbf{k}}\}} \rho_{\mathbf{k}}^{(d)}(\mathbf{x}) \varepsilon_{\mathbf{k}}(\mathbf{x}).$$

$$1142$$

$$1143$$

1144 Given the constructed $\varepsilon(\mathbf{x})$, it's enough to prove that: $0 < \varepsilon(\mathbf{x}) < 1$, $\varepsilon(\mathbf{x})$ and $\varepsilon(\mathbf{x})\mathcal{F}(\mathbf{x})$ are
 1145 globally Lipschitz over \mathbb{X} . We will show these claims one by one and finish the proof.

1146 First, let's show $0 < \varepsilon(\mathbf{x}) < 1$. As $\rho^{(d)}$ is non-negative and $0 < \varepsilon_{\mathbf{k}}(\mathbf{x}) < 1$, we have
 1147

$$1148 \quad 0 < \varepsilon(\mathbf{x}) < \sum_{\mathbf{k}} \rho_{\mathbf{k}}^{(d)}(\mathbf{x}) = 1$$

$$1149$$

$$1150$$

1151 where $\sum_{\mathbf{k}} \rho_{\mathbf{k}}^{(d)}(\mathbf{x}) = 1$ comes from the fact that each term $\rho(x_i - 2k_i)$ depends only on its spe-
 1152 cific index k_i and not on the others, and hence we can distribute the summation as $\sum_i \sum_j a_i b_j =$
 1153 $(\sum_i a_i)(\sum_j b_j)$. That is,

$$1154 \quad \sum_{\mathbf{k}} \rho_{\mathbf{k}}^{(d)}(\mathbf{x}) = \left(\sum_{k_1 \in \mathbb{Z}} \rho(x_1 - 2k_1) \right) \times \left(\sum_{k_2 \in \mathbb{Z}} \rho(x_2 - 2k_2) \right) \times \cdots \times \left(\sum_{k_d \in \mathbb{Z}} \rho(x_d - 2k_d) \right)$$

$$1155$$

$$1156$$

$$1157 \quad = 1 \times 1 \times \cdots \times 1 = 1.$$

$$1158$$

1159 Second, we prove the Lipschitz continuity of $\varepsilon(\mathbf{x})$. In particular, it holds that
 1160

$$1161 \quad |\varepsilon(\mathbf{x}) - \varepsilon(\hat{\mathbf{x}})| = \left| \sum_{\mathbf{k}} \rho_{\mathbf{k}}^{(d)}(\mathbf{x}) \varepsilon_{\mathbf{k}}(\mathbf{x}) - \sum_{\mathbf{k}} \rho_{\mathbf{k}}^{(d)}(\hat{\mathbf{x}}) \varepsilon_{\mathbf{k}}(\hat{\mathbf{x}}) \right|$$

$$1162$$

$$1163$$

$$1164 \quad = \left| \sum_{\mathbf{k}} \rho_{\mathbf{k}}^{(d)}(\mathbf{x})(\varepsilon_{\mathbf{k}}(\mathbf{x}) - \varepsilon_{\mathbf{k}}(\hat{\mathbf{x}})) + \sum_{\mathbf{k}} (\rho_{\mathbf{k}}^{(d)}(\mathbf{x}) - \rho_{\mathbf{k}}^{(d)}(\hat{\mathbf{x}})) \varepsilon_{\mathbf{k}}(\hat{\mathbf{x}}) \right|$$

$$1165$$

$$1166$$

$$1167 \quad \leq \sum_{\mathbf{k}} \rho_{\mathbf{k}}^{(d)}(\mathbf{x}) \underbrace{|\varepsilon_{\mathbf{k}}(\mathbf{x}) - \varepsilon_{\mathbf{k}}(\hat{\mathbf{x}})|}_{\leq \|\mathbf{x} - \hat{\mathbf{x}}\|} + \sum_{\mathbf{k} \in \{\mathbf{k}: \mathbf{x} \in \mathcal{C}_{\mathbf{k}}\}} \underbrace{|\rho_{\mathbf{k}}^{(d)}(\mathbf{x}) - \rho_{\mathbf{k}}^{(d)}(\hat{\mathbf{x}})|}_{\leq \sqrt{d} \|\mathbf{x} - \hat{\mathbf{x}}\|} \underbrace{|\varepsilon_{\mathbf{k}}(\hat{\mathbf{x}})|}_{\leq 1}$$

$$1168$$

$$1169$$

$$1170 \quad \leq \|\mathbf{x} - \hat{\mathbf{x}}\| + 2^d \sqrt{d} \|\mathbf{x} - \hat{\mathbf{x}}\| = (1 + 2^d \sqrt{d}) \|\mathbf{x} - \hat{\mathbf{x}}\|$$

1171 where 2^d comes from the fact at most 2^d grid cubes overlap at each point \mathbf{x} .
 1172

1173 Third, using the same argument, we can show that $\varepsilon(\mathbf{x})\mathcal{F}(\mathbf{x})$ is globally Lipschitz over \mathbb{X} , and
 1174 the Lipschitz constant is bounded by $(3\sqrt{d} + 1 + 2^d \sqrt{d})$ (Recall that $\text{diam}(\mathcal{C}_{\mathbf{k}}) = 3\sqrt{d}$), which
 1175 finishes the proof. \square

1178 A.2 PROOF OF NECESSITY

1180 For Theorem 2.5, we adopt a similar idea: first considering a bounded domain and then extending
 1181 the results to unbounded domains.

1182 **Theorem A.5.** *Let $\mathbb{X} \subset \mathbb{R}^d$ be a bounded domain and let $\mathcal{G} : \mathbb{R}^n \times \mathbb{X} \rightarrow \mathbb{R}^n$ be regular. Then, for
 1183 every $\mathbf{x} \in \mathbb{X}$, the map $\mathbf{y} \mapsto \mathcal{G}(\mathbf{y}, \mathbf{x})$ has a unique fixed point $\mathbf{y}_*(\mathbf{x})$, and the resulting fixed-point
 1184 map $\mathbf{y}_*(\mathbf{x})$ must be locally Lipschitz on \mathbb{X} .*

1185
 1186 *Proof.* Let $\bar{\mathbb{X}}$ be the closure of \mathbb{X} . In this proof, we will first extend the operator \mathcal{G} to $\mathbb{R}^n \times \bar{\mathbb{X}}$, and
 1187 then analyze its properties on this closed domain.

1188 **Step 1: Extension to $\bar{\mathbb{X}}$.** For any $\mathbf{y} \in \mathbb{R}^n$, $\mathcal{G}(\mathbf{y}, \mathbf{x})$ is globally Lipschitz continuous on \mathbb{X} , hence its
 1189 extension is naturally define by
 1190

$$1191 \mathcal{G}(\mathbf{y}, \bar{\mathbf{x}}) := \lim_{\mathbb{X} \ni \mathbf{x} \rightarrow \bar{\mathbf{x}}} \mathcal{G}(\mathbf{y}, \mathbf{x}), \quad \text{for all } \bar{\mathbf{x}} \in \bar{\mathbb{X}} \setminus \mathbb{X}.$$

1192 Different from the proof of Theorem A.1 where \mathcal{F} might be not locally Lipschitz at $\bar{\mathbf{x}}$ even if it is
 1193 continuous at $\bar{\mathbf{x}}$, here the extended \mathcal{G} must be Lipschitz at $\bar{\mathbf{x}}$ and hence Lipschitz on the overall set
 1194 $\bar{\mathbb{X}}$. This can be verified by examining the difference quotient for $\mathbf{x}_1 \neq \mathbf{x}_2$ and $\mathbf{y} \in \mathbb{R}^n$:
 1195

$$1196 \Delta \mathcal{G}[\mathbf{y}; \mathbf{x}_1, \mathbf{x}_2] := \frac{\|\mathcal{G}(\mathbf{y}, \mathbf{x}_1) - \mathcal{G}(\mathbf{y}, \mathbf{x}_2)\|}{\|\mathbf{x}_1 - \mathbf{x}_2\|}$$

1198 Let $\mathcal{G}(\mathbf{y}, \cdot)$'s Lipschitz constant on \mathbb{X} be $L(\mathbf{y}) := \sup_{\mathbf{x}_1 \neq \mathbf{x}_2 \in \mathbb{X}} \Delta \mathcal{G}[\mathbf{y}; \mathbf{x}_1, \mathbf{x}_2]$. For any $\mathbf{x}_1 \in \mathbb{X}$ and
 1199 $\bar{\mathbf{x}}_2 \in \bar{\mathbb{X}} \setminus \mathbb{X}$, it holds that
 1200

$$1201 \Delta \mathcal{G}[\mathbf{y}; \mathbf{x}_1, \bar{\mathbf{x}}_2] = \lim_{\mathbb{X} \ni \mathbf{x}_2 \rightarrow \bar{\mathbf{x}}_2} \Delta \mathcal{G}[\mathbf{y}; \mathbf{x}_1, \mathbf{x}_2] \leq \sup_{\mathbf{x}_2 \in \mathbb{X}: \mathbf{x}_2 \neq \mathbf{x}_1} \Delta \mathcal{G}[\mathbf{y}; \mathbf{x}_1, \mathbf{x}_2] \leq L(\mathbf{y})$$

1203 For any $\bar{\mathbf{x}}_1 \neq \bar{\mathbf{x}}_2 \in \bar{\mathbb{X}} \setminus \mathbb{X}$, we have

$$1204 \Delta \mathcal{G}[\mathbf{y}; \bar{\mathbf{x}}_1, \bar{\mathbf{x}}_2] = \lim_{\mathbb{X} \ni \mathbf{x}_1 \rightarrow \bar{\mathbf{x}}_1} \lim_{\mathbb{X} \ni \mathbf{x}_2 \rightarrow \bar{\mathbf{x}}_2} \Delta \mathcal{G}[\mathbf{y}; \mathbf{x}_1, \mathbf{x}_2] \leq \sup_{\mathbf{x}_1, \mathbf{x}_2 \in \mathbb{X}: \mathbf{x}_2 \neq \mathbf{x}_1} \Delta \mathcal{G}[\mathbf{y}; \mathbf{x}_1, \mathbf{x}_2] = L(\mathbf{y})$$

1206 Therefore, we obtain an upper bound for $\mathcal{G}(\mathbf{y}, \cdot)$'s Lipschitz constant on $\bar{\mathbb{X}}$:
 1207

$$1208 \sup_{\mathbf{x}_1 \neq \mathbf{x}_2 \in \bar{\mathbb{X}}} \Delta \mathcal{G}[\mathbf{y}; \mathbf{x}_1, \mathbf{x}_2] \\ 1209 = \max \left(\sup_{\mathbf{x}_1 \neq \mathbf{x}_2 \in \mathbb{X}} \Delta \mathcal{G}[\mathbf{y}; \bar{\mathbf{x}}_1, \bar{\mathbf{x}}_2], \sup_{\mathbf{x}_1 \in \mathbb{X}, \mathbf{x}_2 \in \bar{\mathbb{X}} \setminus \mathbb{X}} \Delta \mathcal{G}[\mathbf{y}; \mathbf{x}_1, \bar{\mathbf{x}}_2], \sup_{\mathbf{x}_1 \neq \mathbf{x}_2 \in \bar{\mathbb{X}} \setminus \mathbb{X}} \Delta \mathcal{G}[\mathbf{y}; \bar{\mathbf{x}}_1, \bar{\mathbf{x}}_2] \right) \\ 1212 \leq \max(L(\mathbf{y}), L(\mathbf{y}), L(\mathbf{y})) = L(\mathbf{y})$$

1214 That is, for any $\mathbf{y} \in \mathbb{R}^n$, $\mathcal{G}(\mathbf{y}, \cdot)$ is globally Lipschitz on $\bar{\mathbb{X}}$, and the Lipschitz constant is the same
 1215 with that of \mathbb{X} .
 1216

1217 In the other hand, let's consider the Lipschitz constant (contraction constant) w.r.t. \mathbf{y} when fixing
 1218 $\bar{\mathbf{x}} \in \bar{\mathbb{X}} \setminus \mathbb{X}$:

$$1219 \mu(\bar{\mathbf{x}}) = \lim_{\mathbb{X} \ni \mathbf{x} \rightarrow \bar{\mathbf{x}}} \mu(\mathbf{x})$$

1220 Since $0 < \mu(\mathbf{x}) < 1$ for $\mathbf{x} \in \mathbb{X}$, by taking limit, we have $0 \leq \mu(\bar{\mathbf{x}}) \leq 1$. For those $\bar{\mathbf{x}}$ with $\mu(\bar{\mathbf{x}}) < 1$,
 1221 the operator $\mathcal{G}(\cdot, \bar{\mathbf{x}})$ is still contractive. But if $\mu(\bar{\mathbf{x}}) = 1$, the operator $\mathcal{G}(\cdot, \bar{\mathbf{x}})$ is not contractive.
 1222

1223 **Step 2: Defining \mathbb{D} and \mathbb{D}_r .** We collect all points $\mathbf{x} \in \bar{\mathbb{X}}$ where the operator $\mathcal{G}(\cdot, \mathbf{x})$ is not contractive:
 1224

$$1224 \mathbb{D} := \{\mathbf{x} \in \bar{\mathbb{X}} : \mu(\mathbf{x}) = 1\}$$

1225 and define a “safe” set that is sufficiently far from \mathbb{D} :

$$1227 \mathbb{D}_r := \{\mathbf{x} \in \bar{\mathbb{X}} : d(\mathbf{x}, \mathbb{D}) \geq r\}.$$

1228 Note that $\bar{\mathbb{X}} \setminus \mathbb{D} = \bigcup_{r>0} \mathbb{D}_r$ and $\mathbb{X} \subset \bar{\mathbb{X}} \setminus \mathbb{D}$. We obtain
 1229

$$1230 \mathbb{X} \subset \bigcup_{r>0} \mathbb{D}_r.$$

1232 For any \mathbb{D}_r with $r > 0$, we can obtain a uniform contraction of the operator $\mathcal{G}(\cdot, \mathbf{x})$: There is a
 1233 constant $\mu_r \in (0, 1)$ such that
 1234

$$1235 \|\mathcal{G}(\mathbf{y}_1, \mathbf{x}) - \mathcal{G}(\mathbf{y}_2, \mathbf{x})\| \leq \mu_r \|\mathbf{y}_1 - \mathbf{y}_2\| \quad (13)$$

1236 for all $\mathbf{y}_1, \mathbf{y}_2 \in \mathbb{R}^n$ and $\mathbf{x} \in \mathbb{D}_r$, which follows immediately from the continuity of $\mu(\mathbf{x})$ and the
 1237 compactness of \mathbb{D}_r . By the Banach fixed-point theorem, the operator $\mathcal{G}(\cdot, \mathbf{x})$ must have a unique
 1238 fixed point \mathbf{y}_* for each $\mathbf{x} \in \mathbb{D}_r$.
 1239

1240 To complete the proof of Theorem 2.5, thanks to the fact that $\mathbb{X} \subset \bigcup_{r>0} \mathbb{D}_r$, it's enough to show
 1241 that: For any \mathbb{D}_r with $r > 0$, there is a constant C_r such that

$$1241 \|\mathbf{y}_*(\mathbf{x}_1) - \mathbf{y}_*(\mathbf{x}_2)\| \leq C_r \|\mathbf{x}_1 - \mathbf{x}_2\| \quad (14)$$

1242 holds for all $\mathbf{x}_1, \mathbf{x}_2 \in \mathbb{D}_r$. In the following steps, we will show (14).

1243 **Step 3: A controllable sequence.** Fix $\mathbf{x} \in \mathbb{D}_r$. By defining a sequence $\{\mathbf{y}_k(\mathbf{x})\}_{k \geq 0} \subset \mathbb{R}^n$:

$$1244 \quad 1245 \quad \mathbf{y}_{k+1}(\mathbf{x}) = \mathcal{G}(\mathbf{y}_k(\mathbf{x}), \mathbf{x}), \quad \mathbf{y}_0 \text{ is constant for all } \mathbf{x},$$

1246 we are able to estimate the upper bound of $\|\mathbf{y}_*(\mathbf{x})\|$. In particular, we decompose $\mathbf{y}_0 - \mathbf{y}_*$ by a
1247 series:

$$1248 \quad 1249 \quad \mathbf{y}_0 - \mathbf{y}_* = \lim_{k \rightarrow \infty} (\mathbf{y}_0 - \mathbf{y}_k) = \sum_{k=0}^{\infty} (\mathbf{y}_k - \mathbf{y}_{k+1})$$

1250 Thanks to (13), we have

$$1251 \quad 1252 \quad \|\mathbf{y}_k(\mathbf{x}) - \mathbf{y}_{k+1}(\mathbf{x})\| \leq \mu_r \|\mathbf{y}_{k-1}(\mathbf{x}) - \mathbf{y}_k(\mathbf{x})\| \cdots \leq \mu_r^k \|\mathbf{y}_0 - \mathbf{y}_1(\mathbf{x})\| = \mu_r^k \|\mathbf{y}_0 - \mathcal{G}(\mathbf{y}_0, \mathbf{x})\|$$

1253 for all $\mathbf{x} \in \mathbb{D}_r$. Therefore, it holds that

$$1254 \quad 1255 \quad \|\mathbf{y}_0 - \mathbf{y}_*(\mathbf{x})\| \leq \sum_{k=0}^{\infty} \|\mathbf{y}_k(\mathbf{x}) - \mathbf{y}_{k+1}(\mathbf{x})\| \\ 1256 \quad 1257 \quad \leq \left(\sum_{k=0}^{\infty} \mu_r^k \right) \|\mathbf{y}_0 - \mathcal{G}(\mathbf{y}_0, \mathbf{x})\| = \frac{1}{1 - \mu_r} \|\mathbf{y}_0 - \mathcal{G}(\mathbf{y}_0, \mathbf{x})\|$$

1258 Now we can conclude the boundedness of $\|\mathbf{y}_*(\mathbf{x})\|$ for $\mathbf{x} \in \mathbb{D}_r$ by the compactness of \mathbb{D}_r :

$$1259 \quad 1260 \quad \|\mathbf{y}_*(\mathbf{x})\| \leq \underbrace{\|\mathbf{y}_0\| + \frac{1}{1 - \mu_r} \sup_{\mathbf{x} \in \mathbb{D}_r} \|\mathbf{y}_0 - \mathcal{G}(\mathbf{y}_0, \mathbf{x})\|}_{\text{defined as } M_r \geq 0.}$$

1261 With the same argument, we have $\|\mathbf{y}_k(\mathbf{x})\| \leq M_r$ for all $k \geq 0$ and $\mathbf{x} \in \mathbb{D}_r$. It implies that

$$1262 \quad L(\mathbf{y}_k(\mathbf{x})) \leq L_1 + L_2 M_r$$

1263 for some $L_1, L_2 > 0$ as $L(\mathbf{y})$ grows linearly w.r.t. $\|\mathbf{y}\|$. Consequently, we can estimate an upper
1264 bound for the Lipschitz constant of $\mathbf{y}_k(\mathbf{x})$. In particular, for $\mathbf{x}_1, \mathbf{x}_2 \in \mathbb{D}_r$, it holds that

$$1265 \quad 1266 \quad \begin{aligned} & \|\mathbf{y}_{k+1}(\mathbf{x}_1) - \mathbf{y}_{k+1}(\mathbf{x}_2)\| \\ &= \|\mathcal{G}(\mathbf{y}_k(\mathbf{x}_1), \mathbf{x}_1) - \mathcal{G}(\mathbf{y}_k(\mathbf{x}_2), \mathbf{x}_2)\| \\ &= \|\mathcal{G}(\mathbf{y}_k(\mathbf{x}_1), \mathbf{x}_1) - \mathcal{G}(\mathbf{y}_k(\mathbf{x}_2), \mathbf{x}_1) + \mathcal{G}(\mathbf{y}_k(\mathbf{x}_2), \mathbf{x}_1) - \mathcal{G}(\mathbf{y}_k(\mathbf{x}_2), \mathbf{x}_2)\| \\ &\leq \|\mathcal{G}(\mathbf{y}_k(\mathbf{x}_1), \mathbf{x}_1) - \mathcal{G}(\mathbf{y}_k(\mathbf{x}_2), \mathbf{x}_1)\| + \|\mathcal{G}(\mathbf{y}_k(\mathbf{x}_2), \mathbf{x}_1) - \mathcal{G}(\mathbf{y}_k(\mathbf{x}_2), \mathbf{x}_2)\| \\ &\leq \mu_r \|\mathbf{y}_k(\mathbf{x}_1) - \mathbf{y}_k(\mathbf{x}_2)\| + (L_1 + L_2 M_r) \|\mathbf{x}_1 - \mathbf{x}_2\| \end{aligned}$$

1267 For simplicity, let $L_r := L_1 + L_2 M_r$, $a_k := \|\mathbf{y}_k(\mathbf{x}_1) - \mathbf{y}_k(\mathbf{x}_2)\|$, and $h := \|\mathbf{x}_1 - \mathbf{x}_2\|$. By
1268 recursively applying $a_{k+1} \leq \mu_r a_k + Lh$ and $a_0 = 0$, we have

$$1269 \quad 1270 \quad \|\mathbf{y}_k(\mathbf{x}_1) - \mathbf{y}_k(\mathbf{x}_2)\| = a_k \leq (\mu_r)^k a_0 + (\mu_r^{k-1} + \cdots + \mu_r + 1) L_r h \leq \frac{1}{1 - \mu_r} L_r h = \frac{L_r}{1 - \mu_r} \|\mathbf{x}_1 - \mathbf{x}_2\|.$$

1271 **Step 4: Final proof.** As $\mathcal{G}(\cdot, \mathbf{x})$ is a contractor w.r.t. \mathbf{y} for any $\mathbf{x} \in \mathbb{D}_r$, it holds that $\mathbf{y}_k(\mathbf{x}) \rightarrow \mathbf{y}_*(\mathbf{x})$
1272 for any $\mathbf{x} \in \mathbb{D}_r$. (Here, as for the “convergence,” we mean the pointwise convergence, which is
1273 enough here. We don’t need stronger conditions like the uniform convergence.) For the above
1274 $\mathbf{x}_1, \mathbf{x}_2$, there is a K such that

$$1275 \quad 1276 \quad \|\mathbf{y}_k(\mathbf{x}_1) - \mathbf{y}_*(\mathbf{x}_1)\| \leq \frac{L_r}{1 - \mu_r} \|\mathbf{x}_1 - \mathbf{x}_2\|, \quad \|\mathbf{y}_k(\mathbf{x}_2) - \mathbf{y}_*(\mathbf{x}_2)\| \leq \frac{L_r}{1 - \mu_r} \|\mathbf{x}_1 - \mathbf{x}_2\|$$

1277 for $k \geq K$. Combining the above results, we obtain

$$1278 \quad 1279 \quad \begin{aligned} \|\mathbf{y}_*(\mathbf{x}_1) - \mathbf{y}_*(\mathbf{x}_2)\| &\leq \|\mathbf{y}_*(\mathbf{x}_1) - \mathbf{y}_k(\mathbf{x}_1)\| + \|\mathbf{y}_k(\mathbf{x}_1) - \mathbf{y}_k(\mathbf{x}_2)\| + \|\mathbf{y}_k(\mathbf{x}_2) - \mathbf{y}_*(\mathbf{x}_2)\| \\ &\leq \frac{3L_r}{1 - \mu_r} \|\mathbf{x}_1 - \mathbf{x}_2\| \end{aligned}$$

1280 By letting $C_r = 3L_r/(1 - \mu_r)$, we get (14), which completes the proof. \square

1296 **Remark A.6.** Our result relaxes two uniformity requirements in (Dontchev & Rockafellar, 2009,
 1297 Thm. 1A.4): (i) the contraction modulus $\mu(\mathbf{x})$ is allowed to vary with \mathbf{x} (it only needs to be continuous
 1298 in \mathbf{x}), rather than being a single global constant; and (ii) for each \mathbf{y} , the mapping $\mathbf{x} \mapsto \mathcal{G}(\mathbf{y}, \mathbf{x})$
 1299 is Lipschitz on \mathbb{X} with a constant that may grow linearly in $\|\mathbf{y}\|$, instead of being uniformly bounded
 1300 in \mathbf{y} . Because these bounds are not uniform, we conclude only local (as opposed to global) Lipschitz
 1301 continuity of the fixed-point map $\mathbf{x} \mapsto \mathbf{y}_*(\mathbf{x})$ on \mathbb{X} .

1302 Now we relax the condition in Theorem A.5 to unbounded domains and prove Theorem 2.5 based
 1303 on Theorem A.5.

1305 *Proof of Theorem 2.5.* We cover the domain \mathbb{R}^d using the grid $\mathbf{k} = (2k_1, \dots, 2k_d)$ for $k_i \in \mathbb{Z}$,
 1306 defining closed cubic regions $\mathcal{C}_\mathbf{k}$ of side length 3 centered at each \mathbf{k} :

$$1308 \quad \mathcal{C}_\mathbf{k} = \left[2k_1 - \frac{3}{2}, 2k_1 + \frac{3}{2}\right] \times \left[2k_2 - \frac{3}{2}, 2k_2 + \frac{3}{2}\right] \times \dots \times \left[2k_d - \frac{3}{2}, 2k_d + \frac{3}{2}\right].$$

1310 By applying Theorem A.5 to the bounded set $\mathcal{C}_\mathbf{k} \cap \mathbb{X}$, we guarantee the existence of a unique fixed-
 1311 point map $\mathbf{y}_{\mathbf{k},*} : \mathcal{C}_\mathbf{k} \cap \mathbb{X} \rightarrow \mathbb{R}^n$ which is locally Lipschitz continuous on its domain.

1313 Consider any \mathbf{x} in the intersection of two regions $\mathcal{C}_\mathbf{k} \cap \mathcal{C}_{\mathbf{k}'}$. Since $\mathcal{G}(\cdot, \mathbf{x})$ is a contraction, it admits
 1314 a unique fixed point in \mathbb{R}^n . Therefore, the local solutions must coincide:

$$1315 \quad \mathbf{y}_{\mathbf{k},*}(\mathbf{x}) = \mathbf{y}_{\mathbf{k}'*}(\mathbf{x}).$$

1317 This consistency allows us to define a global fixed-point map $\mathbf{y}_* : \mathbb{X} \rightarrow \mathbb{R}^n$ by setting $\mathbf{y}_*(\mathbf{x}) =$
 1318 $\mathbf{y}_{\mathbf{k},*}(\mathbf{x})$ for any \mathbf{k} such that $\mathbf{x} \in \mathcal{C}_\mathbf{k}$. Since \mathbf{y}_* coincides with a locally Lipschitz function $\mathbf{y}_{\mathbf{k},*}$ on
 1319 every compact neighborhood $\mathcal{C}_\mathbf{k}$, \mathbf{y}_* is locally Lipschitz continuous on \mathbb{X} . \square

B A VARIANT ARCHITECTURE

1323 In practice, many works use a variant of the vanilla model $\mathbf{y}_* = \mathcal{G}(\mathbf{y}_*, \mathbf{x})$:

$$1325 \quad \mathbf{z}_* = \mathcal{G}(\mathbf{z}_*, \mathcal{Q}_1(\mathbf{x})), \quad \mathbf{y}_* = \mathcal{Q}_2(\mathbf{z}_*) \quad (15)$$

1326 where \mathcal{G} is the core implicit model, \mathcal{Q}_1 is an encoding network and \mathcal{Q}_2 is a decoding (readout).

1328 At inference, one iterates $\mathbf{z}_t = \mathcal{G}(\mathbf{z}_{t-1}, \mathcal{Q}_1(\mathbf{x}))$ for $1 \leq t \leq T$ and finally $\mathbf{y}_T = \mathcal{Q}_2(\mathbf{z}_T)$. This
 1329 often improves empirical performance but does not alter the expressivity in Theorems 2.4–2.5.

1330 **Corollary B.1.** *Under Assumption 2.2, for any \mathcal{F} there exists a regular implicit operator \mathcal{G} and
 1331 globally Lipschitz maps $\mathcal{Q}_1, \mathcal{Q}_2$ such that $\mathcal{Q}_2(\text{Fix}(\mathcal{G}(\cdot, \mathcal{Q}_1(\mathbf{x})))) = \mathcal{F}(\mathbf{x})$ for all $\mathbf{x} \in \mathbb{X}$. Con-
 1332 versely, for any regular implicit operator \mathcal{G} any globally Lipschitz $\mathcal{Q}_1, \mathcal{Q}_2$, the fixed point \mathbf{z}_* defined
 1333 by (15) exists uniquely and the induced map $\mathbf{x} \mapsto \mathbf{y}_*$ must be locally Lipschitz on \mathbb{X} .*

1334 *Proof.* The claim follows directly from Theorems 2.4–2.5.

1336 *Sufficiency.* Given any locally Lipschitz target \mathcal{F} on \mathbb{X} , Theorem 2.4 ensures the existence of a
 1337 regular \mathcal{G} whose fixed-point map equals \mathcal{F} . Taking $\mathcal{Q}_1, \mathcal{Q}_2$ as both identity maps recovers the
 1338 sufficiency statement with globally Lipschitz $\mathcal{Q}_1, \mathcal{Q}_2$.

1340 *Necessity.* Suppose \mathcal{G} is regular and $\mathcal{Q}_1, \mathcal{Q}_2$ are globally Lipschitz. Then the composite update
 1341 $\mathcal{G}(\mathbf{z}, \mathcal{Q}_1(\mathbf{x}))$ is still regular in \mathbf{z} and \mathbf{x} . By Theorem 2.5, for every $\mathbf{x} \in \mathbb{X}$, there is a unique
 1342 fixed point $\mathbf{z}_*(\mathbf{x})$ and the map $\mathbf{x} \mapsto \mathbf{z}_*(\mathbf{x})$ is locally Lipschitz on \mathbb{X} . Finally, applying the globally
 1343 Lipschitz readout \mathcal{Q}_2 preserves local Lipschitz continuity, so $\mathbf{x} \mapsto \mathbf{y}_*$ is locally Lipschitz as claimed.
 1344 The proof is finished. \square

C PROOFS OF THEOREMS FOR INVERSE PROBLEMS

1348 This section proves that the target solution mappings, \mathcal{F}_{1a} and \mathcal{F}_{1b} , are single-valued and locally
 1349 Lipschitz on their domain, as stated in Theorems 3.3 and 3.4. Before the proofs, we first provide
 some definitions that used in Assumption 3.1.

1350 Given a close subset $\mathbb{M} \subset \mathbb{R}^n$, its *reach* τ is defined in Federer (1959):
 1351

$$\begin{aligned} 1352 \quad \tau := \sup\{r > 0 : \forall \mathbf{y} \in \mathbb{R}^n \text{ with } \text{dist}(\mathbf{y}, \mathbb{M}) < r, \\ 1353 \quad \text{there exists a unique } \mathbf{z} \in \mathbb{M} \text{ such that } \|\mathbf{y} - \mathbf{z}\| = \text{dist}(\mathbf{y}, \mathbb{M})\}. \end{aligned}$$

1354 A set with positive reach is also called a “prox-regular” set in the literature (Poliquin et al., 2000).
 1355

1356 The Bi-Lipschitz condition refers to: for some $0 < \mu \leq L < +\infty$, it holds that
 1357

$$\mu \|\mathbf{y}_1 - \mathbf{y}_2\| \leq \|\mathbf{A}\mathbf{y}_1 - \mathbf{A}\mathbf{y}_2\| \leq L \|\mathbf{y}_1 - \mathbf{y}_2\| \quad \forall \mathbf{y}_1, \mathbf{y}_2 \in \mathbb{M}. \quad (16)$$

1359 According to the definition, it holds that $0 < \mu \leq L \leq \sigma_{\max} < +\infty$. This condition ensures \mathbf{A}
 1360 can be viewed as an injective mapping when restricted to \mathbb{M} , which is important for the recovery
 1361 guarantee.

1362 *Remark for Assumption 3.1.* The assumption that data (particularly images) lies on a smooth mani-
 1363 fold has a long and influential history (Roweis & Saul, 2000; Donoho & Grimes, 2005), and it is still
 1364 widely used in recent literature. The compactness of the data manifold can be achieved by standard
 1365 techniques like normalization. In addition, reach is an important concept for manifold to ensure the
 1366 uniqueness of its projection (Federer, 1959; Aamari et al., 2019). The overall assumptions on mani-
 1367 folds, smoothness, compactness and **positive** reach, is typically used in recent literature regarding
 1368 image and signal processing (Tang & Yang, 2024; Potapchik et al., 2024; Azangulov et al., 2024).
 1369 The on-manifold bi-Lipschitz condition does *not* require \mathbf{A} to be globally invertible; it merely rules
 1370 out ill-posedness *restricted to* \mathbb{M} . This is closely related to Johnson–Lindenstrauss (JL)–type em-
 1371 beddings in compressive sensing: e.g., Baraniuk & Wakin (2009) shows that random matrices are
 1372 bi-Lipschitz on low-dimensional manifolds with high probability, and JL-style conditions are widely
 1373 analyzed and used (Candes & Tao, 2006; Clarkson, 2008; Wakin, 2010; Iwen & Maggioni, 2013;
 1374 Hegde & Baraniuk, 2012).

1374

1375 *Proof of Theorem 3.3.* For simplicity, we first denote the objective functions in (3) as $F_{1a}(\mathbf{y})$:
 1376

$$F_{1a}(\mathbf{y}) := \frac{1}{2} \|\mathbf{x} - \mathbf{A}\mathbf{y}\|^2 + \frac{\alpha}{2} \text{dist}^2(\mathbf{y}, \mathbb{M})$$

1379 Then we introduce some definitions that will be useful in our proof:
 1380

$$\mathbb{U}_r(\mathbb{M}) := \{\mathbf{y} \in \mathbb{R}^n : \text{dist}(\mathbf{y}, \mathbb{M}) < r\}, \quad \overline{\mathbb{U}}_r(\mathbb{M}) := \{\mathbf{y} \in \mathbb{R}^n : \text{dist}(\mathbf{y}, \mathbb{M}) \leq r\}$$

1382 Here, $\mathbb{U}_r(\mathbb{M})$ is an open tubular neighborhood of the manifold \mathbb{M} and $\overline{\mathbb{U}}_r(\mathbb{M})$ is its closure. As
 1383 $r = \tau$, the open set $\mathbb{U}_r(\mathbb{M})$ is named as the *reach tube* of \mathbb{M} , denoted as $\mathbb{U}_\tau(\mathbb{M})$. As introduced in
 1384 Federer (1959), within the reach tube, some nice properties of the distance function and projection
 1385 mapping can be utilized. For any $\mathbf{y} \in \mathbb{U}_\tau(\mathbb{M})$ or any $\mathbf{y} \in \overline{\mathbb{U}}_r(\mathbb{M})$ with $r < \tau$, the projection
 1386 mapping

$$\mathbf{p}(\mathbf{y}) := \arg \min_{\mathbf{z} \in \mathbb{M}} \|\mathbf{z} - \mathbf{y}\|$$

1388 is single valued and well defined, and $\text{dist}(\mathbf{y}, \mathbb{M}) = \|\mathbf{y} - \mathbf{p}(\mathbf{y})\|$.
 1389

1390 **Step 1: Existence of minimizers of F_{1a} .** As $\mathbf{x} \in \mathbb{X}$, there must be an underlying $\mathbf{y}_* \in \mathbb{M}$ (hence
 1391 $\mathbf{y}_* \in \overline{\mathbb{U}}_r(\mathbb{M})$) and \mathbf{n} such that $\|\mathbf{x} - \mathbf{A}\mathbf{y}_*\| = \|\mathbf{n}\|$. Therefore, it holds that

$$F_{1a}(\mathbf{y}_*) = \frac{1}{2} \|\mathbf{x} - \mathbf{A}\mathbf{y}_*\|^2 + \frac{\alpha}{2} \text{dist}^2(\mathbf{y}_*, \mathbb{M}) = \frac{1}{2} \|\mathbf{n}\|^2 + 0 = \frac{1}{2} \|\mathbf{n}\|^2$$

1395 In the other hand, for any point outside the tube: $\mathbf{y} \notin \overline{\mathbb{U}}_r(\mathbb{M})$, the objective value is lower bounded
 1396 by:

$$F_{1a}(\mathbf{y}) \geq 0 + \frac{\alpha}{2} \text{dist}^2(\mathbf{y}, \mathbb{M}) > \frac{\alpha}{2} r^2$$

1398 As long as we have large enough α :

$$\alpha \geq \frac{\|\mathbf{n}\|^2}{r^2}, \quad (17)$$

1400 we can ensure $F_{1a}(\mathbf{y}) > F_{1a}(\mathbf{y}_*)$ for all $\mathbf{y} \notin \overline{\mathbb{U}}_r(\mathbb{M})$, which implies $\inf_{\mathbf{y} \in \mathbb{R}^n} F_{1a}(\mathbf{y}) =$
 1401 $\inf_{\mathbf{y} \in \overline{\mathbb{U}}_r(\mathbb{M})} F_{1a}(\mathbf{y})$. As \mathbb{M} is compact, $\overline{\mathbb{U}}_r(\mathbb{M})$ must be compact as well. Consequently, the infi-
 1402 1403 mum of F is attainable, which concludes the existence of the minimizer of F_{1a} , denoted by $\hat{\mathbf{y}}$, and

1404 $\hat{\mathbf{y}} \in \overline{\mathbb{U}}_r(\mathbb{M})$. Finally, we have the conclusion: It holds for all $r > 0$ that, condition (17) ensures the
 1405 existence of $\hat{\mathbf{y}}$ and $\hat{\mathbf{y}} \in \overline{\mathbb{U}}_r(\mathbb{M})$.
 1406

1407 **Step 2: Bound of minimizers of F_{1a} .** For any $\mathbf{y} \in \mathbb{U}_\tau(\mathbb{M})$, the projection $\mathbf{p}(\mathbf{y})$ is uniquely defined,
 1408 hence we have

$$\begin{aligned} 1409 \|\mathbf{A}\mathbf{y} - \mathbf{x}\| &= \|\mathbf{A}\mathbf{y} - \mathbf{A}\mathbf{y}_* - \mathbf{n}\| = \|\mathbf{A}\mathbf{y} - \mathbf{A}\mathbf{p}(\mathbf{y}) + \mathbf{A}\mathbf{p}(\mathbf{y}) - \mathbf{A}\mathbf{y}_* - \mathbf{n}\| \\ 1410 &\geq \|\mathbf{A}\mathbf{p}(\mathbf{y}) - \mathbf{A}\mathbf{y}_*\| - \|\mathbf{A}\mathbf{y} - \mathbf{A}\mathbf{p}(\mathbf{y})\| - \|\mathbf{n}\| \\ 1411 &\geq \mu \|\mathbf{p}(\mathbf{y}) - \mathbf{y}_*\| - \sigma_{\max} \|\mathbf{y} - \mathbf{p}(\mathbf{y})\| - \|\mathbf{n}\| \\ 1412 &\geq \mu \|\mathbf{p}(\mathbf{y}) - \mathbf{y}_*\| - \sigma_{\max} \|\mathbf{y} - \mathbf{p}(\mathbf{y})\| - \|\mathbf{n}\| \end{aligned}$$

1414 According to the conclusion in Step 1, as long as

$$1416 \alpha \geq \frac{\|\mathbf{n}\|^2}{r^2} > \frac{\|\mathbf{n}\|^2}{\tau^2}, \quad (18)$$

1418 it holds that the minimizer $\hat{\mathbf{y}}$ exists and $\hat{\mathbf{y}} \in \overline{\mathbb{U}}_r(\mathbb{M})$ for some $r < \tau$ and hence $\hat{\mathbf{y}} \in \mathbb{U}_\tau(\mathbb{M})$, which
 1419 allows us to use the above inequalities at the beginning of Step 2. Now we aim to establish an upper
 1420 bound for $\|\mathbf{p}(\hat{\mathbf{y}}) - \mathbf{y}_*\|$ by contradiction. Suppose

$$1422 \mu \|\mathbf{p}(\hat{\mathbf{y}}) - \mathbf{y}_*\| > \sigma_{\max} \|\hat{\mathbf{y}} - \mathbf{p}(\hat{\mathbf{y}})\| + 2\|\mathbf{n}\|$$

1423 we will obtain

$$1425 \|\mathbf{A}\hat{\mathbf{y}} - \mathbf{x}\| \geq \mu \|\mathbf{p}(\hat{\mathbf{y}}) - \mathbf{y}_*\| - \sigma_{\max} \|\hat{\mathbf{y}} - \mathbf{p}(\hat{\mathbf{y}})\| - \|\mathbf{n}\| > \|\mathbf{n}\|,$$

1426 which implies

$$1428 F_{1a}(\hat{\mathbf{y}}) = \frac{1}{2} \|\mathbf{A}\hat{\mathbf{y}} - \mathbf{x}\|^2 + \frac{\alpha}{2} \text{dist}^2(\hat{\mathbf{y}}, \mathbb{M}) > \frac{1}{2} \|\mathbf{n}\|^2 + 0 = F_{1a}(\mathbf{y}_*).$$

1430 This contradicts with the definition of $\hat{\mathbf{y}}$: the minimizer of function F_{1a} . Therefore, we obtain:

$$1432 \mu \|\mathbf{p}(\hat{\mathbf{y}}) - \mathbf{y}_*\| \leq \sigma_{\max} \|\hat{\mathbf{y}} - \mathbf{p}(\hat{\mathbf{y}})\| + 2\|\mathbf{n}\| \leq \sigma_{\max} r + 2\|\mathbf{n}\|$$

1433 which is equivalent to

$$1434 \|\mathbf{p}(\hat{\mathbf{y}}) - \mathbf{y}_*\| \leq \frac{\sigma_{\max}}{\mu} r + \frac{2}{\mu} \|\mathbf{n}\|$$

1436 and implies that

$$1438 \|\hat{\mathbf{y}} - \mathbf{y}_*\| \leq \|\hat{\mathbf{y}} - \mathbf{p}(\hat{\mathbf{y}})\| + \|\mathbf{p}(\hat{\mathbf{y}}) - \mathbf{y}_*\| \leq \left(1 + \frac{\sigma_{\max}}{\mu}\right) r + \frac{2}{\mu} \|\mathbf{n}\| \quad (19)$$

1440 holds for all $\hat{\mathbf{y}}$ that minimizes $F_{1a}(\mathbf{y})$.

1442 **Step 3: Positive definiteness of the Hessian of F_{1a} .** To prove the uniqueness of the solution, we
 1443 will establish the strict convexity of the objective function $F_{1a}(\mathbf{y})$ within a neighborhood around
 1444 any point of \mathbb{M} . To achieve this, we establish the positive definiteness of the Hessian of $F_{1a}(\mathbf{y})$ in
 1445 this step.

1446 For any $\mathbf{y} \in \mathbb{U}_\tau(\mathbb{M})$, the projection mapping is single valued and the objective function can be
 1447 written as

$$1448 F_{1a}(\mathbf{y}) = \frac{1}{2} \underbrace{\|\mathbf{x} - \mathbf{A}\mathbf{y}\|^2}_{f(\mathbf{y})} + \frac{\alpha}{2} \underbrace{\|\mathbf{y} - \mathbf{p}(\mathbf{y})\|^2}_{g(\mathbf{y})}$$

1451 The smoothness of \mathbb{M} implies the smoothness of g and of the projection mapping, and hence we can
 1452 take first and second orders of derivatives on g (Leobacher & Steinicke, 2021, Theorem 2). Thanks
 1453 to (Federer, 1959, Theorem 4.8), the gradient and Hessian of g are given by

$$1454 \nabla g(\mathbf{y}) = 2(\mathbf{y} - \mathbf{p}(\mathbf{y})), \quad \nabla^2 g(\mathbf{y}) = 2(\mathbf{I} - D\mathbf{p}(\mathbf{y})),$$

1455 where $D\mathbf{p}$ denotes the Jacobian of the projection mapping. The overall Hessian of F_{1a} is provided
 1456 by

$$1457 \nabla^2 F_{1a}(\mathbf{y}) = \mathbf{A}^\top \mathbf{A} + \alpha(\mathbf{I} - D\mathbf{p}(\mathbf{y})). \quad (20)$$

To further present the properties of the above Hessian, we introduce a space decomposition according to $\mathbf{p}(\mathbf{y})$:

$$\mathbb{R}^n = \mathbb{T}_{\mathbf{p}(\mathbf{y})}(\mathbb{M}) \oplus \mathbb{N}_{\mathbf{p}(\mathbf{y})}(\mathbb{M})$$

where $\mathbb{T}_{\mathbf{p}(\mathbf{y})}(\mathbb{M})$ denotes the tangent space of \mathbb{M} at the point $\mathbf{p}(\mathbf{y}) \in \mathbb{M}$, and $\mathbb{N}_{\mathbf{p}(\mathbf{y})}(\mathbb{M})$ represents the normal space. According to (Leobacher & Steinicke, 2021, Theorem C and Definition 7), the matrix $D\mathbf{p}(\mathbf{y})$ is actually restricted to the tangent space. In other words, for any decomposition \mathbf{h} with $\mathbf{h} = \mathbf{h}_T + \mathbf{h}_N$ where $\mathbf{h}_T \in \mathbb{T}_{\mathbf{p}(\mathbf{y})}(\mathbb{M})$ and $\mathbf{h}_N \in \mathbb{N}_{\mathbf{p}(\mathbf{y})}(\mathbb{M})$, it holds that

$$D\mathbf{p}(\mathbf{y})\mathbf{h}_N = \mathbf{0}, \quad D\mathbf{p}(\mathbf{y})\mathbf{h}_T \in \mathbb{T}_{\mathbf{p}(\mathbf{y})}(\mathbb{M}). \quad (21)$$

In addition, function $g(\mathbf{y})$ is $(\frac{s}{\tau-s})$ -weakly convex where τ is the reach of \mathbb{M} and $s = \text{dist}(\mathbf{y}, \mathbb{M})$ (Nacry & Thibault, 2022, Section 5), and hence the spectrum of $\nabla^2 g$ can be lower bounded by

$$\langle \mathbf{h}_T, \nabla^2 g(\mathbf{y}) \mathbf{h}_T \rangle \geq -\frac{2s}{\tau-s} \|\mathbf{h}_T\|^2, \quad (22)$$

Now, let's turn to the first term in the Hessian: $\mathbf{A}^\top \mathbf{A}$. It can be shown using the JL condition (16) that, the spectrum of $\mathbf{A}^\top \mathbf{A}$ restricted to the tangent space can also be lower bounded. In particular, we pick an arbitrary tangent vector $\mathbf{h}_T \in \mathbb{T}_{\mathbf{p}(\mathbf{y})}(\mathbb{M})$. According to the definition of tangent space, there must be a curve $\gamma : (-\delta, \delta) \rightarrow \mathbb{M}$ with $\delta > 0$, $\gamma(0) = \mathbf{p}(\mathbf{y})$, and $\gamma'(0) = \mathbf{h}_T$. For any $0 \leq t < \delta$, $\gamma(t) \in \mathbb{M}$. By applying condition (16) with the pair $(\gamma(t), \gamma(0))$ and divide by t^2 , we have

$$\mu^2 \frac{\|\gamma(t) - \gamma(0)\|^2}{t^2} \leq \frac{\|\mathbf{A}\gamma(t) - \mathbf{A}\gamma(0)\|^2}{t^2} \leq L^2 \frac{\|\gamma(t) - \gamma(0)\|^2}{t^2}$$

By differentiability and the continuity of the operator \mathbf{A} , it holds that

$$\lim_{t \rightarrow 0} \frac{\gamma(t) - \gamma(0)}{t} = \mathbf{h}_T, \quad \lim_{t \rightarrow 0} \frac{\mathbf{A}\gamma(t) - \mathbf{A}\gamma(0)}{t} = \mathbf{A}\mathbf{h}_T$$

which implies

$$\mu^2 \|\mathbf{h}_T\|^2 \leq \|\mathbf{A}\mathbf{h}_T\|^2 \leq L^2 \|\mathbf{h}_T\|^2. \quad (23)$$

Combining (20), (21), (22), and (23), we have

$$\begin{aligned} & \langle \mathbf{h}, \nabla^2 F_{1a}(\mathbf{y}) \mathbf{h} \rangle \\ &= \underbrace{\langle \mathbf{h}_T, \mathbf{A}^\top \mathbf{A} \mathbf{h}_T \rangle}_{\geq \mu^2 \|\mathbf{h}_T\|^2} + 2 \langle \mathbf{h}_T, \mathbf{A}^\top \mathbf{A} \mathbf{h}_N \rangle + \underbrace{\langle \mathbf{h}_N, \mathbf{A}^\top \mathbf{A} \mathbf{h}_N \rangle}_{\geq 0} \\ &+ \alpha \underbrace{\langle \mathbf{h}_T, (\mathbf{I} - D\mathbf{p}(\mathbf{y})) \mathbf{h}_T \rangle}_{\geq -\frac{s}{\tau-s} \|\mathbf{h}_T\|^2} + 2\alpha \underbrace{\langle \mathbf{h}_T, (\mathbf{I} - D\mathbf{p}(\mathbf{y})) \mathbf{h}_N \rangle}_{=\langle \mathbf{h}_T, \mathbf{h}_N \rangle = 0} + \alpha \underbrace{\langle \mathbf{h}_N, (\mathbf{I} - D\mathbf{p}(\mathbf{y})) \mathbf{h}_N \rangle}_{=\|\mathbf{h}_N\|^2} \\ &\geq \left(\mu^2 - \alpha \frac{s}{\tau-s} \right) \|\mathbf{h}_T\|^2 + \alpha \|\mathbf{h}_N\|^2 - 2 \|\mathbf{A}\mathbf{h}_T\| \cdot \|\mathbf{A}\mathbf{h}_N\| \\ &\geq \left(\mu^2 - \alpha \frac{s}{\tau-s} \right) \|\mathbf{h}_T\|^2 + \alpha \|\mathbf{h}_N\|^2 - 2L \|\mathbf{h}_T\| \cdot \sigma_{\max} \|\mathbf{h}_N\| \\ &= [\|\mathbf{h}_T\| \quad \|\mathbf{h}_N\|] \begin{bmatrix} \mu^2 - \alpha \frac{s}{\tau-s} & -\sigma_{\max} L \\ -\sigma_{\max} L & \alpha \end{bmatrix} \begin{bmatrix} \|\mathbf{h}_T\| \\ \|\mathbf{h}_N\| \end{bmatrix} \end{aligned}$$

Therefore, to ensure $\langle \mathbf{h}, \nabla^2 F_{1a}(\mathbf{y}) \mathbf{h} \rangle > 0$ for any $\mathbf{h} \neq \mathbf{0}$, it's enough to ensure the 2×2 matrix to be positive definite:

$$\mu^2 - \alpha \frac{s}{\tau-s} > 0 \quad \text{and} \quad \alpha \left(\mu^2 - \alpha \frac{s}{\tau-s} \right) - \sigma_{\max}^2 L^2 > 0. \quad (24)$$

In other words, (24) will guarantee the positive definiteness of $\nabla^2 F_{1a}(\mathbf{y})$ for all $\mathbf{y} \in \overline{\mathbb{U}}_s(\mathbb{M})$ and any $s < \tau$.

Step 4: Uniqueness of minimizers of F_{1a} . In this step, we will combine the results from Steps 2 and 3. Then we are able to prove that the objective function $F_{1a}(\mathbf{y})$ is strictly convex in a neighborhood of its minimizers, which implies the uniqueness of the minimizer. To achieve this, it's enough to ensure

$$\|\hat{\mathbf{y}} - \mathbf{y}_*\| \leq s \quad (25)$$

1512 for all $\hat{\mathbf{y}} \in \arg \min_{\mathbf{y}} F_{1a}(\mathbf{y})$, where s satisfies (24). With this condition (25), it holds that
 1513

$$1514 \hat{\mathbf{y}} \in \mathbb{B}(\mathbf{y}_*, s) \subset \overline{\mathbb{U}}_s(\mathbb{M}).$$

1515 Along with the fact that $\mathbb{B}(\mathbf{y}_*, s)$ is convex and that $\nabla^2 F_{1a}(\mathbf{y})$ is positive definite for all $\mathbf{y} \in$
 1516 $\overline{\mathbb{U}}_s(\mathbb{M})$, F_{1a} is strictly convex within $\mathbb{B}(\mathbf{y}_*, s)$ (Boyd & Vandenberghe, 2004, Section 3.1.4). As
 1517 all minimizers of the strict convex function belong to this convex set, $\mathbb{B}(\mathbf{y}_*, s)$, the minimizer $\hat{\mathbf{y}}$
 1518 must be unique.
 1519

1520 Now the question is: How to guarantee (25)? According to (19), Condition (18) along with
 1521

$$1522 \left(1 + \frac{\sigma_{\max}}{\mu}\right) r + \frac{2}{\mu} \|\mathbf{n}\| \leq s \quad (26)$$

1523 can guarantee (25). Finally, it's enough to choose α , s , and r such that (18), (24), and (26) are
 1524 satisfied together. In particular, we choose
 1525

$$1526 s = \frac{4}{\mu} \|\mathbf{n}\|, \quad r = \frac{1}{\sigma_{\max}} \|\mathbf{n}\|, \quad \alpha = \frac{2\sigma_{\max}^2 L^2}{\mu^2}$$

1527 where α merely depends on \mathbf{A} and \mathbb{M} but is independent of \mathbf{x} . Such a parameter choice implies
 1528 (26):
 1529

$$1530 \left(1 + \frac{\sigma_{\max}}{\mu}\right) r + \frac{2}{\mu} \|\mathbf{n}\| \leq 2 \frac{\sigma_{\max}}{\mu} r + \frac{2}{\mu} \|\mathbf{n}\| = \frac{2}{\mu} \|\mathbf{n}\| + \frac{2}{\mu} \|\mathbf{n}\| = s.$$

1531 As $\|\mathbf{n}\| < \frac{1}{20} \frac{\mu^5}{\sigma_{\max}^2 L^2} \tau$, it holds that
 1532

$$1533 s = \frac{4}{\mu} \|\mathbf{n}\| < \frac{\mu^4}{5\sigma_{\max}^2 L^2} \tau \implies \frac{s}{\tau - s} < \frac{\frac{\mu^4}{5\sigma_{\max}^2 L^2} \tau}{\tau - \frac{\mu^4}{5\sigma_{\max}^2 L^2} \tau} \leq \frac{\frac{\mu^4}{5\sigma_{\max}^2 L^2} \tau}{\tau - \frac{1}{5} \tau} = \frac{\mu^4}{4\sigma_{\max}^2 L^2}$$

1534 and therefore (24) is satisfied:
 1535

$$1536 \mu^2 - \alpha \frac{s}{\tau - s} > \mu^2 - \frac{2\sigma_{\max}^2 L^2}{\mu^2} \frac{\mu^4}{4\sigma_{\max}^2 L^2} = \frac{1}{2} \mu^2 > 0$$

1537 and

$$1538 \alpha \left(\mu^2 - \alpha \frac{s}{\tau - s} \right) > \frac{2\sigma_{\max}^2 L^2}{\mu^2} \cdot \frac{1}{2} \mu^2 = \sigma_{\max}^2 L^2.$$

1539 Finally, by choosing α as before, condition (18) is satisfied:
 1540

$$1541 \alpha = 2\sigma_{\max}^2 \cdot \frac{L^2}{\mu^2} \geq 2\sigma_{\max}^2 = \frac{2\|\mathbf{n}\|^2}{r^2}, \quad r = \frac{1}{\sigma_{\max}} \|\mathbf{n}\| < \frac{1}{\sigma_{\max}} \cdot \frac{1}{20} \frac{\mu^5}{\sigma_{\max}^2 L^2} \tau < \tau,$$

1542 which finishes the proof of the uniqueness of minimizers of F_{1a} .
 1543

1544 **Step 5: Local Lipschitz continuity of \mathcal{F}_{1a} .** Previous results from Steps 1-4 indicate that, for any
 1545 $\mathbf{x} \in \mathbb{X}$, there is a unique $\hat{\mathbf{y}}(\mathbf{x})$ that minimizes F_{1a} , but the continuity of $\hat{\mathbf{y}}$ w.r.t. \mathbf{x} has not been
 1546 established. In this step, we will show this continuity via the implicit function theorem. Firstly, as $\hat{\mathbf{y}}$
 1547 minimizes F_{1a} , by first-order optimality conditions for smooth minimization, it holds that
 1548

$$1549 \nabla F_{1a}(\hat{\mathbf{y}}) = \underbrace{\mathbf{A}^\top (\mathbf{A}\hat{\mathbf{y}} - \mathbf{x}) + \alpha(\hat{\mathbf{y}} - \mathbf{p}(\hat{\mathbf{y}}))}_{=: \mathcal{H}(\mathbf{x}, \hat{\mathbf{y}})} = \mathbf{0}$$

1550 Now, let's pick a point \mathbf{x}_0 from \mathbb{X} . Previous results from Steps 1-4 indicate that, operator $\mathcal{H}(\mathbf{x}, \mathbf{y})$ is
 1551 continuously differentiable within a neighborhood of $(\mathbf{x}_0, \hat{\mathbf{y}}(\mathbf{x}_0))$, and its Jacobian matrix w.r.t. \mathbf{y}
 1552

$$1553 D_{\mathbf{y}} \mathcal{H}(\mathbf{x}, \mathbf{y}) = \nabla^2 F_{1a}(\mathbf{y})$$

1554 is positive definite within that neighborhood of $(\mathbf{x}_0, \hat{\mathbf{y}}(\mathbf{x}_0))$. Therefore, we are able to apply the
 1555 implicit function theorem (Folland, 2023, Theorem 3.9) and conclude that $\hat{\mathbf{y}}(\mathbf{x})$ is Lipschitz continuous
 1556 within a neighborhood of \mathbf{x}_0 . This argument applies for any points \mathbf{x}_0 in \mathbb{X} . Therefore,
 1557 $\hat{\mathbf{y}} = \mathcal{F}_{1a}(\mathbf{x})$ is locally Lipschitz continuous on \mathbb{X} . \square

The proof line of Theorem 3.4 largely follows the proof of Theorem 3.3. Here we will highlight the difference of proofs between the two theorems, so that Theorem 3.4 will be rigorously proved without too much redundancy.

Proof of Theorem 3.4. For simplicity, we denote the objective function in (4) as $F_{1b}(\mathbf{y}, \mathbf{z})$:

$$F_{1b}(\mathbf{y}, \mathbf{z}) := \frac{1}{2} \|\mathbf{x} - \mathbf{A}\mathbf{y}\|^2 + \frac{\alpha}{2} \text{dist}^2(\mathbf{z}, \mathbb{M}) + \frac{\beta}{2} \|\mathbf{z} - \mathbf{y}\|^2,$$

and we will study its properties analogously to F_{1a} .

Step 1: Existence of minimizers of F_{1b} . For any $r > 0$, as

$$\alpha \geq \frac{\|\mathbf{n}\|^2}{r^2}, \quad \beta \geq \frac{\|\mathbf{n}\|^2}{r^2},$$

it holds that

$$\inf_{\mathbf{y}, \mathbf{z}} F_{1b}(\mathbf{y}, \mathbf{z}) = \inf_{(\mathbf{y}, \mathbf{z}): \text{dist}(\mathbf{z}, \mathbb{M}) \leq r \text{ and } \|\mathbf{z} - \mathbf{y}\| \leq r} F_{1b}(\mathbf{y}, \mathbf{z}). \quad (27)$$

This can be proved by contradiction: (I) Suppose $F_{1b}(\hat{\mathbf{y}}, \hat{\mathbf{z}})$ is lower than the right-hand-side of (27) and $\text{dist}(\hat{\mathbf{z}}, \mathbb{M}) > r$, we have

$$F_{1b}(\hat{\mathbf{y}}, \hat{\mathbf{z}}) \geq 0 + \frac{\|\mathbf{n}\|^2}{2r^2} \text{dist}^2(\hat{\mathbf{z}}, \mathbb{M}) + 0 > \frac{1}{2} \|\mathbf{n}\|^2 = F_{1b}(\mathbf{y}_*, \mathbf{y}_*)$$

which contradicts with the hypothesis regarding $(\hat{\mathbf{y}}, \hat{\mathbf{z}})$. (II) Suppose $F_{1b}(\hat{\mathbf{y}}, \hat{\mathbf{z}})$ is lower than the right-hand-side of (27) and $\|\hat{\mathbf{z}} - \hat{\mathbf{y}}\| > r$, we have

$$F_{1b}(\hat{\mathbf{y}}, \hat{\mathbf{z}}) \geq 0 + 0 + \frac{\|\mathbf{n}\|^2}{2r^2} \|\hat{\mathbf{z}} - \hat{\mathbf{y}}\|^2 > \frac{1}{2} \|\mathbf{n}\|^2 = F_{1b}(\mathbf{y}_*, \mathbf{y}_*)$$

which also derives a contradiction. Arguments in (I) and (II) together prove (27). Similar to the proof of Theorem 3.3, (27) implies the existence of minimizers of F_{1b} (i.e., minimizers are attainable.)

Step 2: Bound of minimizers of F_{1b} . To extend the proof regarding F_{1a} to F_{1b} , we consider the following inequality that holds for all $\mathbf{y}, \mathbf{z} \in \mathbb{U}_\tau(\mathbb{M})$

$$\|\mathbf{y} - \mathbf{p}(\mathbf{y})\| \leq \|\mathbf{y} - \mathbf{p}(\mathbf{z})\| \leq \|\mathbf{y} - \mathbf{z}\| + \|\mathbf{z} - \mathbf{p}(\mathbf{z})\| = \|\mathbf{y} - \mathbf{z}\| + \text{dist}(\mathbf{z}, \mathbb{M}) \leq 2r.$$

Therefore, we need $2r < \tau$ and

$$\alpha \geq \frac{\|\mathbf{n}\|^2}{r^2} > \frac{4\|\mathbf{n}\|^2}{\tau^2}, \quad \beta \geq \frac{\|\mathbf{n}\|^2}{r^2} > \frac{4\|\mathbf{n}\|^2}{\tau^2} \quad (28)$$

to ensure $\hat{\mathbf{y}}, \hat{\mathbf{z}} \in \mathbb{U}_\tau(\mathbb{M})$. Following the same argument as the proof of Theorem 3.3, the above condition (28) implies

$$\|\mathbf{p}(\hat{\mathbf{y}}) - \mathbf{y}_*\| \leq \frac{\sigma_{\max}}{\mu} (2r) + \frac{2}{\mu} \|\mathbf{n}\|$$

and hence

$$\|\hat{\mathbf{y}} - \mathbf{y}_*\| \leq \|\hat{\mathbf{y}} - \mathbf{p}(\hat{\mathbf{y}})\| + \|\mathbf{p}(\hat{\mathbf{y}}) - \mathbf{y}_*\| \leq 2 \left(1 + \frac{\sigma_{\max}}{\mu} \right) r + \frac{2}{\mu} \|\mathbf{n}\| \quad (29)$$

and

$$\|\hat{\mathbf{z}} - \mathbf{y}_*\| \leq \|\hat{\mathbf{z}} - \hat{\mathbf{y}}\| + \|\hat{\mathbf{y}} - \mathbf{y}_*\| \leq \left(3 + 2 \frac{\sigma_{\max}}{\mu} \right) r + \frac{2}{\mu} \|\mathbf{n}\| \quad (30)$$

holds for all $(\hat{\mathbf{y}}, \hat{\mathbf{z}})$ that minimizes $F_{1b}(\mathbf{y}, \mathbf{z})$.

Step 3: Positive definiteness of the Hessian of F_{1b} . Function $F_{1b}(\mathbf{y}, \mathbf{z})$'s Hessian matrix is of size $2n \times 2n$ and can be written as a 2×2 block w.r.t. \mathbf{y} and \mathbf{z} :

$$\nabla^2 F_{1b}(\mathbf{y}, \mathbf{z}) = \begin{bmatrix} \mathbf{A}^\top \mathbf{A} & \mathbf{0} \\ \mathbf{0} & \mathbf{0} \end{bmatrix} + \alpha \begin{bmatrix} \mathbf{0} & \mathbf{0} \\ \mathbf{0} & \mathbf{I} - D\mathbf{p}(\mathbf{z}) \end{bmatrix} + \beta \begin{bmatrix} \mathbf{I} & -\mathbf{I} \\ -\mathbf{I} & \mathbf{I} \end{bmatrix}$$

For any $\mathbf{h} = [\mathbf{u}^\top \ \mathbf{v}^\top]^\top \in \mathbb{R}^{2n}$, the quadratic form $\langle \mathbf{h}, \nabla^2 F_{1b}(\mathbf{y}, \mathbf{z}) \mathbf{h} \rangle$ can be calculated through:

$$\langle \mathbf{h}, \nabla^2 F_{1b}(\mathbf{y}, \mathbf{z}) \mathbf{h} \rangle = \mathbf{u}^\top \mathbf{A}^\top \mathbf{A} \mathbf{u} + \alpha \mathbf{v}^\top (\mathbf{I} - D\mathbf{p}(\mathbf{z})) \mathbf{v} + \beta \|\mathbf{u} - \mathbf{v}\|^2$$

Decompose $u = u_T + u_N$ and $v = v_T + v_N$ in $\mathbb{T}_{p(z)}(\mathbb{M}) \oplus \mathbb{N}_{p(z)}(\mathbb{M})$. Using the same argument as the proof of Theorem 3.3, we have

$$\begin{aligned} & \langle \mathbf{h}, \nabla^2 F_{1b}(\mathbf{y}, \mathbf{z}) \mathbf{h} \rangle \\ & \geq \left(\mu^2 \|\mathbf{u}_T\|^2 - 2\sigma_{\max} L \|\mathbf{u}_T\| \|\mathbf{u}_N\| \right) + \alpha \left(-\frac{s}{\tau-s} \|\mathbf{v}_T\|^2 + \|\mathbf{v}_N\|^2 \right) + \beta \|\mathbf{u} - \mathbf{v}\|^2 \end{aligned}$$

which implies

$$\begin{aligned}
& \langle \mathbf{h}, \nabla^2 F_{1b}(\mathbf{y}, \mathbf{z}) \mathbf{h} \rangle \\
\geq & \left(\mu^2 \|\mathbf{u}_T\|^2 - 2\sigma_{\max} L \|\mathbf{u}_T\| \|\mathbf{u}_N\| \right) \\
& + \alpha \left(-\frac{s}{\tau-s} \|\mathbf{v}_T\|^2 + \|\mathbf{v}_N\|^2 \right) + \beta \left(\|\mathbf{u}_T - \mathbf{v}_T\|^2 + \|\mathbf{u}_N - \mathbf{v}_N\|^2 \right) \\
\geq & \left(\mu^2 \|\mathbf{u}_T\|^2 - 2\sigma_{\max} L \|\mathbf{u}_T\| \|\mathbf{u}_N\| \right) \\
& + \alpha \left(-\frac{s}{\tau-s} \|\mathbf{v}_T\|^2 + \|\mathbf{v}_N\|^2 \right) + \beta \left((\|\mathbf{u}_T\| - \|\mathbf{v}_T\|)^2 + (\|\mathbf{u}_N\| - \|\mathbf{v}_N\|)^2 \right) \\
= & [\|\mathbf{u}_T\| \ \ \|\mathbf{u}_N\| \ \ \|\mathbf{v}_T\| \ \ \|\mathbf{v}_N\|] \underbrace{\begin{bmatrix} \mu^2 + \beta & -\sigma_{\max} L & -\beta & -\beta \\ -\sigma_{\max} L & \beta & \beta - \alpha \frac{s}{\tau-s} & -\beta \\ -\beta & \beta - \alpha \frac{s}{\tau-s} & \alpha + \beta & \alpha + \beta \end{bmatrix}}_{=: \mathbf{B}} \begin{bmatrix} \|\mathbf{u}_T\| \\ \|\mathbf{u}_N\| \\ \|\mathbf{v}_T\| \\ \|\mathbf{v}_N\| \end{bmatrix}
\end{aligned}$$

To ensure the positive definiteness of $\nabla^2 F_{1b}(\mathbf{y}, \mathbf{z})$, it's enough to ensure $\mathbf{B} \succ \mathbf{0}$. For simplicity, we define

$$\theta := \alpha \frac{s}{\tau - s}, \quad \mathbf{B}_1 := \begin{bmatrix} \mu^2 + \beta & -\sigma_{\max} L \\ -\sigma_{\max} L & \beta \end{bmatrix} \quad \mathbf{B}_2 := \begin{bmatrix} -\beta & \\ & -\beta \end{bmatrix} \quad \mathbf{B}_3 := \begin{bmatrix} \beta - \theta & \\ & \alpha + \beta \end{bmatrix}$$

Then $B = \begin{bmatrix} B_1 & B_2 \\ B_2^\top & B_3 \end{bmatrix}$ is positive definite if and only if B_3 and its Schur complement S are both positive definite:

$$\mathbf{B}_3 \succ \mathbf{0}, \quad \mathbf{S} = \mathbf{B}_1 - \mathbf{B}_2 \mathbf{B}_3^{-1} \mathbf{B}_2^\top \succ \mathbf{0}$$

As B_2 and B_3 are both diagonal, so $B_2 B_3^{-1} B_2^\top$ is straight forward to calculate: $B_2 B_3^{-1} B_2^\top = \text{diag}\left(\frac{\beta^2}{\beta-\theta}, \frac{\beta^2}{\alpha+\beta}\right)$. Then the Schur complement can be calculated:

$$S = \begin{bmatrix} \mu^2 + \beta - \frac{\beta^2}{\beta - \theta} & -\sigma_{\max} L \\ -\sigma_{\max} L & \beta - \frac{\beta^2}{\alpha + \beta} \end{bmatrix} = \begin{bmatrix} \mu^2 - \frac{\beta\theta}{\beta - \theta} & -\sigma_{\max} L \\ -\sigma_{\max} L & \frac{\alpha\beta}{\alpha + \beta} \end{bmatrix}$$

Note that $B_3 \succ 0$ if.f $\beta > \theta$. Therefore, $B \succ 0$ if.f

$$\beta > \theta, \quad \mu^2 > \frac{\beta\theta}{\beta - \theta}, \quad \left(\mu^2 - \frac{\beta\theta}{\beta - \theta} \right) \frac{\alpha\beta}{\alpha + \beta} > \sigma_{\max}^2 L^2, \quad (31)$$

where $\theta = \alpha \frac{s}{\tau-s}$. Finally, we obtain that (31) ensures $\nabla^2 F_{1b}(\mathbf{y}, \mathbf{z}) \succ \mathbf{0}$ for all $\mathbf{y} \in \mathbb{R}^n$ and all $\mathbf{z} \in \overline{\mathbb{U}}_s(\mathbb{M})$ with $s < \tau$.

Step 4: Uniqueness of minimizers of F_{1b} . Comparable to the Step 4 in Theorem 3.3, we need $\|\hat{z} - y_*\| \leq s$ for all $(\hat{y}, \hat{z}) \in \arg \min F_{1b}(\mathbf{y}, \mathbf{z})$. Based on (30), it's enough to guarantee

$$\left(3 + 2\frac{\sigma_{\max}}{\mu}\right)r + \frac{2}{\mu}\|\mathbf{n}\| \leq s \quad (32)$$

Now we choose

$$s = \frac{4}{\mu} \|n\|, \quad r = \frac{2}{5\sigma_{\max}} \|n\|$$

1674 which directly satisfies (32). As $\|\mathbf{n}\| < \frac{1}{76} \frac{\mu^5}{\sigma_{\max}^2 L^2} \tau$, we have
 1675

$$1676 \quad s = \frac{4}{\mu} \|\mathbf{n}\| < \frac{1}{19} \frac{\mu^4}{\sigma_{\max}^2 L^2} \tau, \quad \frac{s}{\tau - s} < \frac{\frac{1}{19} \frac{\mu^4}{\sigma_{\max}^2 L^2} \tau}{\tau - \frac{1}{19} \frac{\mu^4}{\sigma_{\max}^2 L^2} \tau} \leq \frac{\frac{1}{19} \frac{\mu^4}{\sigma_{\max}^2 L^2} \tau}{\tau - \frac{1}{19} \tau} = \frac{1}{18} \frac{\mu^4}{\sigma_{\max}^2 L^2}$$

1679 As long as we take

$$1681 \quad \alpha = \frac{9\sigma_{\max}^2 L^2}{\mu^2}, \quad \beta \geq \max \left(\alpha, \frac{3}{2} \mu^2 \right)$$

1683 it holds that

$$1685 \quad \theta = \alpha \frac{s}{\tau - s} < \frac{9\sigma_{\max}^2 L^2}{\mu^2} \frac{1}{18} \frac{\mu^4}{\sigma_{\max}^2 L^2} = \frac{1}{2} \mu^2$$

1687 which implies $\beta > 3\theta$ and hence $\beta > \theta$. Moreover, we can verify the remaining part of (31):

$$1689 \quad \frac{\beta\theta}{\beta - \theta} < \frac{\beta\theta}{\beta - \beta/3} = \frac{3}{2}\theta < \frac{3}{4}\mu^2 < \mu^2,$$

$$1691 \quad \left(\mu^2 - \frac{\beta\theta}{\beta - \theta} \right) \frac{\alpha\beta}{\alpha + \beta} > \left(\mu^2 - \frac{3}{4}\mu^2 \right) \frac{\alpha\beta}{\beta + \beta} = \frac{1}{8}\mu^2\alpha = \frac{1}{8}\mu^2 \cdot \frac{9\sigma_{\max}^2 L^2}{\mu^2} > \sigma_{\max}^2 L^2.$$

1694 which finishes the proof of (31). Finally, it's enough to verify (28):

$$1695 \quad 2r \leq \frac{\|\mathbf{n}\|}{\sigma_{\max}} \leq \frac{1}{76} \frac{\mu^5}{\sigma_{\max}^3 L^2} \tau < \tau, \quad \frac{\|\mathbf{n}\|^2}{r^2} = \frac{25}{4} \sigma_{\max}^2 \leq \alpha \leq \beta,$$

1698 which finishes Step 4, and concludes the uniqueness of $(\hat{\mathbf{y}}, \hat{\mathbf{z}})$.

1699 **Step 5: Local Lipschitz continuity of \mathcal{F}_{1b} .** By largely following Step 5 in the proof of Theorem 3.3
 1700 and changing $\nabla^2 F_{1a}(\mathbf{y})$ to $\nabla^2 F_{1b}(\mathbf{y}, \mathbf{z})$, one can directly conclude that the mapping \mathcal{F}_{1b} is locally
 1701 Lipschitz continuous on \mathbb{X} . \square

1703 C.1 PROXIMAL OPERATOR NEAR A MANIFOLD

1705 We collect here the definition and basic properties of the proximal map used in the main text and
 1706 relate them to the convergence condition proposed in Ryu et al. (2019).

1707 **Theorem C.1** (Contractivity of the proximal residual near a \mathcal{C}^2 manifold). *Let $\mathbb{M} \subset \mathbb{R}^n$ be a
 1708 compact \mathcal{C}^2 embedded submanifold with reach $\tau > 0$. For $\sigma > 0$ define, for each $\mathbf{z} \in \mathbb{U}_\tau(\mathbb{M})$,*

$$1710 \quad \phi_\sigma(\mathbf{y}, \mathbf{z}) := \frac{\sigma}{2} \text{dist}^2(\mathbf{y}, \mathbb{M}) + \frac{1}{2} \|\mathbf{y} - \mathbf{z}\|^2.$$

1712 Then ϕ_σ must yield a unique minimizer, and hence we are able to define

$$1714 \quad \text{prox}_\sigma(\mathbf{z}) := \arg \min_{\mathbf{y}} \phi_\sigma(\mathbf{y}, \mathbf{z}), \quad \mathcal{S}_\sigma(\mathbf{z}) := \text{prox}_\sigma(\mathbf{z}) - \mathbf{z}.$$

1716 Then \mathcal{S}_σ is a contractive operator within a tubular neighborhood of \mathbb{M} . In particular, it holds that

$$1718 \quad \|\mathcal{S}_\sigma(\mathbf{z}) - \mathcal{S}_\sigma(\mathbf{z}')\| \leq \frac{\sigma}{1 + \sigma} \|\mathbf{z} - \mathbf{z}'\| \tag{33}$$

1720 for all $\mathbf{z}, \mathbf{z}' \in \mathbb{U}_r(\mathbb{M})$ where $r \leq \tau/4$ and $\|\mathbf{z} - \mathbf{z}'\| \leq \tau/4$.

1722 Relation to plug-and-play (PnP): Condition (A) of Ryu et al. (2019) assumes a (nearly) contractive
 1723 *denoiser residual*—precisely the kind of property (33) guarantees for the proximal residual $\text{prox}_\sigma - \mathbf{I}$
 1724 on a neighborhood of \mathbb{M} . In practice, \mathbb{M} is unknown; one therefore learns a parameterized operator
 1725 (e.g., a neural network) whose residual is constrained to be (nearly) σ -contractive and plugs it into
 1726 PGD/HQS in place of the exact proximal map. Whereas Ryu et al. (2019) posits Condition (A) to
 1727 ensure convergence, Theorem C.1 shows this condition arises naturally when the prior corresponds
 to the manifold-penalty $\frac{\sigma}{2} \text{dist}^2(\cdot, \mathbb{M})$.

1728 *Proof of Theorem C.1.* We first note that, for any \mathbf{y} , if $\|\mathbf{y} - \mathbf{z}\| > \|\mathbf{z} - \mathbf{p}(\mathbf{z})\|$, then it holds that
 1729

$$1730 \quad \phi_\sigma(\mathbf{p}(\mathbf{z}), \mathbf{z}) = 0 + \frac{1}{2}\|\mathbf{z} - \mathbf{p}(\mathbf{z})\|^2 < \frac{\sigma}{2}\text{dist}^2(\mathbf{y}, \mathbb{M}) + \frac{1}{2}\|\mathbf{y} - \mathbf{z}\|^2 = \phi_\sigma(\mathbf{y}, \mathbf{z})$$

1732 which implies

$$1733 \quad \inf_{\mathbf{y}} \phi_\sigma(\mathbf{y}, \mathbf{z}) = \inf_{\mathbf{y}: \|\mathbf{y} - \mathbf{z}\| \leq \|\mathbf{z} - \mathbf{p}(\mathbf{z})\|} \phi_\sigma(\mathbf{y}, \mathbf{z})$$

1735 Let $r = \|\mathbf{z} - \mathbf{p}(\mathbf{z})\|$. We further notice that, for any \mathbf{y} with $\|\mathbf{y} - \mathbf{z}\| = s \leq r$, we are able to define
 1736 $\tilde{\mathbf{y}}$

$$1737 \quad \tilde{\mathbf{y}} := \frac{r - s}{r}\mathbf{z} + \frac{s}{r}\mathbf{p}(\mathbf{z})$$

1739 which satisfies $\mathbf{p}(\tilde{\mathbf{y}}) = \mathbf{p}(\mathbf{z})$ and hence it holds that
 1740

$$\begin{aligned} 1741 \quad \text{dist}(\tilde{\mathbf{y}}, \mathbb{M}) &= \|\tilde{\mathbf{y}} - \mathbf{p}(\mathbf{z})\| = \|\mathbf{z} - \mathbf{p}(\mathbf{z})\| - \|\tilde{\mathbf{y}} - \mathbf{z}\| \\ 1742 &< \|\mathbf{z} - \mathbf{p}(\mathbf{y})\| - \|\tilde{\mathbf{y}} - \mathbf{z}\| \\ 1743 &\leq \|\mathbf{z} - \mathbf{y}\| + \|\mathbf{y} - \mathbf{p}(\mathbf{y})\| - \|\tilde{\mathbf{y}} - \mathbf{z}\| \\ 1744 &= s + \|\mathbf{y} - \mathbf{p}(\mathbf{y})\| - s = \|\mathbf{y} - \mathbf{p}(\mathbf{y})\| = \text{dist}(\mathbf{y}, \mathbb{M}) \\ 1745 \end{aligned}$$

1746 which implies

$$1747 \quad \phi_\sigma(\tilde{\mathbf{y}}, \mathbf{z}) = \frac{\sigma}{2}\text{dist}^2(\tilde{\mathbf{y}}, \mathbb{M}) + \frac{1}{2}\|\tilde{\mathbf{y}} - \mathbf{z}\|^2 < \frac{\sigma}{2}\text{dist}^2(\mathbf{y}, \mathbb{M}) + \frac{1}{2}\|\mathbf{y} - \mathbf{z}\|^2 = \phi_\sigma(\mathbf{y}, \mathbf{z})$$

1750 Consequently, we conclude that minimizing ϕ_σ is equal to minimizing it over the line segment
 1751 between \mathbf{z} and its projection $\mathbf{p}(\mathbf{z})$:

$$1752 \quad \inf_{\mathbf{y}} \phi_\sigma(\mathbf{y}, \mathbf{z}) = \inf_{\xi \in [0, 1]} \phi_\sigma(\xi\mathbf{z} + (1 - \xi)\mathbf{p}(\mathbf{z}), \mathbf{z}).$$

1754 Now define $\psi(\xi) = \phi_\sigma(\xi\mathbf{z} + (1 - \xi)\mathbf{p}(\mathbf{z}), \mathbf{z})$. We have
 1755

$$\begin{aligned} 1756 \quad \psi(\xi) &= \frac{\sigma}{2} \left\| (\xi\mathbf{z} + (1 - \xi)\mathbf{p}(\mathbf{z})) - \mathbf{p}(\mathbf{z}) \right\|^2 + \frac{1}{2} \left\| (\xi\mathbf{z} + (1 - \xi)\mathbf{p}(\mathbf{z})) - \mathbf{z} \right\|^2 \\ 1757 &= \frac{\sigma}{2}\xi^2\|\mathbf{z} - \mathbf{p}(\mathbf{z})\|^2 + \frac{1}{2}(1 - \xi)^2\|\mathbf{z} - \mathbf{p}(\mathbf{z})\|^2 \\ 1758 &= (\sigma\xi^2 + (1 - \xi)^2) \cdot \frac{1}{2}\|\mathbf{z} - \mathbf{p}(\mathbf{z})\|^2 \\ 1759 \\ 1760 \\ 1761 \end{aligned}$$

1762 Therefore, $\inf_{\xi \in [0, 1]} \psi(\xi)$ is attainable, and the minimizer is $\xi_* = \frac{1}{1 + \sigma}$, which implies ϕ_σ must yield
 1763 a unique minimizer at
 1764

$$1765 \quad \mathbf{y}_* = \frac{\mathbf{z} + \sigma\mathbf{p}(\mathbf{z})}{1 + \sigma}.$$

1766 Consequently, we have
 1767

$$1768 \quad \mathcal{S}_\sigma(\mathbf{z}) = \mathbf{y}_* - \mathbf{z} = \frac{\sigma}{1 + \sigma}(\mathbf{p}(\mathbf{z}) - \mathbf{z})$$

1769 and hence
 1770

$$1771 \quad D\mathcal{S}_\sigma(\mathbf{z}) = \frac{\sigma}{1 + \sigma}(D\mathbf{p}(\mathbf{z}) - \mathbf{I}).$$

1772 According to (Leobacher & Steinicke, 2021, Theorem C), $D\mathbf{p}(\mathbf{z})$ is actually restricted to the tangent
 1773 space $\mathbb{T}_{\mathbf{p}(\mathbf{z})(\mathbb{M})}$:

$$1775 \quad D\mathbf{p}(\mathbf{z}) = \left(\mathbf{I}_{\mathbb{T}_{\mathbf{p}(\mathbf{z})(\mathbb{M})}} - r\mathcal{L}_{\mathbf{p}(\mathbf{z}), \mathbf{v}} \right)^{-1} P_{\mathbb{T}_{\mathbf{p}(\mathbf{z})(\mathbb{M})}}$$

1777 where $r = \|\mathbf{p}(\mathbf{z}) - \mathbf{z}\|$, $\mathbf{v} = (\mathbf{p}(\mathbf{z}) - \mathbf{z})/r$, and $\mathcal{L}_{\mathbf{p}(\mathbf{z}), \mathbf{v}}$ is the shape operator in direction \mathbf{v} at
 1778 $\mathbf{p}(\mathbf{z})$. The shape operator's eigenvalues $\kappa_1, \dots, \kappa_d$ (In this context, d means the dimension of the
 1779 tangent space) are the principal curvatures of \mathbb{M} (Do Carmo, 2016), which implies the eigenvalues
 1780 of $D\mathbf{p}(\mathbf{z})$, when restricted to the tangent space, are

$$1781 \quad \frac{1}{1 - r\kappa_1}, \dots, \frac{1}{1 - r\kappa_d}.$$

1782 All the curvatures are bounded by the reciprocal of the reach: $|\kappa_i| \leq 1/\tau$ (Aamari et al., 2019).
 1783 Therefore, it holds that

$$1785 \frac{\tau}{\tau+r} \mathbf{I} \Big|_{\mathbb{T}_{\mathbf{p}(\mathbf{z})(\mathbb{M})}} \preceq D\mathbf{p}(\mathbf{z}) \Big|_{\mathbb{T}_{\mathbf{p}(\mathbf{z})(\mathbb{M})}} \preceq \frac{\tau}{\tau-r} \mathbf{I} \Big|_{\mathbb{T}_{\mathbf{p}(\mathbf{z})(\mathbb{M})}}.$$

1787 Moreover, as $D\mathbf{p}(\mathbf{z})$ is restricted to and acts only on the tangent space $\mathbb{T}_{\mathbf{p}(\mathbf{z})(\mathbb{M})}$, we have $\mathbf{0} \preceq$
 1788 $D\mathbf{p}(\mathbf{z}) \preceq \frac{\tau}{\tau-r} \mathbf{I}$, which implies

$$1790 -\mathbf{I} \preceq D\mathbf{p}(\mathbf{z}) - \mathbf{I} \preceq \frac{r}{\tau-r} \mathbf{I}.$$

1792 For $r \leq \tau/2$, we have $\frac{r}{\tau-r} \leq 1$ and hence $\|D\mathcal{S}_\sigma(\mathbf{z})\| \leq \frac{\sigma}{1+\sigma}$. As long as $\mathbf{z}, \mathbf{z}' \in \mathbb{U}_r(\mathbb{M})$ where
 1793 $r \leq \tau/4$ and $\|\mathbf{z} - \mathbf{z}'\| \leq \tau/4$, the two points \mathbf{z}, \mathbf{z}' can be included in a convex subset (actually a
 1794 ball) of $\mathbb{U}_r(\mathbb{M})$ with $r = \tau/2$. By the mean value theorem, we finish the proof of (33). \square

1796 C.2 DISCUSSIONS REGARDING PNP

1798 **Derivation of HQS.** Consider (4):

$$1800 \min_{\mathbf{y}, \mathbf{z} \in \mathbb{R}^n} \frac{1}{2} \|\mathbf{x} - \mathbf{A}\mathbf{y}\|^2 + \frac{\alpha}{2} \text{dist}^2(\mathbf{z}, \mathbb{M}) + \frac{\beta}{2} \|\mathbf{y} - \mathbf{z}\|^2.$$

1802 A typically method to solve it is applying block coordinate descent on it, which is also named ‘‘Half-
 1803 quadratic-splitting (HQS)’’ in the literature (Yang, 1995):

$$1805 \mathbf{y}_{t+1} = \arg \min_{\mathbf{y} \in \mathbb{R}^n} \frac{1}{2} \|\mathbf{A}\mathbf{y} - \mathbf{x}\|^2 + \frac{\beta}{2} \|\mathbf{y} - \mathbf{z}_t\|^2 = (\mathbf{A}^\top \mathbf{A} + \beta \mathbf{I})^{-1} (\mathbf{A}^\top \mathbf{x} + \beta \mathbf{z}_t)$$

$$1807 \mathbf{z}_{t+1} = \arg \min_{\mathbf{z} \in \mathbb{R}^n} \frac{\alpha}{2} \text{dist}^2(\mathbf{z}, \mathbb{M}) + \frac{\beta}{2} \|\mathbf{z} - \mathbf{y}_{t+1}\|^2 = \text{prox}_\sigma(\mathbf{y}_{t+1}) \quad (\text{let } \sigma = \alpha/\beta)$$

1810 Similarly, we can parameterize prox_σ as a neural network $\mathcal{H}_{\theta, \sigma}$. Therefore, HQS suggests an implicit
 1811 model

$$1812 \mathcal{G}_\Theta(\mathbf{z}, \mathbf{x}) = \mathcal{H}_{\theta, \sigma} \left((\mathbf{A}^\top \mathbf{A} + \beta \mathbf{I})^{-1} (\mathbf{A}^\top \mathbf{x} + \beta \mathbf{z}) \right)$$

1814 where $\Theta = \{\theta, \sigma, \beta\}$ includes all trainable parameters, which derives (6).

1815 **Bibliographical notes.** Here we adopt the long-standing ‘‘plug-in denoiser’’ idea. It originated with
 1816 Plug-and-Play (PnP) ADMM, which replaces a proximal operator with an off-the-shelf denoiser in-
 1817 side ADMM (Venkatakrishnan et al., 2013). The framework has since been developed and analyzed
 1818 extensively—see, e.g., (Chan et al., 2016; Kamilov et al., 2017; Buzzard et al., 2018; Sun et al.,
 1819 2019) and the recent survey (Kamilov et al., 2023). In the PGD setting, one pretrains \mathcal{H} for Gaus-
 1820 sian denoising and plugs it into (5) (Ryu et al., 2019; Gavaskar & Chaudhury, 2020; Liu et al., 2021;
 1821 Hurault et al., 2022b). The same plug-in idea applies to HQS via (6) (Zhang et al., 2021; Hurault
 1822 et al., 2022a; Rasti-Meymandi et al., 2023). In contrast to training a denoiser off-the-shelf and plug-
 1823 ging it in, one can train the *entire* \mathcal{G}_Θ via deep equilibrium methods for the target task (the approach
 1824 closest to this paper) in both PGD-style (Gilton et al., 2021; Winston & Kolter, 2020; Zou et al.,
 1825 2023; Yu & Dansereau, 2024; Daniele et al., 2025; Shenoy et al., 2025) and HQS-style (Gkillas
 1826 et al., 2023).

1827 D PROOFS REGARDING NS EQUATIONS

1830 To rigorously state and prove the theorems, we present some definitions here. First, We denote by
 1831 $H^m(\Omega)$ the Sobolev space of functions which are in $L^2(\Omega)$ together with all their derivatives of
 1832 order $\leq m$. Then $H_p^m(\Omega) \subset H^m(\Omega)$ is the collection of functions in $H^m(\Omega)$ that satisfies the
 1833 periodic boundary condition on Ω with zero mean (ref. to (Temam, 1995, Remark 1.1)). Then, we
 1834 can define the spaces considered in this paper:

$$1835 \mathbb{H} := \left\{ u \in \{H_p^0(\Omega)\}^2 : \nabla \cdot u = 0 \right\}, \quad \mathbb{V} := \left\{ u \in \{H_p^1(\Omega)\}^2 : \nabla \cdot u = 0 \right\}$$

1836 For the NS equation (7), we consider $f \in \mathbb{H}$ and $u \in \mathbb{V}$. Moreover, we denote \mathbb{V}' as the dual space
 1837 of \mathbb{V} and have

$$\mathbb{V} \subset \mathbb{H} \subset \mathbb{V}'.$$

1839 We then equip \mathbb{H} with the standard L^2 inner product and norm for vector fields:
 1840

$$1841 \langle u, v \rangle_{\mathbb{H}} := \int_{\Omega} \langle u(\xi), v(\xi) \rangle d\xi, \quad \|u\|_{\mathbb{H}} := \sqrt{\langle u, u \rangle_{\mathbb{H}}} = \left(\int_{\Omega} \|u(\xi)\|^2 d\xi \right)^{1/2} = \|u\|_{L^2(\Omega)}$$

1843 The space \mathbb{V} is equipped with the L^2 norm on the first-order derivatives of u . In particular,
 1844

$$1845 \langle u, v \rangle_{\mathbb{V}} := \sum_{i=1}^2 \int_{\Omega} \left\langle \frac{\partial u}{\partial \xi_i}(\xi), \frac{\partial v}{\partial \xi_i}(\xi) \right\rangle d\xi$$

$$1848 \|u\|_{\mathbb{V}} := \sqrt{\langle u, u \rangle_{\mathbb{V}}} = \left(\sum_{i=1}^2 \int_{\Omega} \left\| \frac{\partial u}{\partial \xi_i}(\xi) \right\|^2 d\xi \right)^{1/2} = \|\nabla u\|_{L^2(\Omega)}$$

1851 and $\|\cdot\|_{\mathbb{V}'}$ is defined as the dual norm of $\|\cdot\|_{\mathbb{V}}$. By Poincare and Cauchy-Schwartz inequalities, we
 1852 have

$$1853 \|v\|_{\mathbb{H}} \leq c_1 \|v\|_{\mathbb{V}}, \quad \forall v \in \mathbb{V}$$

1854 and

$$1855 \|v\|_{\mathbb{V}'} \leq c_2 \|v\|_{\mathbb{H}}, \quad \forall v \in \mathbb{H}$$

1856 where c_1, c_2 are constants depending on the domain Ω . The above definitions and results are standard
 1857 in the literature and we largely follow the notation in (Temam, 1995, Section 2).

1859 *Proof of Theorem 3.6.* (Temam, 1995, Theorem 10.1) states that, for any $f \in \mathbb{V}'$, if $\|f\|_{\mathbb{V}'} \leq c_0 \nu^2$
 1860 (with $c_0 > 0$ depending only on Ω), then the steady NS problem (7) has a unique solution u_* . Since
 1861 $\mathbb{H} \subset \mathbb{V}'$ and $\|f\|_{\mathbb{V}'} \leq c_2 \|f\|_{\mathbb{H}}$, this yields uniqueness on

$$1862 \mathbb{H}_{\nu}^{(1)} := \left\{ f \in \mathbb{H} : \|f\|_{\mathbb{H}} \leq \frac{c_0}{c_2} \nu^2 \right\}.$$

1865 Moreover, by (Temam, 1995, Theorem 10.4), there exists an open dense set $\mathbb{H}_{\nu}^{(2)} \subset \mathbb{H}$ such that,
 1866 on each connected component of $\mathbb{H}_{\nu}^{(2)}$, the solution u_* depends C^∞ on f ; in particular, $f \mapsto u_*$
 1867 is locally Lipschitz there. Define $\mathbb{H}_{\nu} := \mathbb{H}_{\nu}^{(1)} \cap \mathbb{H}_{\nu}^{(2)}$. Since $\mathbb{H}_{\nu}^{(2)}$ is open and dense in \mathbb{H} , the set
 1868 \mathbb{H}_{ν} is dense in $\mathbb{H}_{\nu}^{(1)}$. On \mathbb{H}_{ν} , the solution is unique and the map $f \mapsto u_*$ is locally Lipschitz. This
 1869 completes the proof. \square
 1870

1871 Before moving to Corollary 3.7, let's reclarify lifting and projection operators: Let the lifting (or
 1872 extension) operator $\mathcal{E}_h : \mathbb{R}^{N_h \times 2} \rightarrow \{L^2(\Omega)\}^2$ be the piecewise-constant reconstruction $\mathcal{E}_h(\mathbf{x}) :=$
 1873 $\sum_{C \in \Omega_h} x_C \mathbf{1}_C$, and let $\mathcal{P} : \{L^2(\Omega)\}^2 \rightarrow \mathbb{H}$ be the orthogonal projection onto divergence-free,
 1874 zero-mean fields. Then we move on to Corollary 3.7.
 1875

1876 *Proof of Corollary 3.7.* The mapping $\mathcal{F}_2 : \mathbf{x} \mapsto \mathbf{y}_*$ can be viewed as a composition of multiple
 1877 mappings: We first map $\mathbf{x} \in \mathbb{R}^{N_h \times 2}$ to a continuous version $f \in \mathbb{H}$ by $\mathcal{P} \circ \mathcal{E}_h$, then f can be
 1878 mapped to its corresponding solution u_* by a Locally Lipschitz operator as stated in Theorem 3.6.
 1879 Here we denote this mapping by $\mathcal{S} : f \mapsto u_*$. Then u_* is mapped to ω_* by vorticity: $\nabla \times u_*$, and
 1880 finally ω_* can be mapped to \mathbf{y}_* by a restriction operator \mathcal{R}_h :
 1881

$$\mathcal{F}_2 = \mathcal{R}_h \circ (\nabla \times) \circ \mathcal{S} \circ \mathcal{P} \circ \mathcal{E}_h.$$

1883 Then let's analyze the norm of the above operators one by one. Firstly, the restriction operator \mathcal{R}_h
 1884 has a norm no greater than 1 as:

$$1885 \|\mathcal{R}_h(\omega)\|_{\ell_h^2}^2 = \sum_{C \in \Omega_h} |C| \left| \frac{1}{|C|} \int_C \omega(\xi) d\xi \right|^2$$

$$1888 \leq \sum_{C \in \Omega_h} \frac{1}{|C|} \left(\int_C |\omega(\xi)| d\xi \right)^2 \leq \sum_{C \in \Omega_h} \int_C |\omega(\xi)|^2 d\xi = \|\omega\|_{L^2(\Omega)}^2$$

1890 Note that \mathcal{R}_h is a linear operator, hence its bounded norm immediately leads to its bounded Lipschitz
 1891 constant:

$$1892 \quad \|\mathcal{R}_h(\omega) - \mathcal{R}_h(\omega')\|_{\ell_h^2}^2 = \|\mathcal{R}_h(\omega - \omega')\|_{\ell_h^2}^2 \leq \|\omega - \omega'\|_{L^2(\Omega)}^2.$$

1893 Second, the curl operator $\nabla \times$ must be a bounded linear operator because the solution $u_* \in \mathbb{V}$, where
 1894 first-order derivatives must be L^2 . Third, the solution mapping \mathcal{S} has been discussed in Theorem
 1895 3.6, it is a nonlinear operator, but it is locally Lipschitz continuous. Fourth, the projection operator
 1896 \mathcal{P} must be linear and have a norm no greater than 1. Finally, the lifting operator is linear and has a
 1897 bounded norm as:

$$1898 \quad \|\mathcal{E}_h(\mathbf{x})\|_{L^2(\Omega)}^2 = \sum_{C \in \Omega_h} |C| |x_C|^2 = \|\mathbf{x}\|_{\ell_h^2}^2$$

1900 Therefore, except for the nonlinear operator \mathcal{S} , the other four operators are all linear and bounded
 1901 and hence are globally Lipschitz continuous. As long as we can show that the input of \mathcal{S} must be
 1902 taken from the unique solution regime \mathbb{H}_ν , we will complete the proof that \mathcal{F}_2 is locally Lipschitz
 1903 everywhere on $\mathbb{X}_{\nu,h}$. This can be proved because $\mathbf{x} \in \mathbb{X}_{\nu,h}$ implies $\mathcal{P}(\mathcal{E}_h(\mathbf{x})) \in \mathbb{H}_\nu$. Finally, by
 1904 applying Theorem 2.4, we conclude the existence of \mathcal{G} described in Corollary 3.7, which finishes
 1905 the entire proof. \square

1907 E PROOFS REGARDING LINEAR PROGRAMMING

1909 Although Lipschitz continuity of LP solution maps has been studied (e.g., (Mangasarian & Shiu,
 1910 1987; Dontchev & Rockafellar, 2009)), we are not aware of a reference that states Theorem 3.8 in
 1911 the precise form needed here—particularly allowing perturbations of \mathbf{A} (rather than treating \mathbf{A} as
 1912 fixed). For completeness, we therefore include a self-contained discussion and proof.

1913 To work with a standard form, we rewrite the general-form problem (8) in standard form. Suppose
 1914 there are p equality constraints and q inequality constraints. Without loss of generality, we assume
 1915 \circ_i equals to “=” for $1 \leq i \leq p$ and \circ_i equals to “ \leq ” for $p+1 \leq i \leq m$. Then we denote \mathbf{A}_p as the
 1916 first p rows of matrix \mathbf{A} and \mathbf{A}_q as the remaining part:

$$1918 \quad \mathbf{A}_p := \mathbf{A}[1 : p, :], \quad \mathbf{A}_q := \mathbf{A}[p+1 : m, :]$$

1919 And therefore the general form LP (8) can be written as

$$1921 \quad \min_{\mathbf{y} \in \mathbb{R}^n} \mathbf{c}^\top \mathbf{y}, \quad \text{s.t. } \mathbf{A}_p \mathbf{y} = \mathbf{b}_p, \quad \mathbf{A}_q \mathbf{y} \leq \mathbf{b}_q, \quad \mathbf{l} \leq \mathbf{y} \leq \mathbf{u}.$$

1923 Let $\hat{\mathbf{y}} := \mathbf{y} - \mathbf{l}$, $\mathbf{s} := \mathbf{b}_q - \mathbf{A}_q \mathbf{y}$, and $\mathbf{t} := \mathbf{u} - \mathbf{y}$, the above problem can be transformed to

$$1925 \quad \min_{\mathbf{y} \in \mathbb{R}^n} \mathbf{c}^\top \hat{\mathbf{y}}, \quad \text{s.t. } \begin{bmatrix} \mathbf{A}_p & & \\ \mathbf{A}_q & \mathbf{I} & \\ \mathbf{I} & & \mathbf{I} \end{bmatrix} \begin{bmatrix} \hat{\mathbf{y}} \\ \mathbf{s} \\ \mathbf{t} \end{bmatrix} = \begin{bmatrix} \mathbf{b}_p - \mathbf{A}_p \mathbf{l} \\ \mathbf{b}_q - \mathbf{A}_q \mathbf{l} \\ \mathbf{u} - \mathbf{l} \end{bmatrix}, \quad \hat{\mathbf{y}} \geq \mathbf{0}, \mathbf{s} \geq \mathbf{0}, \mathbf{t} \geq \mathbf{0}$$

1928 By letting

$$1929 \quad \tilde{\mathbf{c}} := \begin{bmatrix} \mathbf{c} \\ \mathbf{0} \\ \mathbf{0} \end{bmatrix}, \quad \tilde{\mathbf{A}} := \begin{bmatrix} \mathbf{b}_p - \mathbf{A}_p \mathbf{l} \\ \mathbf{b}_q - \mathbf{A}_q \mathbf{l} \\ \mathbf{u} - \mathbf{l} \end{bmatrix}, \quad \tilde{\mathbf{b}} := \begin{bmatrix} \mathbf{b}_p - \mathbf{A}_p \mathbf{l} \\ \mathbf{b}_q - \mathbf{A}_q \mathbf{l} \\ \mathbf{u} - \mathbf{l} \end{bmatrix}, \quad \tilde{\mathbf{y}} := \begin{bmatrix} \hat{\mathbf{y}} \\ \mathbf{s} \\ \mathbf{t} \end{bmatrix}$$

1932 The problem is equivalently expressed in standard form as

$$1933 \quad \min_{\tilde{\mathbf{y}}} \tilde{\mathbf{c}}^\top \tilde{\mathbf{y}}, \quad \text{s.t. } \tilde{\mathbf{A}} \tilde{\mathbf{y}} = \tilde{\mathbf{b}}, \quad \tilde{\mathbf{y}} \geq \mathbf{0}.$$

1935 In fact, every LP can be rewritten in an equivalent standard form. While concepts such as basic
 1936 feasible solutions, degeneracy, and complementary slackness are most naturally and cleanly stated
 1937 in standard form, each admits a closely related analogue (with minor adjustments) for the general
 1938 form. Accordingly—without loss of generality and to keep the focus on core ideas—we carry out
 1939 the proof in the standard-form setting:

$$1940 \quad \min_{\mathbf{y}} \mathbf{c}^\top \mathbf{y}, \quad \text{s.t. } \mathbf{A} \mathbf{y} = \mathbf{b}, \quad \mathbf{y} \geq \mathbf{0},$$

1942 with dual

$$1943 \quad \min_{\mathbf{z}} \mathbf{b}^\top \mathbf{z}, \quad \text{s.t. } \mathbf{A}^\top \mathbf{z} \leq \mathbf{c}.$$

1944 Here, we follow the standard settings in the literature: $\mathbf{y}, \mathbf{c} \in \mathbb{R}^n$, $\mathbf{z}, \mathbf{b} \in \mathbb{R}^m$, $\mathbf{A} \in \mathbb{R}^{m \times n}$,
 1945 $\text{rank}(\mathbf{A}) = m$ (ensured by preprocessing with removing redundant equalities), and $m \leq n$. In
 1946 this context, we define the domain of LP that we work on:

$$1947 \quad \mathbb{X} := \{(\mathbf{A}, \mathbf{b}, \mathbf{c}) : \text{The resulting standard LP is feasible and bounded}\}$$

1949 Note that, to match the rest of the paper, we reserve \mathbf{x} for machine learning model inputs (in this
 1950 context, it is $\mathbf{x} = (\mathbf{A}, \mathbf{b}, \mathbf{c})$) and hence write the primal LP variable as \mathbf{y} and the dual LP variable as
 1951 \mathbf{z} . This departs from the common (\mathbf{x}, \mathbf{y}) convention. Note also that in the main text the symbol \mathbf{z}
 1952 denotes a latent variable; here, in the appendix regarding LP’s technical details, it denotes the dual
 1953 variable. These meanings are unrelated and should be clear from context.

1954 Now let’s present some definitions used in this appendix. Fix a *basis* by selecting an index set
 1955 $B \subset \{1, 2, \dots, n\}$ with $|B| = m$ such that the $m \times m$ submatrix $\mathbf{B} := \mathbf{A}[:, B]$ is *nonsingular*.
 1956 Let $N = \{1, 2, \dots, n\} \setminus B$ be the complement of the basis and let $\mathbf{N} := \mathbf{A}[:, N]$. Then the equality
 1957 constraints read

$$1958 \quad \mathbf{B}\mathbf{y}_B + \mathbf{N}\mathbf{y}_N = \mathbf{b}$$

1959 Setting $\mathbf{y}_N = \mathbf{0}$ yields $\mathbf{y}_B = \mathbf{B}^{-1}\mathbf{b}$. Such a $\mathbf{y} = [\mathbf{y}_B, \mathbf{0}]$ is called a *basic solution*. If additionally
 1960 $\mathbf{y}_B \geq \mathbf{0}$, this basic solution is feasible, then it is called a *basic feasible solution (BFS)*. On the dual
 1961 side, we define the slack variable \mathbf{s} and its sub-vector restricted to B and N :

$$1963 \quad \mathbf{s} := \mathbf{c} - \mathbf{A}^\top \mathbf{z}, \quad \mathbf{s}_B := \mathbf{c}_B - \mathbf{B}^\top \mathbf{z}, \quad \mathbf{s}_N := \mathbf{c}_N - \mathbf{N}^\top \mathbf{z}.$$

1964 A pair (\mathbf{y}, \mathbf{z}) is primal–dual optimal (i.e., satisfies KKT for LP) iff

$$1966 \quad \mathbf{A}\mathbf{y} = \mathbf{b}, \quad \mathbf{c} = \mathbf{A}^\top \mathbf{z} + \mathbf{s}, \quad \mathbf{y} \odot \mathbf{s} = \mathbf{0}, \quad \mathbf{y} \geq \mathbf{0}, \quad \mathbf{s} \geq \mathbf{0} \quad (34)$$

1968 for some $\mathbf{s} \in \mathbb{R}^n$. If, in addition, there exists a basis B such that

$$1969 \quad \mathbf{y}_B \geq \mathbf{0}, \quad \mathbf{y}_N = \mathbf{0}, \quad \mathbf{s}_B = \mathbf{0}, \quad \mathbf{s}_N \geq \mathbf{0}, \quad (35)$$

1971 then the tuple $(\mathbf{y}, \mathbf{z}, \mathbf{s})$ is called an optimal BFS with a complementary dual. By the fundamental
 1972 theorem of linear programming, any feasible instance with finite optimal value $(\mathbf{A}, \mathbf{b}, \mathbf{c}) \in \mathbb{X}$ admits
 1973 an optimal BFS with a complementary dual satisfying (34) and (35) together (Bertsimas & Tsitsiklis,
 1997).

1975 While conditions (34) and (35) are enough to ensure the existence of the optimal basic solutions,
 1976 they are not enough to ensure that the optimal solution is unique and local Lipschitz continuous w.r.t.
 1977 the inputs $(\mathbf{A}, \mathbf{b}, \mathbf{c})$. To ensure these points, we present two additional conditions based on (34) and
 1978 (35):

$$1979 \quad \mathbf{y}_B > \mathbf{0} \quad (\text{Non-degeneracy}) \quad (36)$$

$$1980 \quad \mathbf{s}_N > \mathbf{0} \quad (\text{Strict complementary slackness}) \quad (37)$$

1982 All the conditions together are enough to the uniqueness and local Lipschitz continuity. Let’s introduce
 1983 a set consisting of all “good” LP instances:

$$1984 \quad \mathbb{X}_{\text{sub}} := \{(\mathbf{A}, \mathbf{b}, \mathbf{c}) \in \mathbb{X} : \text{The LP yields a tuple } (\mathbf{y}, \mathbf{z}, \mathbf{s}) \text{ satisfying (34), (35), (36) and (37).}\}$$

1986 With all the preparations, we can prove Theorem 3.8 now. Actually, proving Theorem 3.8 in the
 1987 context of standard-form LP is equivalent to proving the following two theorems.

1988 **Theorem E.1.** *For any LP $(\mathbf{A}, \mathbf{b}, \mathbf{c}) \in \mathbb{X}_{\text{sub}}$, it must yield a unique optimal solution \mathbf{y}_* , and the
 1989 solution mapping $(\mathbf{A}, \mathbf{b}, \mathbf{c}) \mapsto \mathbf{y}_*$ is locally Lipschitz continuous everywhere on \mathbb{X}_{sub} .*

1990 **Theorem E.2.** \mathbb{X}_{sub} is a dense subset of \mathbb{X} .

1992 Theorem E.1 follows from Dontchev & Rockafellar (1996), which develops Robinson’s notion of
 1993 strong regularity (Robinson, 1980) for nonlinear programs. For completeness—and to keep notation
 1994 consistent with linear programming—we restate the relevant lemma in an LP-adapted form and then
 1995 verify its hypotheses for LP. We begin by quoting the result from Dontchev & Rockafellar (1996).

1996 **Lemma E.3** (Dontchev & Rockafellar (1996)). *Consider a parameteric nonlinear program:*

$$1997 \quad \min_{\mathbf{y} \in \mathbb{R}^n} \mathbf{c}^\top \mathbf{y} + g_0(\mathbf{w}, \mathbf{y})$$

1998 s.t. $g_i(\mathbf{w}, \mathbf{y}) = u_i, \quad 1 \leq i \leq r$
 1999 $g_i(\mathbf{w}, \mathbf{y}) \leq u_i, \quad r + 1 \leq i \leq d$
 2000
 2001 where $g_i(0 \leq i \leq d)$ are all \mathcal{C}^2 functions, and \mathbf{c}, \mathbf{w} and $\mathbf{u} = [u_1, \dots, u_d]^\top$ are parameters to
 2002 describe the program, and consider its Lagrangian with multipliers $\lambda = [\lambda_1, \dots, \lambda_d] \in \mathbb{R}^d$ given
 2003

$$L(\mathbf{w}, \mathbf{y}, \lambda) = g_0(\mathbf{w}, \mathbf{y}) + \sum_{i=1}^d \lambda_i g_i(\mathbf{w}, \mathbf{y}).$$

Let $(\bar{y}, \bar{\lambda})$ be a KKT point at $(\bar{c}, \bar{w}, \bar{u})$, and define the index sets at $(\bar{y}, \bar{\lambda})$

$$\begin{aligned} I_1 &= \left\{ r+1 \leq i \leq d : g_i(\bar{\mathbf{w}}, \bar{\mathbf{y}}) = u_i, \bar{\lambda}_i > 0 \right\} \cup \left\{ 1, \dots, r \right\}, \\ I_2 &= \left\{ r+1 \leq i \leq d : g_i(\bar{\mathbf{w}}, \bar{\mathbf{y}}) = u_i, \bar{\lambda}_i = 0 \right\}, \\ I_3 &= \left\{ r+1 \leq i \leq d : g_i(\bar{\mathbf{w}}, \bar{\mathbf{y}}) < u_i, \bar{\lambda}_i = 0 \right\}. \end{aligned}$$

If the following conditions hold:

- The constraint gradients $\nabla_{\bar{\mathbf{y}}} g_i(\bar{\mathbf{w}}, \bar{\mathbf{y}})$ for $i \in I_1 \cup I_2$ are linearly independent; and
- It holds that

$$\langle \mathbf{y}', \nabla_{\mathbf{y}\mathbf{y}}^2 L(\bar{\mathbf{w}}, \bar{\mathbf{y}}, \bar{\lambda}) \mathbf{y}' \rangle > 0$$

for all $\mathbf{y}' \neq \mathbf{0}$ in the subspace $\mathbb{M} = \left\{ \mathbf{y}' : \mathbf{y}' \perp \nabla_{\mathbf{y}} g_i(\bar{\mathbf{w}}, \bar{\mathbf{y}}) \text{ for all } i \in I_1 \right\}$,

then the KKT solution map $(\mathbf{c}, \mathbf{w}, \mathbf{u}) \mapsto (\mathbf{y}, \lambda)$ is locally single-valued and Lipschitz around $(\bar{\mathbf{c}}, \bar{\mathbf{w}}, \bar{\mathbf{u}}, \bar{\mathbf{y}}, \bar{\lambda})$.

Proof of Theorem E.1. Taking $r = m$ and $d = m + n$. Let \mathbf{a}_i^\top be the i -th row of \mathbf{A} in standard LP, and let

$$g_i(\mathbf{w}, \mathbf{y}) = \begin{cases} \mathbf{a}_i^\top \mathbf{y}, & i = 1, \dots, m, \\ -y_{i-m}, & i = m+1, \dots, m+n, \end{cases} \quad u_i = \begin{cases} b_i, & i = 1, \dots, m, \\ 0, & i = m+1, \dots, m+n, \end{cases}$$

with w collecting the coefficients of A . The Lagrangian in Lemma E.3 becomes

$$L(\mathbf{w}, \mathbf{y}, \lambda) = \mathbf{c}^\top \mathbf{y} + \sum_{i=1}^m \lambda_i \mathbf{a}_i^\top \mathbf{y} + \sum_{j=1}^n \lambda_{m+j} (-y_j).$$

Introduce the usual dual/primal-slack variables

$$z := -\lambda_{1:m} \in \mathbb{R}^m \quad \quad s := \lambda_{m+1:m+n} \in \mathbb{R}^n.$$

to rewrite stationarity as $\nabla_y L = c - A^\top z - s = 0$, i.e., $s = c - A^\top z$. Primal feasibility is $Ay = b$, $y \geq 0$; dual feasibility is $s \geq 0$; and complementarity is $y \odot s = 0$. Thus the KKT system in Lemma E.3 coincides with the standard LP KKT conditions.

Assume $(\mathbf{A}, \mathbf{b}, \mathbf{c}) \in \mathbb{X}_{\text{sub}}$, i.e., the LP admits a tuple $(\bar{\mathbf{y}}, \bar{\mathbf{z}}, \bar{\mathbf{s}})$ satisfying (34), (35), (36) and (37) (A nondegenerate and strict complementary basic point). In this context, the index sets I_1, I_2, I_3 at $(\bar{\mathbf{y}}, \bar{\mathbf{z}}, \bar{\mathbf{s}})$ become:

$$\begin{aligned}I_1 &= \{1, \dots, m\} \cup \{m + j : \bar{y}_j = 0, \bar{s}_j > 0\}, \\I_2 &= \{m + j : \bar{y}_j = 0, \bar{s}_j = 0\}, \\I_3 &= \{m + j : \bar{y}_i > 0, \bar{s}_j = 0\}.\end{aligned}$$

which implies:

- For each j , either $\bar{y}_j > 0$ or $\bar{s}_j > 0$, which implies $I_2 = \emptyset$.
- I_3 is substantially the basis set: $I_3 = \{m + j : j \in B\}$

2052 • I_1 includes all the indices in the complement of basis: $I_1 = \{1, \dots, m\} \cup \{m+j : j \in N\}$
 2053

2054 To verify the hypotheses of Lemma E.3, we examine the gradients:
 2055

$$2056 \quad \{\nabla_{\mathbf{y}} g_i\}_{i \in I_1} = \{\mathbf{a}_i\}_{i=1}^m \cup \{-\mathbf{e}_j\}_{j \in N}$$

2057 In the context of standard LP, $|N| = n - m$. Hence, $\{\nabla_{\mathbf{y}} g_i\}_{i \in I_1}$ consists of n vectors in \mathbb{R}^n . Now
 2058 we create a matrix \mathbf{G} by stacking these vectors as rows:
 2059

$$2060 \quad \mathbf{G} := \begin{bmatrix} \mathbf{a}_1^\top \\ \vdots \\ \mathbf{a}_m^\top \\ \mathbf{e}_{j_1}^\top \\ \vdots \\ \mathbf{e}_{j_{n-m}}^\top \end{bmatrix}$$

2066 By properly permuting the columns of \mathbf{G} , it becomes
 2067

$$2068 \quad \tilde{\mathbf{G}} = \begin{bmatrix} \mathbf{B} & \mathbf{N} \\ \mathbf{0} & \mathbf{I} \end{bmatrix}$$

2071 where \mathbf{I} represents the identity matrix in \mathbb{R}^{n-m} . Since \mathbf{B} (the basis matrix) and \mathbf{I} are both nonsingular,
 2072 $\tilde{\mathbf{G}}$ (and hence \mathbf{G}) must be nonsingular. Therefore, the rows of \mathbf{G} are linearly independent,
 2073 i.e., $\{\nabla_{\mathbf{y}} g_i\}_{i \in I_1}$ is linearly independent. With $I_2 = \emptyset$, the first hypothesis of Lemma E.3 holds.
 2074 Moreover, because these gradients $\{\nabla_{\mathbf{y}} g_i\}_{i \in I_1}$ span \mathbb{R}^n , the \mathbb{M} subspace must be trivial: $\mathbb{M} = \{\mathbf{0}\}$.
 2075 Therefore, the second hypothesis of Lemma E.3 is automatically satisfied.

2076 By Lemma E.3, the KKT solution map is locally single-valued and Lipschitz around the given
 2077 point, which yields the desired local uniqueness and Lipschitz dependence of \mathbf{y}_* on $(\mathbf{A}, \mathbf{b}, \mathbf{c})$ for
 2078 every $(\mathbf{A}, \mathbf{b}, \mathbf{c}) \in \mathbb{X}_{\text{sub}}$. \square
 2079

2080 Theorem E.2 can be proved by fundamental concepts in real analysis.
 2081

2082 *Proof of Theorem E.2.* To prove \mathbb{X}_{sub} is dense in \mathbb{X} , it's enough to show that: For any $(\mathbf{A}, \mathbf{b}, \mathbf{c}) \in \mathbb{X}$,
 2083 one can always create a sequence of LP $\{(\mathbf{A}_k, \mathbf{b}_k, \mathbf{c}_k)\}_{k \geq 1} \subset \mathbb{X}_{\text{sub}}$ such that

$$2084 \quad \mathbf{A}_k \rightarrow \mathbf{A}, \quad \mathbf{b}_k \rightarrow \mathbf{b}, \quad \mathbf{c}_k \rightarrow \mathbf{c}.$$

2086 Now let's fix $(\mathbf{A}, \mathbf{b}, \mathbf{c}) \in \mathbb{X}$. As we previously discussed, there must be a tuple $(\mathbf{y}, \mathbf{z}, \mathbf{s})$ satisfying
 2087 (34) and (35). Define:
 2088

$$2089 \quad \mathbf{y}_k := \mathbf{y} + \frac{1}{k} \mathbf{e}_B, \quad \mathbf{s}_k := \mathbf{s} + \frac{1}{k} \mathbf{e}_N, \quad \mathbf{z}_k := \mathbf{z}$$

2091 so that $(\mathbf{y}_k, \mathbf{z}_k, \mathbf{s}_k)$ must satisfy the nondegeneracy and strict complementary slackness: (35), (36),
 2092 and (37). Accordingly, define
 2093

$$2094 \quad \mathbf{A}_k := \mathbf{A}, \quad \mathbf{b}_k := \mathbf{A}_k \mathbf{y}_k, \quad \mathbf{c}_k := \mathbf{A}_k^\top \mathbf{z}_k + \mathbf{s}_k$$

2095 Then one can verify that the tuple $(\mathbf{y}, \mathbf{z}, \mathbf{s})$ satisfies (34), (35), (36) and (37) for the LP instance
 2096 $(\mathbf{A}_k, \mathbf{b}_k, \mathbf{c}_k)$, hence $(\mathbf{A}_k, \mathbf{b}_k, \mathbf{c}_k) \in \mathbb{X}_{\text{sub}}$ for all $k \geq 1$. Finally, such a perturbed LP instance can be
 2097 arbitrarily close to $(\mathbf{A}, \mathbf{b}, \mathbf{c})$ as $k \rightarrow \infty$:
 2098

$$2099 \quad \|\mathbf{A}_k - \mathbf{A}\| = 0$$

$$2100 \quad \|\mathbf{b}_k - \mathbf{b}\| = \left\| \mathbf{A} \left(\frac{1}{k} \mathbf{e}_B \right) \right\| \leq \frac{1}{k} \|\mathbf{A}\| \|\mathbf{e}_B\| = \frac{\sqrt{m}}{k} \|\mathbf{A}\| \rightarrow 0$$

$$2102 \quad \|\mathbf{c}_k - \mathbf{c}\| = \left\| \frac{1}{k} \mathbf{e}_N \right\| = \frac{\sqrt{n-m}}{k} \rightarrow 0$$

2104 which finishes the proof. \square
 2105

2106 **F TRAINING STRATEGIES**
 2107

2108 **Unrolling vs implicit differentiation.** There are two training strategies adopted in this paper. One
 2109 is named “unrolling” (minimizing $\ell(\mathbf{y}_T)$):

$$2110 \quad \min_{\theta} \ell(\mathbf{y}_T), \quad \mathbf{y}_{t+1} = \mathcal{G}_{\theta}(\mathbf{y}_t, \mathbf{x}), \quad t = 0, 1, 2, \dots, T-1$$

2112 and the other is named “implicit differentiation” (minimizing $\ell(\mathbf{y}_*)$):

$$2114 \quad \min_{\theta} \ell(\mathbf{y}_*), \quad \mathbf{y}_* = \mathcal{G}_{\theta}(\mathbf{y}_*, \mathbf{x}).$$

2115 These two strategies are closely related. In particular,

- 2117 • As established in prior literature, unrolled training is mathematically equivalent to a Neumann
 2118 series approximation of the implicit gradient (Geng et al., 2021). Specifically, implicit differ-
 2119 entiation requires inverting the Jacobian $(\mathbf{I} - \mathbf{J}_{\mathcal{G}_{\theta}})^{-1}$; finite unrolling effectively approximates
 2120 this inverse via a Neumann series expansion. This is a widely adopted technique in the implicit
 2121 model community to avoid the instability and cost of exact inversion.
- 2122 • Implicit training is simply the limit of unrolled training: as $T \rightarrow \infty$, the gradient $\nabla_{\theta} \ell(\mathbf{y}_T)$
 2123 converges to the implicit gradient $\nabla_{\theta} \ell(\mathbf{y}_*)$ (Geng et al., 2021).

2124 Overall, unrolling and root-finding are merely two numerical implementations for approximating
 2125 the same fixed point, $\mathbf{y}_*(\mathbf{x})$, and technically speaking, there is no significant gap or distinction
 2126 between the two. Theoretically, infinite unrolling converges exactly to $\mathbf{y}_*(\mathbf{x})$. In practice, unrolling
 2127 depth simply controls the trade-off between accuracy and computational cost: a dynamic strictly
 2128 analogous to setting the error tolerance in implicit root-finding solvers.

2129 Particularly in our paper, for Case Studies 1 & 2, we employ implicit differentiation (minimizing
 2130 $\ell(\mathbf{y}_*)$) via root-finding; for Case Study 3, we adopt unrolling to train implicit GNNs, which serves
 2131 as a truncated Neumann approximation of the implicit GNN gradient; for Case Study 4, we directly
 2132 use the pretrained model from Geiping et al. (2025).

2134 **Guarantees of Regularity and the Expressivity Trade-off.** While our experiments demonstrate
 2135 that standard training (either unrolling and implicit differentiation defined above) empirically results
 2136 in regular implicit operators, *we do not explicitly enforce this property in the loss function*. Designing
 2137 training mechanisms that theoretically guarantee regularity without sacrificing the model’s unique
 2138 expressive capabilities remains an open and interesting future topic.

2139 Recall that regularity (Definition 2.3) comprises two conditions: the Lipschitz continuity of the
 2140 map $\mathbf{x} \mapsto \mathcal{G}_{\theta}(\mathbf{y}, \mathbf{x})$ and the contractivity of the map $\mathbf{y} \mapsto \mathcal{G}_{\theta}(\mathbf{y}, \mathbf{x})$. The first condition is largely
 2141 inherent to standard deep learning architectures; compositions of affine layers with bounded weights
 2142 and 1-Lipschitz activations (e.g., ReLU) naturally preserve Lipschitz continuity with respect to the
 2143 input Miyato et al. (2018); Virmaux & Scaman (2018). Therefore, the critical challenge lies in
 2144 guaranteeing the second condition: contractivity with respect to the state \mathbf{y} .

2145 A substantial body of literature has sought to enforce this contractivity by construction (e.g.,
 2146 El Ghaoui et al. (2021); Winston & Kolter (2020); Jafarpour et al. (2021); Revay et al. (2020);
 2147 Havens et al. (2023)). These approaches typically impose rigid structural constraints, such as pa-
 2148 rameterizing the model as a one-layer nonlinear MLP: $\mathcal{G}_{\theta}(\mathbf{y}, \mathbf{x}) = \sigma(\mathbf{A}\mathbf{y} + \mathbf{B}\mathbf{x} + \mathbf{b})$ and strictly
 2149 bounding the spectral norm of \mathbf{A} , or enforcing global monotonicity.

2150 However, these methods generally enforce a *uniform* contraction modulus μ across the entire domain
 2151 $\mathbf{x} \in \mathbb{X}$. Our theoretical analysis suggests that such uniformity fundamentally undercuts the unique
 2152 expressive advantage of implicit models. As illustrated in Figure 1, for a sequence of continuous
 2153 iterates $\mathbf{y}_t(\mathbf{x})$ to converge to a target $\mathcal{F}(\mathbf{x})$ that is discontinuous or has singularities, the conver-
 2154 gence *cannot* be uniform. This implies that the convergence rate—and consequently the operator’s
 2155 contraction modulus $\mu(\mathbf{x})$ —must be adaptive, varying with \mathbf{x} to allow for slower convergence in
 2156 complex regions. Enforcing a globally uniform μ severs this adaptive capability, thereby severely
 2157 constraining the model’s expressive power.

2158 Therefore, developing novel regularization techniques that can guarantee *adaptive* contractivity (en-
 2159 suring $0 < \mu(\mathbf{x}) < 1$ locally while allowing it to vary over \mathbf{x}) is a critical direction for future
 research to balance theoretical stability with maximal expressivity.

2160 **G EXPERIMENT DETAILS REGARDING IMAGE RECONSTRUCTION**
2161

2162 This section complements the main text with additional implementation and dataset details for the
2163 inverse-problem experiments.

2164 **Experiment settings.** We consider an image deblurring task, $\mathbf{x} = \mathbf{A}(\mathbf{y}_*) + \mathbf{n}$, where \mathbf{A} is the
2165 blur operator and \mathbf{n} is the Gaussian noise ($\sigma = 0.03$). We use a motion-blur operator, and the
2166 blur kernel is the first of the eight kernels from Levin et al. (2009). Ground-truth images \mathbf{y}_* come
2167 from BSDS500 (Martin et al., 2001). We follow the official splits (200 train / 100 validation / 200
2168 test) and apply a random 128×128 crop to each image. For each \mathbf{y}_* , we generate the corresponding
2169 \mathbf{x} by applying \mathbf{A} and adding noise. The resulting pairs $(\mathbf{x}, \mathbf{y}_*)$ form three datasets $\mathbb{D}_{\text{inv,train}}$,
2170 $\mathbb{D}_{\text{inv,valid}}$, and $\mathbb{D}_{\text{inv,test}}$ for training, validation, and testing, respectively. In both PGD and HQS style
2171 parameterizations ((5) and (6)), the operator \mathcal{H} is implemented with DRUNet (Zhang et al., 2021).

2172 **Training.** We initialize \mathcal{H} using pretrained weights from the Deepinv library (Tachella et al., 2025)
2173 and then fine-tune the full implicit models on the BSDS500 training set for this deblurring task.
2174 Training follows the vanilla Jacobian-based implicit differentiation and is implemented on top of the
2175 official Deepinv framework. All models were trained with Adam (learning rate 10^{-4} , batch size 3).
2176 Explicit baselines were trained for 20 epochs, and the implicit models for 10 epochs. After each
2177 epoch we evaluated on the validation set and saved the checkpoint; the final model used for testing
2178 is the one with the lowest validation loss. These epoch budgets were sufficient for validation-loss
2179 convergence.

2180 **PSNR.** PSNR (Peak Signal-to-Noise Ratio) is defined between a reference \mathbf{y}^* and reconstructed
2181 image \mathbf{y} as

2182
$$\text{PSNR}(\mathbf{y}, \mathbf{y}^*) := 10 \log_{10} \left(\frac{n \cdot \text{MAX}^2}{\|\mathbf{y} - \mathbf{y}^*\|^2} \right)$$
2183

2184 where n is the dimension of \mathbf{y} and \mathbf{y}^* , and MAX means the max possible pixel value (e.g., 255 for
2185 8-bit, or 1 if images are in $[0, 1]$. In our context, it is 1. Higher PSNR means better (more accurate)
2186 reconstruction.

2187 **Standard test set.** Evaluation uses the 200 images from the official BSDS500 test split, randomly
2188 cropped to 128×128 . Let $\mathbb{D}_{\text{inv,test}} = \{(\mathbf{x}_i, \mathbf{y}_i^*)\}_{i=1}^{200}$, where

2189
$$\mathbf{x}_i = \mathbf{A}(\mathbf{y}_i^*) + \mathbf{n}_i, \quad \mathbf{n}_i \sim \mathcal{N}(\mathbf{0}, \sigma^2 \mathbf{I}), \quad \sigma = 0.03.$$

2190 Here \mathbf{y}_i^* denotes the clean (ground-truth) image and \mathbf{x}_i its corresponding blurred-noisy observation
2191 under the forward model \mathbf{A} .

2192 **Perturbed test set.** To empirically validate our theory, we created a perturbed version of the test
2193 set. To create a diverse and representative set of perturbations, we generate perturbations that
2194 correspond to different frequency levels. Image frequencies represent different levels of detail, where
2195 low frequencies capture smooth, large-scale areas, and high frequencies capture sharp edges and fine
2196 textures. By probing the model with perturbations across this spectrum, we can comprehensively
2197 evaluate its behavior.

2198 Specifically, we construct each perturbation by targeting a singular vector of the forward operator
2199 \mathbf{A} . Because \mathbf{A} is (circular) convolution, its singular vectors are Fourier modes. For each image
2200 \mathbf{y}_i^* and each frequency magnitude $f \in \{0.1, 0.3, 0.5, 0.7, 0.9\}$, we first identify the 2D discrete
2201 Fourier frequencies and sort them by their geometric distance from the origin. We then select the
2202 frequency coordinate (u, v) at the f -th percentile of this sorted list. A one-hot tensor is created in
2203 the Fourier domain with a value of 1.0 at the chosen (u, v) position and zeros elsewhere. This sparse
2204 frequency representation is transformed back into the image domain by applying the adjoint of the
2205 blur operator, \mathbf{A}^\top . These perturbations are visualized in Figure 9. Adding them to \mathbf{y}_i^* respectively
2206 yields perturbed clean images $\mathbf{y}_{i,j}^*$ ($j = 1, \dots, 5$); we then form the corresponding observation

2207
$$\mathbf{x}_{i,j} = \mathbf{A}(\mathbf{y}_{i,j}^*) + \mathbf{n}_i, \quad \mathbf{n}_i \sim \mathcal{N}(\mathbf{0}, \sigma^2 \mathbf{I}).$$

2208 The perturbed evaluation set is

2209
$$\mathbb{D}'_{\text{inv,test}} = \{(\mathbf{x}_{i,j}, \mathbf{y}_{i,j}^*) : 1 \leq i \leq 200, 1 \leq j \leq 5\}.$$

2210 For convenience we also define the unperturbed index $j = 0$ by $\mathbf{x}_{i,0} := \mathbf{x}_i$ and $\mathbf{y}_{i,0}^* := \mathbf{y}_i^*$.

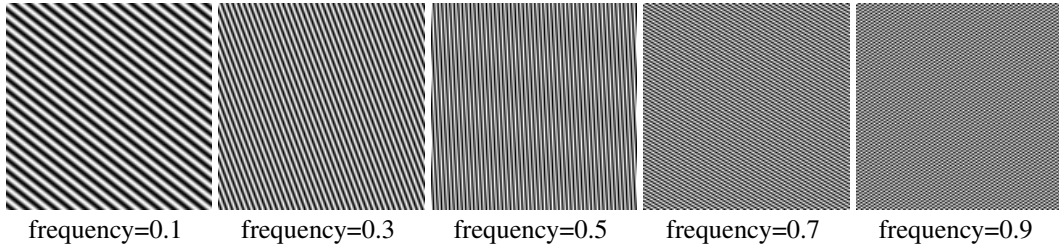


Figure 9: Visualized perturbations for inverse problems.

Table 3: Deeper explicit models vs implicit models for image deblurring (PGD architecture). “Exp ($\times T$)” represents an explicit model T times deeper than the implicit baseline. O/M denotes CUDA Out of Memory during training.

	Exp ($\times 1$)	Exp ($\times 2$)	Exp ($\times 4$)	Exp ($\times 8$)	Exp ($\times 16$)	Exp ($\times 32$)	Implicit
Params.	32.641 M	65.282 M	130.56 M	261.13 M	522.26 M	1044.5 M	32.641 M
PSNR	27.14 dB	27.64 dB	27.89 dB	28.11 dB	28.27 dB	O/M	28.21 dB

Table 4: Deeper explicit models vs implicit models for image deblurring (HQS architecture). “Exp ($\times T$)” represents an explicit model T times deeper than the implicit baseline. O/M denotes CUDA Out of Memory during training.

	Exp ($\times 1$)	Exp ($\times 2$)	Exp ($\times 4$)	Exp ($\times 8$)	Exp ($\times 16$)	Exp ($\times 32$)	Implicit
Params.	32.641 M	65.282 M	130.56 M	261.13 M	522.26 M	1044.5 M	32.641 M
PSNR	26.94 dB	28.02 dB	28.35 dB	28.69 dB	28.87 dB	O/M	29.18 dB

Platform. All experiments were run on a workstation with eight Quadro RTX 6000 GPUs.

Additional Experiments. Implicit models often excel on imaging tasks, but a natural question is whether simply stacking more explicit layers (i.e., deepening the model) can close the gap. To probe this, we construct explicit counterparts to implicit models by untying the parameters across iterations:

$$\min_{\Theta} \mathbb{E}_{\mathbf{x}} \ell(\mathbf{y}_T, \mathbf{y}_*), \quad \text{s.t. } \mathbf{y}_t = \mathcal{G}_{\Theta^{(t)}}(\mathbf{y}_{t-1}, \mathbf{x}), \quad t = 1, \dots, T$$

where each block $\mathcal{G}_{\Theta^{(t)}}$ has the same architecture as in the implicit case (PGD or HQS), but $\Theta^{(t)}$ are separate for each t . This is equivalent to stacking T blocks to form a deeper explicit model with more learnable parameters. Unlike implicit models (which can use different iteration counts at train vs. test), these explicit models must use the same T for both training and testing. We evaluated $T \in \{1, 2, 4, 8, 16, 32\}$ to compare against the corresponding implicit models.

Tables 3 and 4 report results on image deblurring. Across both PGD and HQS settings, deepening explicit models increases parameter counts massively (up to ~ 1 billion) but yields diminishing returns in PSNR. Crucially, the implicit models achieve performance comparable to or better than explicit models that are $16\times$ deeper, while using a fraction of the parameters (32.6 M vs. 522 M). For instance, in the HQS setting, the implicit model (29.18 dB) outperforms the explicit model with 16 unrolled blocks (28.87 dB).

Furthermore, training extremely deep explicit models (e.g., $T = 32$) becomes infeasible due to memory constraints (O/M). This highlights the distinct efficiency advantage of the weight-tied implicit approach: it theoretically allows for infinite depth (realized here as 100 test-time iterations) while maintaining constant parameter counts (32.6 M) and memory usage.

H EXPERIMENT DETAILS REGARDING SCIENTIFIC COMPUTING

Model structure and training. Given cell-averaged forces $\mathbf{x} \in \mathbb{R}^{H \times W \times 2}$ and vorticities $\mathbf{y} \in \mathbb{R}^{H \times W \times 1}$, where H means the height and W means the width, we learn

$$\mathbf{z}_* = \mathcal{G}_{\Theta}(\mathbf{z}_*, \mathcal{Q}_{\Phi}(\mathbf{x})), \quad \mathbf{y}_* = \mathcal{Q}_{\Psi}(\mathbf{z}_*),$$

2268 where $\mathbf{z}_* \in \mathbb{R}^{H \times W \times C}$ is a latent field with C channels. At inference, we iterate
 2269

$$\mathbf{z}_t = \mathcal{G}_\Theta(\mathbf{z}_{t-1}, \mathcal{Q}_\Phi(\mathbf{x})),$$

2271 for $1 \leq t \leq T$ and finally call $\mathbf{y}_T = \mathcal{Q}_\Phi(\mathbf{z}_T)$.
 2272

2273 The projection \mathcal{Q}_Φ is a *pointwise* linear encoder applied at each grid cell to lift into C channels. In
 2274 particular, $\mathbf{g} = \mathcal{Q}_\Phi(\mathbf{x})$ reads

$$\mathbf{g} = \mathbf{W}_1 \mathbf{x} + \mathbf{b}_1 \in \mathbb{R}^{H \times W \times C}$$

2275 where $\Phi = (\mathbf{W}_1, \mathbf{b}_1)$ are learnable parameters.
 2276

2277 The core map $\mathcal{G}_\Theta(\mathbf{z}, \mathbf{g})$ stacks L identical FNO layers with input injection:
 2278

$$\mathbf{z}^{(0)} = \mathbf{z}$$

$$\mathbf{z}^{(l)} = \sigma \left(\mathbf{g} + \mathbf{W}_2^{(l)} \mathbf{z}^{(l-1)} + \mathbf{b}_2^{(l)} + \text{IFFT}(\mathbf{R}^{(l)} \cdot \text{FFT}(\mathbf{z}^{(l-1)})) \right), \quad l = 1, 2, \dots, L,$$

$$\mathcal{G}_\Theta(\mathbf{z}, \mathbf{g}) = \mathbf{z}^{(L)}$$

2284 where $\Theta = \{\mathbf{W}_2^{(l)}, \mathbf{b}_2^{(l)}, \mathbf{R}^{(l)}\}_{l=1}^L$ are learnable parameters. Each layer: (i) performs a global spec-
 2285 tral convolution on \mathbf{z} : take an FFT of the C -channel tensor, keep only a small set of low Fourier
 2286 modes. Suppose the number of retained Fourier modes is $K \times K$ (2D FFT), $\text{FFT}(\mathbf{z}) \in \mathbb{C}^{K \times K \times C}$.
 2287 For each retained mode (k_1, k_2) multiply the C -dimensional channel vector by a learnable dense ma-
 2288 trix $\mathbf{R}_{k_1, k_2}^{(l)} \in \mathbb{C}^{C \times C}$ (mixing channels) and hence the overall matrix is of size $\mathbf{R}^{(l)} \in \mathbb{C}^{K \times K \times C \times C}$,
 2289 then apply an inverse FFT; (ii) adds a local pointwise transform, adds the injected encoder features
 2290 $\mathcal{Q}_\Phi(\mathbf{x})$, and applies a nonlinearity. This realizes a resolution-invariant, globally receptive operator
 2291 that naturally respects periodic boundary conditions.

2292 Finally, we decode with the pointwise readout \mathcal{Q}_Ψ (a small per-cell two-layer MLP) to produce
 2293 $\mathbf{y} \in \mathbb{R}^{H \times W \times 1}$ where Ψ are learnable parameters.
 2294

2295 All samples use $H = W = 128$. Unless stated otherwise, we set the latent width $C = 32$, retain
 2296 $K = 12$ Fourier modes per dimension in the FNO blocks, and use $L = 3$ FNO layers inside \mathcal{G}_Θ .
 2297 Training differentiates implicitly through the fixed point, and the fixed-point solver uses Anderson
 2298 acceleration. We optimize with Adam (learning rate 5×10^{-3} , batch size 16). For explicit baselines,
 2299 we train for 500 epochs, which suffices for the training loss to converge.

2300 **Perturbed data generation.** In this paragraph, we describe how we generate perturbed samples
 2301 in $\mathbb{D}'_{\text{pde,test}}$. We take the dataset of Marwah et al. (2023) as the unperturbed set $\mathbb{D}_{\text{pde,test}}$ and create
 2302 perturbations by linearizing the steady NS equation (7). Each sample (f, ω) comprises a forcing
 2303 term f and its vorticity solution ω . Directly prescribing f and solving for ω is computationally
 2304 costly; following Marwah et al. (2023), we instead prescribe ω and obtain the corresponding f by
 2305 evaluating the PDE operator (not by solving the PDE). In our setting, the base samples are given;
 2306 thus we first construct a solution perturbation $\delta\omega$ and then compute the induced forcing perturbation
 2307 δf via the linearization, yielding the perturbed pair $(f + \delta f, \omega + \delta\omega)$.
 2308

2309 Note that, while the dataset is discrete, we use the continuous notation f, ω, u in this section to ease
 2310 reading and to remain consistent with the PDE literature. In addition, we use $\xi = (\xi_1, \xi_2)$ as the
 2311 special domain variable to keep consistent with our main text, and use $k = (k_1, k_2)$ as the frequency
 2312 domain variable.
 2313

(Generate $\delta\omega$). Fix a target wavenumber $k_* \in \mathbb{N}$ and a desired L^2 -magnitude $\eta > 0$. We construct
 2314 $\delta\omega$ by

$$\delta\omega(\xi_1, \xi_2) = A \sin(k_* \xi_1 + k_* \xi_2), \quad A \text{ chosen so that } \|\delta\omega\|_{L^2(\Omega)} = \eta.$$

2315 The wavenumber is selected from a user-specified frequency percentile p_{freq} relative to the maxi-
 2316 mum resolvable frequency $k_{\text{max}} = H/2 = W/2$, namely

$$k_* = p_{\text{freq}} \times k_{\text{max}} \quad (\text{rounded to the nearest integer mode}).$$

2317 In our code we set the grid size $H = W = 128$, the perturbation strength $\eta = 0.01$, and choose
 2318

$$p_{\text{freq}} \in \{0.01, 0.02, 0.03, 0.04, 0.05, 0.1, 0.3, 0.5, 0.7, 0.9, 0.95, 0.96, 0.97, 0.98, 0.99\}.$$

2319 Accordingly, each original sample yields 15 perturbed samples.
 2320

2322 Table 5: Implicit FNO vs deeper Explicit FNO. “ $\text{Exp}(\times l)$ ” denotes an explicit model that is l times
 2323 deeper than the implicit FNO. O/M indicates a CUDA out-of-memory error during training.

	Exp($\times 1$)	Exp($\times 2$)	Exp($\times 4$)	Exp($\times 8$)	Exp($\times 16$)	Exp($\times 32$)	Implicit
Params.	2.376 M	4.155 M	7.713 M	14.83M	29.06M	57.52M	2.376 M
Rel. Err.	0.1787	0.1526	0.1410	0.1380	0.1360	O/M	0.0785

2329 Table 6: Implicit FNO vs wider Explicit FNO. “ $\text{Exp}(\times w)$ ” denotes an explicit model that is w times
 2330 wider than the implicit FNO. O/M indicates a CUDA out-of-memory error during training.

	Exp($\times 1$)	Exp($\times 2$)	Exp($\times 4$)	Exp($\times 8$)	Implicit
Params.	2.376 M	9.504 M	38.01 M	152.0M	2.376 M
Rel. Err.	0.1787	0.1555	0.1401	O/M	0.0785

2337 (Generate velocity from vorticity). Given a scalar vorticity field ω (and its perturbation $\delta\omega$), we
 2338 recover the corresponding velocities u via a streamfunction ψ given by

$$u = (\partial_2\psi, -\partial_1\psi), \quad \omega = -\Delta\psi.$$

2341 Hence ψ is obtained by solving the Poisson equation $\Delta\psi = -\omega$, after which we obtain u . On a
 2342 periodic grid, these operators are implemented efficiently in the Fourier domain.

2343 (Linearization and the perturbed vorticity forcing δg). Applying the (scalar) curl “ $\nabla \times$ ” to both sides
 2344 of (7) yields the steady vorticity form

$$(u \cdot \nabla) \omega - \nu \Delta \omega = g, \quad g = \nabla \times f = \partial_1 f_2 - \partial_2 f_1,$$

2348 where $f = (f_1, f_2)$ is the body force and g is its curl. Introducing perturbations $(\delta u, \delta\omega, \delta g)$ and
 2349 expanding

$$(u + \delta u) \cdot \nabla (\omega + \delta\omega) - \nu \Delta (\omega + \delta\omega) = g + \delta g,$$

2351 then subtracting the base equation and discarding higher-order terms gives the first-order relation

$$\delta g = (u \cdot \nabla) \delta\omega + (\delta u \cdot \nabla) \omega - \nu \Delta \delta\omega.$$

2355 Again, for numerical implementation on a periodic grid, the differential operators are applied effi-
 2356 ciently in the Fourier domain.

2357 (Recover the vector force δf from its curl δg). We recover a periodic $\delta f = (\delta f_1, \delta f_2)$ satisfying
 2358 $\nabla \times \delta f = \delta g$ by solving a Poisson equation for an auxiliary streamfunction ψ and obtain δf exactly
 2359 as in “Generate velocity from vorticity.”

2360 **Additional Experiments: Scaling Explicit Models.** A natural question is whether the performance
 2361 gap between implicit and explicit models can be bridged simply by scaling up the explicit architec-
 2362 ture (i.e., stacking more layers or increasing channel width). To investigate this, we compared the
 2363 implicit FNO against explicit baselines scaled significantly in two dimensions: depth (up to $32\times$)
 2364 and width (up to $8\times$). The results, summarized in Table 5 and Table 6, demonstrate that while
 2365 scaling explicit models yields modest accuracy gains, it faces severe diminishing returns and com-
 2366 putational bottlenecks (eventually leading to CUDA Out-of-Memory errors). Crucially, the implicit
 2367 model achieves markedly better performance (lowest relative error of 0.0785) than even the largest
 2368 viable explicit models, despite the explicit counterparts using over $10\times$ the number of parameters
 2369 (e.g., 29.06 M for $\text{Exp}(\times 16)$ vs. 2.376 M for Implicit). This confirms that the implicit formulation
 2370 provides an expressive advantage that cannot be efficiently replicated by simply allocating more
 2371 capacity to an explicit solver.

2372 Note: These findings are broadly consistent with Marwah et al. (2023). We follow their setup with
 2373 two minor deviations: we use a smaller training batch size (16) due to hardware limits, and while
 2374 we keep $T = 24$ training iterations for the implicit model, at inference we run $T = 50$, because we
 2375 observe that the trained implicit models remain stable and often benefit from additional fixed-point
 iterations at test time.

2376 **I EXPERIMENT DETAILS REGARDING LP**
 2377

2378 **GNN model details.** We implement (9):
 2379

$$z_* = \mathcal{G}_\Theta(z_*, \mathcal{Q}_\Phi(x)), \quad y_* = \mathcal{Q}_\Psi(z_*)$$

2381 with an L -layer message-passing GNN (Scarselli et al., 2008; Xu et al., 2019) on the bipartite graph.
 2382 Let $\mathcal{N}(i)$ (resp. $\mathcal{N}(j)$) be the neighbors of constraint node W_i (resp. variable node V_j). With shared
 2383 MLPs across all nodes and edges, the GNN structure is given by:
 2384

$$\begin{aligned} \text{Input-embedding:} \quad W_i^{(0)} &= \text{MLP}_{\phi_1}(b_i, \circ_i), \\ V_j^{(0)} &= \text{MLP}_{\phi_2}(c_j, l_j, u_j, z_{\text{in},j}) \\ \text{Message-passing } (1 \leq l \leq L-1): \quad W_i^{(l)} &= \text{MLP}_{\theta_1^{(l)}} \left(W_i^{(l)}, \sum_{j \in \mathcal{N}(i)} A_{ij} \cdot \text{MLP}_{\theta_2^{(l)}}(V_j^{(l-1)}) \right), \\ V_j^{(l)} &= \text{MLP}_{\theta_3^{(l)}} \left(V_j^{(l)}, \sum_{i \in \mathcal{N}(j)} A_{ij} \cdot \text{MLP}_{\theta_4^{(l)}}(W_i^{(l-1)}) \right) \\ \text{Output-embedding:} \quad z_{\text{out},j} &= \text{MLP}_{\theta_5}(V_j^{(L)}) \end{aligned}$$

2385 We write this compactly as follows.
 2386

$$z_{\text{out}} = \mathcal{G}_\Theta(z_{\text{in}}, \mathcal{Q}_\Phi(x))$$

2387 where $\Theta = \{\{\theta_1^{(l)}\}_{l=1}^{L-1}, \{\theta_2^{(l)}\}_{l=1}^{L-1}, \{\theta_3^{(l)}\}_{l=1}^{L-1}, \{\theta_4^{(l)}\}_{l=1}^{L-1}, \theta_5\}$ are trainable parameters in the GNN,
 2388 $\Phi = \{\phi_1, \phi_2\}$ includes the trainable parameters of the input embedding. The input x includes all
 2389 static information $x := (A, b, c, \circ, l, u)$. Finally, the output embedding $y = \mathcal{Q}_\Psi(z)$ is given by
 2390

$$y_j = \text{MLP}_\Psi(z_j)$$

2391 for every variable node j . All MLPs in \mathcal{G}_Θ , \mathcal{Q}_Φ , and \mathcal{Q}_Ψ use two layers with ReLU activations. We
 2392 sweep widths (or embedding sizes) in $\{4, 8, 16, 32\}$ and report results in the main text.
 2393

2394 Note that l is the layer index within the GNN structure, not the iteration number t . All parameters
 2395 in Θ are independent of the iteration number, so this GNN can be applied iteratively. x is the static
 2396 features and z is the dynamic feature. In addition, removing the dynamic input z_{in} and decoding
 2397 directly to y recovers the standard (explicit) GNN baseline.
 2398

2399 **Dataset generation.** We largely follow Chen et al. (2023) to construct the training set $\mathbb{D}_{\text{LP,train}}$ and
 2400 test set $\mathbb{D}_{\text{LP,test}}$, drawing (A, b, c, \circ, l, u) i.i.d. from the same distribution. Each LP has 50 variables
 2401 and 10 constraints. The matrix A is sparse with 100 nonzeros whose locations are chosen uniformly
 2402 at random and whose values are sampled from a standard normal distribution. Entries of b and c are
 2403 sampled i.i.d. from $\text{Unif}[-1, 1]$, after which c is scaled by 0.01. Variable bounds l, u are sampled
 2404 coordinatewise from $\mathcal{N}(0, 10)$; whenever $l_j > u_j$ we swap them. Constraint types are sampled
 2405 independently with $\Pr(\circ_i = "\leq") = 0.7$ and $\Pr(\circ_i = "=") = 0.3$. Under this generator, the
 2406 feasibility probability is approximately 0.53; we retain only feasible instances, yielding 2,500 LPs
 2407 for training and 1,000 for testing. Solutions are computed with `scipy.optimize`.
 2408

2409 To build the perturbed datasets $\mathbb{D}_{\text{LP,test}}^{(j)}$, we perturb one component at a time while holding the others
 2410 fixed. For c , draw δc with i.i.d. standard normal entries, normalize, and scale to magnitude 10^{-4} :
 2411

$$c' = c + 10^{-4} \times \frac{\delta c}{\|\delta c\|}.$$

2412 We apply the same procedure to b , l , and u . For A , we perturb only existing nonzeros to preserve
 2413 the sparsity pattern: let $\mathbb{S} = \{(i_k, j_k)\}_{k=1}^{\text{nnz}(A)}$ be the nonzero locations and draw $\delta a \in \mathbb{R}^{|\mathbb{S}|}$ i.i.d.
 2414 standard normal; normalize and scale so $\|\delta a\| = 10^{-4}$, then set
 2415

$$A'_{i_k, j_k} = A_{i_k, j_k} + (\delta a)_k \text{ for } (i_k, j_k) \in \mathbb{S}, \quad A'_{i, j} = A_{i, j} \text{ otherwise.}$$

2430 This yields five perturbed versions (perturbing \mathbf{A} , \mathbf{b} , \mathbf{c} , \mathbf{l} , or \mathbf{u} separately). We evaluate the estimated
 2431 Lipschitz constants L_t and relative errors E_t on each version and report the results in the main text.
 2432

2433 **Training method.** To train our implicit GNNs, we employ a two-stage curriculum strategy. The
 2434 model is trained by unrolling its iterative updates for a fixed number of steps, T , and minimizing the
 2435 loss on the final output:

$$\begin{aligned} 2436 \quad & \min_{\Theta, \Phi, \Psi} \sum_{(\mathbf{x}, \mathbf{y}_*) \in \mathbb{D}_{\text{LPtrain}}} \ell(\mathbf{y}_T, \mathbf{y}_*) \\ 2437 \\ 2438 \quad & \text{s.t. } \mathbf{z}_0 = \mathbf{0} \\ 2439 \\ 2440 \quad & \mathbf{z}_t = \mathcal{G}_\Theta(\mathbf{z}_{t-1}, \mathcal{Q}_\Phi(\mathbf{x})), \quad t = 1, 2, \dots, T \\ 2441 \\ 2442 \quad & \mathbf{y}_T = \mathcal{Q}_\Psi(\mathbf{z}_T) \end{aligned}$$

2442 We set the final unroll horizon to $T = 6$, as we observed no significant improvements with longer
 2443 sequences. Training directly with $T = 6$ is inefficient, so we adopt a two-stage curriculum. This
 2444 approach is a standard practice in the Learning to Optimize field for training implicit or unrolled
 2445 models that solve optimization problems (Chen et al., 2022c). This approach begins with a shorter
 2446 unroll horizon and a larger learning rate, using the trained model to warm-start the subsequent stage
 2447 with a longer horizon and a reduced learning rate. This strategy is often described as “layerwise
 2448 training” (Chen et al., 2018; Liu et al., 2019) or “curriculum learning” (Chen et al., 2020). In our
 2449 settings: Stage 1 uses $T = 3$ with a learning rate 0.01; Stage 2 uses $T = 6$ with a learning rate 10^{-4} .
 2450 Both stages use Adam optimizer.

2451 For a fair comparison, the non-iterative explicit GNNs are trained using the same two-stage learning-
 2452 rate schedule. This regimen proved effective, as the training errors for our explicit baselines
 2453 surpassed those reported in prior work (Chen et al., 2023).

2454 At the inference time, T can be chosen as the unroll length in the training stage, or moderately
 2455 longer. In our experiments, we use $T = 8$ at the inference time, as we do not observe significant
 2456 improvement with a larger number of iterations.

2457 *Remark.* While we employ unrolled training rather than the vanilla Jacobian-based implicit differ-
 2458 entiation, we classify our approach as an “implicit model” because the underlying architecture, a
 2459 weight-tied update $\mathbf{z}_t = \mathcal{G}_\Theta(\mathbf{z}_{t-1}, \mathcal{Q}_\Phi(\mathbf{x}))$, remains identical. The distinction lies solely in the
 2460 numerical implementation: as established by Geng et al. (2021), unrolled training is mathemati-
 2461 cally equivalent to a Neumann series approximation of the implicit gradient. Thus, unrolling and
 2462 root-finding are simply two valid strategies for approximating the same fixed point, $\mathbf{y}_*(\mathbf{x})$. This
 2463 equivalence is widely recognized in the Implicit GNN literature, where Neumann approximations
 2464 are standard for scaling to large graphs (e.g., (Baker et al., 2023)). Since our focus is on expressiv-
 2465 ity rather than optimization mechanics, we treat both formulations as belonging to the same model
 2466 class.

2467 J BROADER CONTEXTUAL DISCUSSIONS

2470 While our work primarily establishes the expressive power of implicit models through the lens of
 2471 fixed-point iterations, we situate our contributions within the broader landscape of implicit model
 2472 theory in this section.

2473 **Universality and expressivity.** Despite its foundational importance, a general and systematic theory
 2474 of expressive power for implicit models remains largely open. To our knowledge, existing results
 2475 address only specific facets of the problem. For example, while Bai et al. (2019) demonstrated that
 2476 an operator g exists such that its fixed point reproduces any explicit network f , this existence result
 2477 crucially does not guarantee that the fixed-point iteration (1) actually converges. Other works have
 2478 established universality within restricted domains, such as steady-state PDEs Marwah et al. (2023),
 2479 or proven separation results where implicit models outperform explicit counterparts in specific set-
 2480 tings Wu et al. (2024). While insightful, none of these studies provide a complete characterization
 2481 of the general function class representable by implicit models, nor do they directly address the fun-
 2482 damental questions (Q1) and (Q2) raised in our introduction.

2483 **Contrast with explicit models.** First, consider the setting where the model is subject to a global
 2484 Lipschitz constraint (e.g., $\text{Lip}(f_\theta) \leq 1$), which is common for robustness and stability. In this

2484 case, explicit feedforward networks are mathematically strictly limited to representing globally 1-
 2485 Lipschitz maps (Murari et al., 2025). Consequently, they are fundamentally incapable of expressing
 2486 locally Lipschitz targets whose gradients become arbitrarily large (such as $1/x$ near zero). In
 2487 contrast, our work demonstrates that implicit models break this barrier: a simple, globally regular
 2488 operator (Lipschitz in x , contractive in y) can generate complex, locally Lipschitz fixed-point maps
 2489 via iteration. This “Simple Operator → Complex Fixed Point” mechanism is the core difference
 2490 claimed in our paper.

2491 Second, if we remove constraints, Beneventano et al. (2021) have shown that deep ReLU networks
 2492 can indeed approximate locally Lipschitz functions on arbitrary compact sets. However, achieving
 2493 high precision for such complex targets requires the explicit model size (depth/width) to grow ar-
 2494 bitrarily large. Here lies the crucial distinction: explicit models scale expressivity with model size,
 2495 whereas implicit models are able to scale expressivity with test-time iterations. This allows implicit
 2496 models to represent increasingly complex functions dynamically without adding parameters.

2497 **Training Dynamics and Convergence.** A significant body of work focuses on the optimization
 2498 mechanics of implicit models. Geng et al. (2021) rigorously established the equivalence between
 2499 unrolled training and implicit differentiation via Neumann series approximations, validating the
 2500 training methodologies used in our case studies. Ling et al. (2023); Truong (2025) provide global
 2501 convergence guarantees and rate analyses for the training in over-parameterized deep equilibrium
 2502 models. While these studies ensure that training algorithms can successfully minimize the loss,
 2503 our work addresses the fundamental antecedent question: whether a model exists that is capable of
 2504 representing the target function in the first place.

2505 **Generalization.** Distinct from expressivity, Fung & Berkels (2024) derive generalization bounds for
 2506 families of implicit networks, characterizing their ability to perform on unseen data. Our analysis
 2507 focuses on approximation capacity—the ability to construct an operator that exactly reproduces a
 2508 target map—which is orthogonal to the sample complexity and generalization bounds discussed in
 2509 their work.

2510 **Infinite-Width Limits and Kernel Connections.** Recent research has sought to bridge the gap
 2511 between implicit models, explicit deep networks, and kernel methods. Gao et al. (2022) extend the
 2512 over-parameterization theory of explicit networks to implicit models, establishing well-posedness
 2513 and convergence even in finite-width regimes where standard infinite-depth results do not directly
 2514 apply. In the infinite-width limit, Feng & Kolter (2023) formally derive the Neural Tangent Ker-
 2515 nel (NTK) for equilibrium models, characterizing their training dynamics in the linear regime. On
 2516 the architectural side, Ling et al. (2024) show that for high-dimensional Gaussian mixtures, deep
 2517 equilibrium models can be functionally equivalent to shallow explicit networks. In contrast to these
 2518 kernel-based or distribution-specific analyses, *our work adopts a non-parametric function-space*
 2519 *perspective*; we demonstrate that for general locally Lipschitz targets, the expressive power of im-
 2520 plicit models is not static but scales dynamically with test-time computation, a property distinct from
 2521 the linear regimes often studied in kernel theory.

2522 K LLM USAGE STATEMENT

2523 We used LLMs solely as a writing-polish assistant across all sections in the main text and appendix.
 2524 Its role was limited to grammar fixes, wording/flow improvements, and rephrasing of text that we
 2525 originally drafted. All model suggestions were reviewed, verified, and, when necessary, edited by
 2526 the authors to ensure accuracy. The authors take full responsibility for the final manuscript, including
 2527 any text influenced by LLM assistance.

2528
 2529
 2530
 2531
 2532
 2533
 2534
 2535
 2536
 2537